Structural Characterization of the Heterobactin Siderophores from *Rhodococcus erythropolis* PR4 and Elucidation of their Biosynthetic Machinery

---

Strukturelle Charakterisierung des Heterobactin Siderophors aus *Rhodococcus erythropolis* PR4 und Untersuchung seiner biosynthetischen Maschinerie

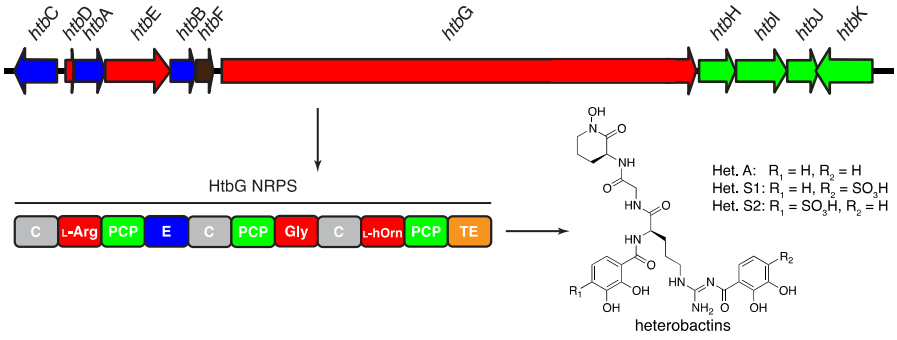

Dissertation

zur

Erlangung des Doktorgrades

der Naturwissenschaften

(Dr. rer. nat.)

dem Fachbereich Chemie

der Philipps-Universität Marburg

vorgelegt von

Mustafa Adnan Mustafa Zeyadi

Aus Jeddah, Saudi Arabien

Marburg an der Lahn, 2015

Die Untersuchungen zur vorliegenden Arbeit wurden am Fachbereich Chemie der Philipps-Universität Marburg unter der Leitung von Herrn Prof. Dr. Mohamed A. Marahiel durchgeführt.

Vom Fachbereich Chemie der Philipps-Universität Marburg als Dissertation angenommen am 27 October 2015.

Erstgutachter: Prof. Dr. Mohamed A. Marahiel (Philipps-Universität Marburg)

Zweitgutachter: Dr.Gert Bange (Philipps-Universität Marburg)

Tag der mündlichen Prüfung am: 10 December 2015

The majority of the work presented herein has been published:

Mattia Bosello, **Mustafa Zeyadi**, Femke I. Kraas, Uwe Linne, Xiulan Xie and Mohamed A. Marahiel.

Structural Characterization of the Heterobactin Siderophores from *Rhodococcus erythropolis* PR4 and Elucidation of their Biosynthetic Machinery.

Journal of Natural Products **2013** 76, 2282-2290

Dedicated to my

Parents & Family

Table of contents

Table of contents

Abbreviation

List of abbreviation

ABC	ATP Binding Cassette
A-domain	adenylation domain
aa	amino acid
Ac-CoA	acetyl coenzyme A
ArCP	aryl carrier protein
ACP	acyl carrier protein
ADP	adenosine diphosphate
AMP	adenosine monophosphate
AT	acetyltransferase
ATP	adenosine triphosphate
ATR-IR	attenuated total reflection infrared spectroscopy
BLAST	Basic Local Alignment Search Tool
BSA	Bovine Serum Albumine
bp	bases pairs
CAS	chrome azurol sulfonate
CD	Circular dichroism spectroscopy
C-domain	condensation domain
Cy-domain	cyclization domain
CoA	coenzyme A
COSY	correlation spectroscopy
ddH_2O	double-distilled water
DHB	2,3-dihydroxybenzoic acid
DAD	diode-array detector
DMSO	dimethylsulfoxide
DNA	deoxyribonucleic acid
EDTA	ethylenediaminetetraacetic acid
E-domain	epimerization domain
EIC	extracted ion chromatogram
ESI	electron-spray ionization
F-domain	formylation domain
FA	fatty acid

FAD	flavin adenine dinucleotide
FDAA	*N*-α-(2,4-dinitro-5-fluorophenyl)-L alaninamide
FMN	flavin mononucleotide
FPLC	fast protein liquid chromatography
GC	Guanine-Cytocine content
haOrn	δ-*N*-acetyl-δ-N-hydroxyornithine
HEPES	4-(2-hydroxyethyl)-1-piperazine ethanesulfoni acid
HMO	Heterobactin monooxygenase
hOrn	δ-*N*-hydroxyornithine
HPLC	high performance liquid chromatography
HR-MS	high-resolution mass spectrometry
IPTG	isopropyl-β-D-thiogalactopyranoside
K_D	Dissociation constant
LC-MS	liquid chromatography-mass spectrometry
LTQ	linear trap quadrupole
MALDI	Matrix Assisted Laser Desorption Ionization
MT-domain	methyltransferase domain
MeOH	methanol
mRNA	messenger ribonucleic acid
MS	mass spectrometery
NADH	nicotinamide adenine dinucleotide
NADPH	nicotinamide adenine dinucleotide (phosphate)
NFPA	nonafluoropentanoic acid, n-perfluoropentanoic
Ni-NTA	Ni-nitrilotriacetic acid
NIS	NRPS independent siderophore
NMO	*N*-hydroxylating flavoprotein monooxygenases
NMR	nuclear magnetic resonance
NOESY	nuclear Overhauser effect spectroscopy
NRP	non-ribosomal peptide
NRPS	non-ribosomal peptide synthetase
NTP	nucleoside triphosphate
OD	optical density
OMTs	Outer membrane transporters

ORF	open reading frame
Orn	ornithine
Ox-domain	oxidation domain
PBP	Periplasmic binding protein
PCP-domain	peptidyl- carrier –protein domain
PCR	polymerase chain reaction
PK	polyketide
PKS	polyketide synthase
Ppan	4'-phosphopantetheine
PPi	inorganic pyrophosphate
Pptase	4'-phosphopantetheinyl-transferase
qTOF	quadrupole time-of-flight
RNA	ribonucleic acid
ROS	reactive oxygen species
RP	reversed-phase
RT	Room temperature
SBPs	Siserophore-binding protein
SDS	sodium dodecyl sulfate
SDS-PAGE	sodium dodecyl sulfate polyacrylamide gel electrophoresis
SIC	selected (single) ion chromatogram
Sfp	4'-phosphopantetheinyl-transferase involved in surfactin production
Spp.	Species
T-domain	thiolation domain
TE-domain	thioesterase domain
TFA	trifluroacetic acid
TIC	total ion chromatogram
TOCSY	total correlation spectroscopy
tR	retention time
TRIS	tris-(hydroxymethyl)-aminomethane
tRNA	transfer ribonucleic acid
v/v	Volume/volume
w/v	weight/volume
w.t.	wild-type

Table 1 Overview of the proteinogenic amino acids. The three- and one-letter codes are given for each amino acid, as well as the molecular weight.

Amino acid	Three letter code	One letter code	Mw(Da)
alanine	Ala	A	89
arginine	Arg	R	174
asparagine	Asn	N	132
aspartic acid	Asp	D	133
cysteine	Cys	C	121
glutamic acid	Glu	E	147
glutamine	Gln	Q	146
glycine	Gly	G	75
histidine	His	H	155
isoleucine	Ile	I	131
leucine	Leu	L	131
lysine	Lys	K	146
methonine	Met	M	149
phenylalanine	Phe	F	165
proline	Pro	P	115
serine	Ser	S	105
threonine	Thr	T	119
tryptophan	Trp	W	204
tyrosisne	Tyr	Y	181
valine	Val	V	117

Summary

The genus *Rhodococcus* belong to the order actinomycetes, which are gram-positive bacteria with high GC content. They produce a broad range of bioactive secondary metabolites that found use in the pharmaceutical industry and in other biotechnological applications. Most of these bioactive metabolites were derived from nonribosomal peptides (NRP) or polyketides (PK). However, only few natural products have been isolated and characterized so far. In particular, within the *Rhodococcus genus*, substantial chemical diversity has been observed among the iron-chelating siderophores through the structure elucidation of rhodochelin, rhodobactin and heterobactin A1. Therefore this work was focused on isolation and structural characterization of further new iron-chelating molecules to explore the possible chemical potential of this genus on secondary metabolite production. In this study we accomplished the isolation, the structural characterization and the elucidation of the biosynthetic origin of heterobactins, a catecholate-hydroxamate mixed-type siderophores from *Rhodococcus erythropolis* PR4. The structure elucidation of the extracted and purified siderophore heterobactin A was accomplished via MS^n analysis and NMR spectroscopy and revealed the noteworthy presence of a peptide bond between the guanidine group of an arginine residue and a 2,3- dihydroxybenzoate moiety. The two other purified siderophores heterobactin S1 and S2 were found to be derivatives of heterobactin A that have sulfonation modifications on the aromatic rings. The bioinformatic analysis of the *R. erythropolis* PR4 genome and the subsequent genetic and biochemical characterization of the putative biosynthetic machinery identified the gene cluster responsible for the biosynthesis of the heterobactins to encode the three modules comprising nonribosomal peptide synthetase (NRPS) HtbG. Interestingly, the HtbG NRPS contains an unprecedented C-PCP-A domain organization within the second module of the HtbG-synthetase that may help the correct elongation of the peptide intermediate. The present work also revises the structure of heterobactin A that was described by Carrano et al. in 2001. Also, the biochemical characterization of the monooxygenase HMO (encoded by the *hmo* gene within the gene cluster) established a route for the biosynthesis of the non- proteinogenic amino acid L-hOrn, prior to its incorporation by the NRPS HtbG into the siderophore scaffold. The insights gained from the structural and biochemical characterization of the siderophore heterobactins, together with the genetic and biochemical characterization of the respective biosynthetic gene clusters, allowed us to establish a biosynthetic model for heterobactins assembly. The iron-siderophore binding protein HtbH (encoded by *htbH* gene within the gene cluster) was also biochemically characterized and was shown to display a novel mix-type catecholate-hydroxamate binding behavior.

Zusammenfassung

Der Genus *Rhodococcus* gehört zu der Ordnung der *Actinomycetales*. Diese sind gram-positive Bakterien mit einem hohen GC-Gehalt, welche eine große Anzahl an Sekundärmetaboliten produzieren, die in der pharmazeutischen Industrie und in der Biotechnologie Anwendung gefunden haben. Die meisten dieser bioaktiven Verbindungen stammen entweder von nicht-ribosomalen Peptiden (NRP) oder Polyketiden (PK), von denen bisher jedoch nur wenige isoliert wurden. Nichtsdestotrotz wurde insbesondere innerhalb des *Rhodococcus*-Genus eine bemerkenswerte strukturelle Vielfalt von Siderophoren durch die Strukturaufklärung von Rhodochelin, Rhodobactin und Heterobactin A1 nachgewiesen. Deshalb wurde der Fokus dieser Arbeit auf die Isolierung und Charakterisierung von neuen Siderophor-Strukturen gelegt, um das chemische Potential in diesem Genus noch stärker hervorzuheben. In der vorliegenden Arbeit wird über die Isolierung, strukturelle Charakterisierung und Aufklärung des Biosyntheseursprungs des Siderophors Heterobactin berichtet. Dieser ist ein Catecholat-Hydroxamat-Mischtyp aus *Rhodococcus erythropolis*. Die Strukturaufklärung des extrahierten und gereinigten Siderophors Heterobactin A wurde mittels MS^n-Analytik und NMR- Spektroskopie durchgeführt und zeigte die Anwesenheit einer besonderen Peptidbindung zwischen der Guanidingruppe eines Argininrestes und einer 2,3-Dihydroxybenzoatgruppe. Die beiden isolierten Heterobactin-Varianten S1 und S2 sind zudem Derivate von Heterobactin A, die eine Sulfonierung an den Aromaten aufweisen. Die bioinformatische Untersuchung des *R. erythropolis* PR4 Genoms und die anschließende biochemische Charakterisierung der putativen Biosynthesemaschinerie halfen das Gencluster zu identifizieren, das für die Biosynthese der Heterobactine verantwortlich ist. Interessanterweise verfügt die HtbG NRPS-Synthetase, die aus drei Modulen besteht, innerhalb ihres zweiten Moduls über eine nie zuvor beobachtete C-PCP-A Domänenorganisation, welche notwendig sein könnte für die korrekte Verlängerung der Peptidintermediate. Die vorliegende Arbeit korrigiert zudem die von Carrano et al. in 2001 beschriebene Heterobactin A Struktur. Die biochemische Charakterisierung der Monooxygenase HMO (kodiert vom Gen *hmo*) etablierte zudem die Biosyntheseroute der nicht-proteinogenen Aminosäure L-hOrn, bevor diese durch die NRPS-Maschinerie in das Peptidgerüst (Siderophor) eingefügt wird. Die Ergebnisse aus der strukturellen und biochemischen Charakterisierung der Heterobactine erlauben, zusammen mit der genetischen und biochemischen Charakterisierung der jeweiligen Biosynthesegencluster, den Vorschlag eines Biosynthesemodells für die Heterobactin-Assemblierung, In dieser arbeit wurde auch das Siderophor-Bindungsprotein htbH biochemisch untersucht, wobei seine hohe Affinität zum Mischtyp Catecholat-Hydroxamat Siderophor gezeigt werden konnte.

Chapter 1

Introduction

1. Introduction

1.1 *Rhodococcus erythropolis* PR4

The genus *Rhodococcus* belong to the order actinomycetes, which are Gram-positive bacteria that have high guanine-cytosine (GC) content. They produce potential secondary metabolites, such as nonribosomal peptides (NRP) and polyketides (PK).[1] *Rhodococcus erythropolis* PR4 has been isolated from the deep sea at a depth of 1,000 m south of Okinawa Island, Japan (the Pacific Ocean).[1,2] *R.erythropolis* PR4 can degrade normal and branched alkanes as sources of carbon and energy.[3] In recent years, increasing information from microbial genome sequencing and the bioinformatics tools for genome mining have assisted improvements for novel natural product discovery.[4]

1.2 Iron in the environment and in microbiology

Being the fourth most common element on earth (and the second most common metal), iron is an essential element in many biological systems and takes part as an essential cofactor in many enzymes of cellular metabolism, which include photosynthesis, respiration, krebs cycle, oxygene transport, gene regulation and DNA biosynthesis. Under aerobic conditions, soluble Fe^{II} spontaneously oxidized to Fe^{III}, which, in the presence of oxygen and water and at neutral pH, forms insoluble ferric oxide hydrate complexes, leading to a free Fe^{III} concentration of up to 10^{-18} M. In order to cope with iron-limiting conditions, microbes have developed mechanisms for highly selective metal uptake.[5,6,7] The secretion of low molecular weight organic chelators, called siderophores (from Greek: “iron carriers”), is one of the main iron-mobilizing strategies used by both environmental and pathogenic strains to support their growth under strict iron-limiting conditions.[8,9] Most siderophores display a molecular mass < 1 kDa, coordinate the ferric iron via six-donor atoms as an octahedral complex (in a ferric iron:siderophore ratio of 1:1), and have an extremely high affinity (K_f =10^{22}-10^{49} M^{-1}).[10] After siderophore secretion to the extracellular space, the ferric iron-siderophore complex is actively imported into the intracellular space, where the iron is released from the chelator complex and channeled to the intracellular targets.[11–13] Most aerobic and facultative anaerobic microorganisms synthesize at least one siderophore, and some microbial strains may produce more

than one siderophore: for example, *Pseudomonas aeruginosa*, which produces two siderophores, pyoverdine and pyochelin. It must be stressed that not all microbes require iron, and siderophores can be dispensed within these rare cases.[14] Some lactic acid bacteria are not stimulated to greater growth with iron,[15] and manganese and cobalt are used instead.[16] Other microbes need iron but grow anaerobically on Fe^{II}.[17]

1.3 The history of siderophores

The first attempts to isolate the fluorescent pigments (later named pyoverdin) were reported in 1891.[18] In 1902, Twort and Ingram discovered that all mycobacteria needed an essential substance that was vital to their growth.[19] During the period 1949-1952, three different siderophores, mycobactin,[20] ferrichrome[21] and coprogen,[22] were isolated and defined as growth factors. In 1954, Snow characterized mycobactin which possesses a high affinity for Fe^{III}.[23] At the same time, Burton and colleagues isolated the "Terregens Factor" (in 1972, called arthrobactin) as a growth factor and demonstrated that it formed a stable iron complex.[24] In 1956, Garbibaldi and Neilands demonstrated that the production of ferrichrome A was enhanced by growing the organism *Ustilago sphaerogena* in iron-deficient medium.[25]In 1958, characterization of the catecholate siderophores was initiated by the finding that the glycine conjugate of 2,3-dihydroxybenzoic acid was secreted by *Bacillus subtilis* when grown under iron-limiting conditions.[26] In 1961, Emery and Neilands elucidated the structure of ferrichrome and ferrichrome A.[27] In parallel, the ferrioxamines and ferrimycin were isolated by ETZ, Zurich and Ciba.[28–30] In 1963, Schwarzenbach and colleagues reported the affinity constant of the ferrioxamine group.[31] In the mid-1960s, a range of structurally diverse hydroxamates were characterized as iron-binding growth factors. In 1970, the first tricatechol siderophore (enterochelin) was identified[32] and, in same year, enterobactin was isolated by Pollock and Neilands from *Salmonella typhimurium* and by OBrine and Gibson from *E.coli*.[32,33] Since 1970, a large number of siderophores have been characterized, the majority using hydroxmate, catecholate or α-hydroxycarboxylate functional groups.

1.4 Siderophores structures

Siderophores are structurally diverse natural products and display great chemical diversity in both iron coordination and their biosynthesis. These structures are characterized by the presence of one, two and, in most cases, three bidentate chelating groups, generally oxygenated, necessary for the formation of very stable hexacoordinated octahedric complexes between the siderophores and Fe^{III}. These groups are generally either catecholates (better termed as "aryl caps"), hydroxamates, and (α-hydroxy)-carboxylates. However, the continuous discovery of new structures led to a more complex classification, due to the presence of at least two different coordinating groups within one molecule, resulting in "mixed-type" siderophores.[34]

1.4.1 The catecholate and phenolate siderophores

The siderophores possessing exclusively catecholate or phenolate groups are synthesized only by bacteria. The most commonly studied in this group are the tris catecholates enterobactin and bacillibactin isolated from *E.coli* and *Bacillus subtilis,* respectively. In the presence of Fe^{III}, the ligand forms a high-spin octahedric hexacoordinated complex having the highest affinity constant for the siderophore:iron complex, enterobactin = 10^{49} M^{-1} and bacilibactin = 10^{47} M^{-1}. The aryl-capped siderophores are mainly synthesized by nonribosomal peptide synthetases (NRPSs). Prior to NRPS-catalyzed assembly, the aryl acids 2,3dihydroxybenzoate (DHB) and salicylate, which are generally used as aryl caps, have to be provided by specific enzymes. The genes encoding the NRPS and the enzymes for aryl acid synthesis in most bacteria are directly iron-regulated via the Fur repressor.[10]

1.4.2 The hyroxamates siderophores

In contrast to the catecholate and phenolate class, the hydroxamate siderophores can be synthesized by bacteria and also by fungi. They derive generally from 1-amino-hydroxyamino alkanes or N-hydroxyamino acids bound to the rest of the molecule via amide or ester bonds. Hydroxamate siderophores can be classified in four main sub-groups: Ferrichrome, Ferrioxamines, Coprogens and Fusarinines.[35] Furthermore, in contrast to catecholate siderophores, the hydroxamate and carboxylate siderophores

are assembled, in most cases, by NRPS-independent (NIS) mechanisms. The biosynthesis of these classes of siderophores need some enzymes, such as monooxygenase, decarboxylase, aminotransferase or ac(et)yltransferase.[36]

1.4.3 α-hydroxy carboxylate siderophores

α-hydroxy carboxylate siderophores contain only aliphatic amines and/or carboxylate and hydroxy donor groups. The first member of this class was a rhizoferrin siderophore.[36] The free α-hydroxy carboxylate moieties may be derived from hydroxy-carboxylic acids, such as citrate (viboferrin and staphyloferrin), 2-oxo- glutarate (achromobactin) and malonic acid (rhizobactin DM4). The second mechanism for free α-hydroxy carboxylate moieties results from introducing β–cysteine -aspartates into a peptide backbone sequence, such as pyoverdin.[35]

1.4.4 Mixed-type siderophores

Increasing genome sequencing information about natural products, secondary metabolites and new siderophores led to a more complex classification, since many structures that integrate the chemical features of at least two classes into one molecule, resulting in "mixed-type" siderophores, have become known. Many "mixed-type" siderophores have been reported, such as petrobactin siderophore (a mixed 3,4-catecholate/α-hydroxycarboxylate from *B.subtilis*),[37] Rhodochelin siderophore (a mixed catecholate/hydroxamate from *R.jostii* RH1)[38] and Aerobactin siderophore (citrate/hydroxamate from Enterobacter ssp.).[37] These are representive of different siderophores structures with their producers. Catecholate/phenolate, hydroxamate, carboxylate and the mixed-type structures are shown in (Figure 1.1).

1.5 Siderophore biosynthesis pathways

Siderophore diversity can be also classified on the basis of the biosynthetic origin as NRPS-dependent and NIS. NRPS-dependent is the assembly strategy most used in microorganisms to assemble siderophores.[38] The second pathway for siderophore biosynthesis is the NIS. Aerobactin was the first siderophore assembled by an NIS biosynthetic pathway to be discovered. It is a mixed-type siderophore produced by several Gram-negative bacteria, including *E. coli*, *Shigella species*, *Yersinia species* and

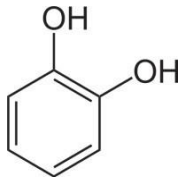

catecholate

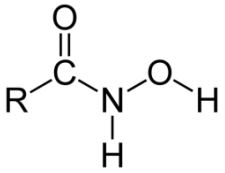

hydroxamate

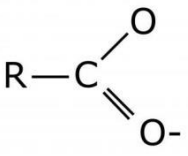

carboxylate

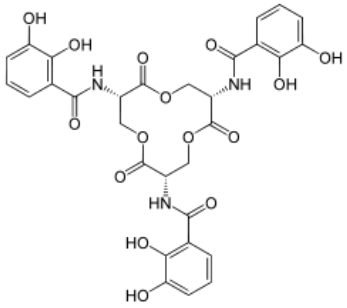

Enterobactin
(entreric bacteri *streptomyces* spp.)

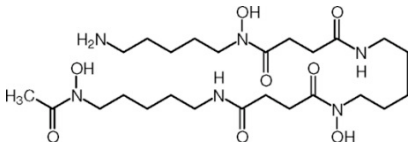

Desferrioxamine

(Streptomyces pilosus)

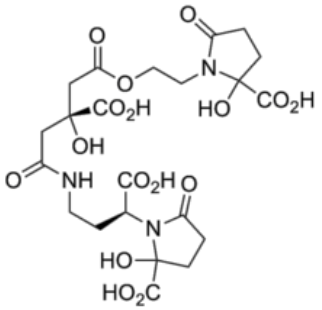

Achromobactin

(*Erwina chrysanthemi)*

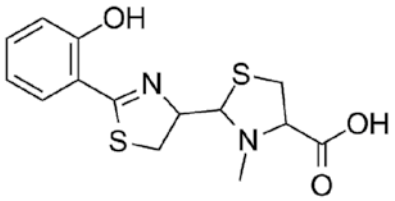

Pyochelin (Phenolate) (Pseudomonas aeruginosa)

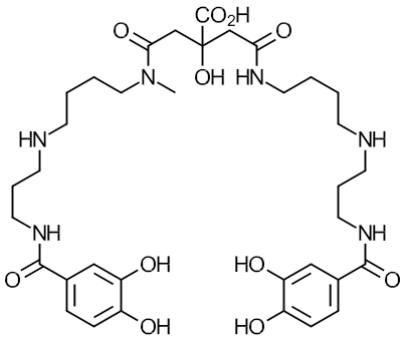

Petrobactin (mixed-type)

Catecholate/carboxylate

(Bacillus anthracis)

Figure 1.1 Different representative siderophore structures with their producers: catecholate/phenolate, hydroxamate, carboxylate and mixed-type structures.

Salmonella species. The gene cluster which is directly responsible for aerobactin biosynthesis consists of four genes.[39] The *iucD* gene encodes a Flavin-dependent monooxygenase that catalyzes hydroxylation of the ε-amino group of L-lysine,[40] and the *iucB* gene encodes an acetyl transferase that catalyzes *N*-acetylation of the hydroxylamino group in the resulting N^6-hydroxy-L-lysine (L-hLys),[41](Figure 1.2).

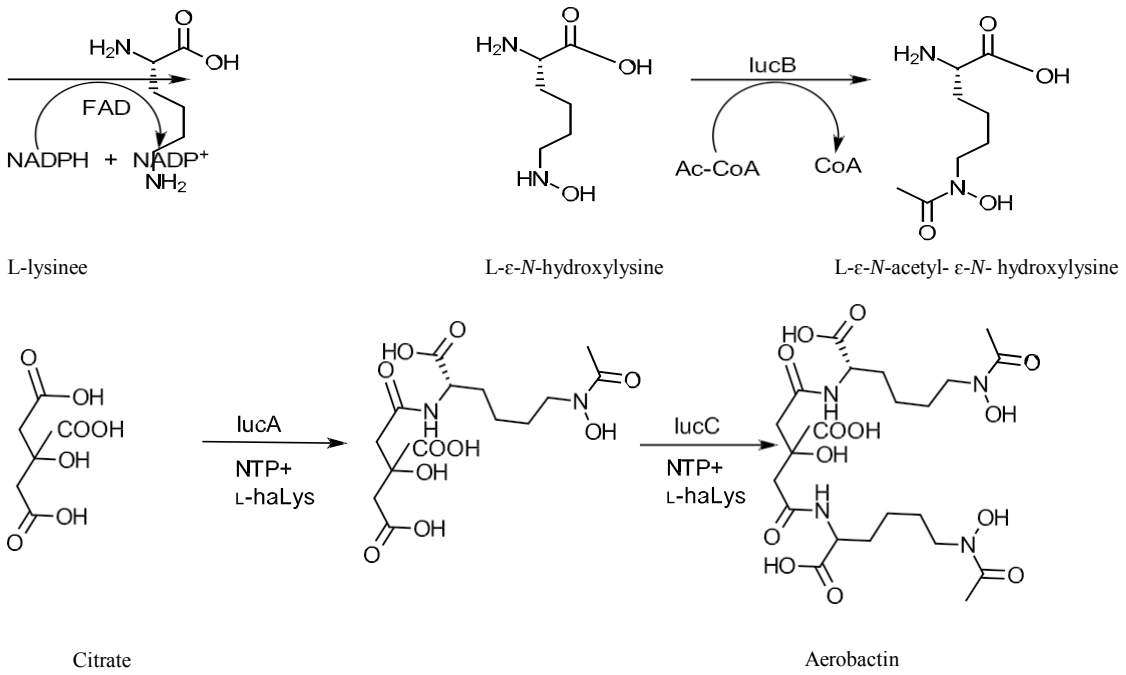

Figure 1.2 The postulated pathway for aerobactin biosynthesis. The FAD-dependent monooxygenase IucD hydroxylates the ε-amino group of L-Lys, subsequently acetylated to LhaLys by the IucB acetyltransferase. The tailored building block is condensed with a carboxyl group of citric acid by IucA. Analogously, IucC catalyzes the second condensation reaction to give rise siderophore aerobactin. In analogy with other NIS synthetases, it is proposed that the condensation reactions take require the consumption of NTPs for the activation of the citrate's carboxylic functions.

Genetic studies indicate that *iucA* encodes a synthetase that catalyzes acylation of the α-amino group in N^6-acetyl-N^6-hydroxy-L-lysine (L-ahLys) with one of the prochiral carboxyl groups of citric acid to form N^6-acetyl-N^2-citryl-N^6 hydroxy-L-lysine These studies also indicate that the *iucC* gene encodes a similar synthetase which catalyses condensation of the product of the *IucA*-catalyzed reaction with a second molecule of hLys to form aerobactin.[42,43]

1.5.1 Siderophore biosynthesis catalyzed by NRPSs

The NRPSs represent large multienzyme complexes that activate and assemble a broad array of amino, carboxy and hydroxyl acids, leading to a high structural variability of the generally macrocyclic peptidic products, which in most cases show biological activity,[4] For example, belomycin is classified as an "antitumor", vancomycin exhibits antibiotics activity and cyclosprin is an immunosuppressive agent. In contrast to ribosomal peptide synthesis, the assembly of the peptidic products is carried out in an mRNA-independent function.[38] This diversity may be enhanced through various substrate modifications occurring during assembly by the action of specialized domains that are integrated into the standard NRPS domain architecture. The NRPSs consist of an array of modules; each module is responsible for the combination and modification of one building block into the final polypeptide product.[45] Modules can be dissected into various catalytic domains responsible for substrate recognition, activation, peptide bond formation, modification, elongation and final product release. There are three essential domains needed to carry out substrate selection and activation (A-domain), hold the activated substrate (PCP-domain) and form the peptide bond (C-domain), which is lacking in initiate NRPSs. The chemical structures of some nonribosomal peptides is shown in (Figure 1.3).[46]

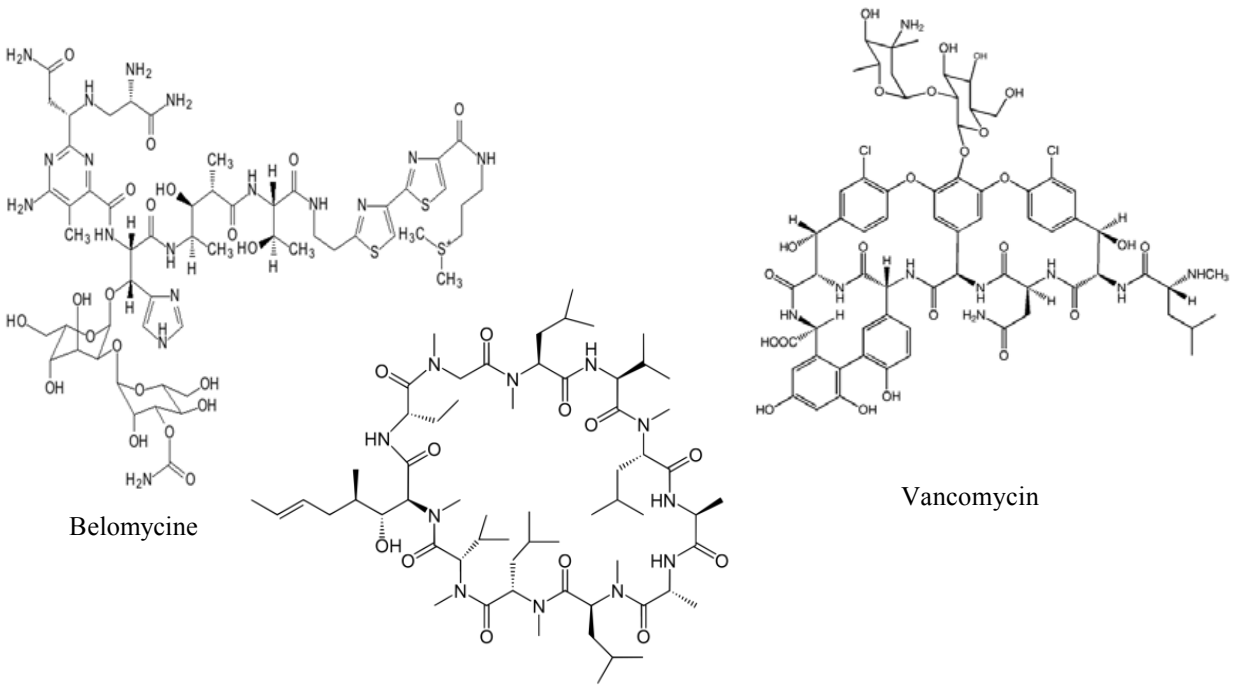

Figure 1.3 Example of nonribosomal peptide (NRP) natural products.

1.5.2 Nonribosomal peptide synthetase domains

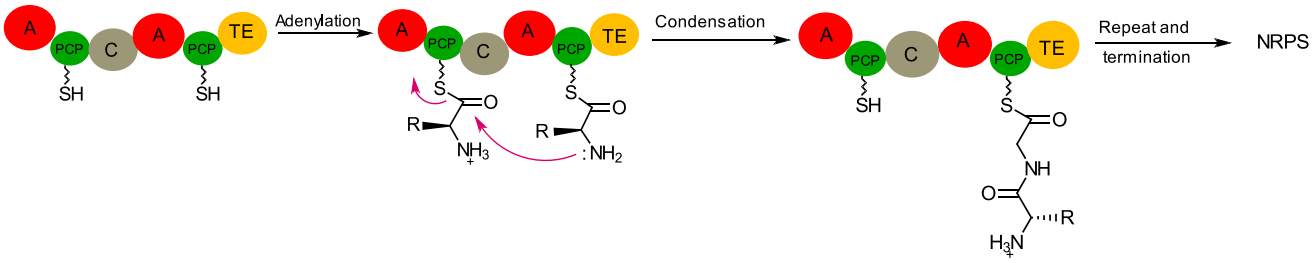

Figure 1.4 Schematic of a nonribosomal peptide synthetase (NRPS) assembly line. The peptidyl carrier domain (PCP) has a phosphopantetheine prosthetic group terminated with a thiol (wavy lines). The adenylation (A) domain activates amino acids and the condensation (C) domain makes the amide linkages. Termination is frequently catalyzed by a thioesterase (TE) domain.[47]

1.5.2.1 Adenylation (A)-domain

The recognition and activation of the amino or carboxy acid substrate as amino acyl adenylate which consumes the ATP is catalyzed by the Adenylation (A) domain, which usually consists of ~550 amino acids and could be divided into the N-terminal core (~450 amino acids) and the C-terminal subdomain (~ 100 amino acids).[38,46] A two-step mechanism is required for substrate activation. Firstly, formation of an aminoacyl adenylate intermediate after the cognate amino acid is activated at the expense of Mg^{2+}-ATP and release of pp_i. Secondly, the enzyme-attached thiol moiety 4'-phosphopantetheine (4'-PP) attacks the amino acyl adenylate to yield the aminoacyl thioester and AMP as a leaving group. However, the similarity in biological activity of the A-domain and aminoacyl-tRNA synthetase are structurally distinct.[48] The first crystal structure of the A-domain was of the phenylalanine-activating A-domain of gramicidin GrsA from *Bacillus brevis* (PheA).[49] Solving the 3D structure of PheA with bound phenylalanine and AMP gave detailed insight into its catalytic mechanism and allowed the assignment of those amino acid residues that play a decisive role in the coordination of the substrate.

1.5.2.2 Peptidyl carrier protein domain

The peptidyl carrier protein (PCP) domain or thiolation (T)-domain is the site of cofactor binding. The protein consists of ~80 amino acids and is located downstream of the A-domain. It has a highly conserved serine residue and serves as a crane for activated substrate delivery. The activated amino acid is transferred onto the thiol group of the Ppan prosthetic group attached to the PCP-domain.[50] The conversion of inactive apo-PCP into its active Ppan-PCP holo form is mediated by PPTase, e.g. Sfp.[51] The first structure of a PCP was solved via NMR spectroscopy with the PCP of the *B.bbrevis* tyrocidin synthetase.[52] The structure of the pepridyl carrier protein (PCP) is a distorted four-helix package with an expanded loop between the first and second helices, which may be significant for binding with Sfp. The PCP is a member of the carrier protein superfamily, such as acyl carrier proteins (ACPs) of fatty acid, PK synthases and aryl carrier proteins. Despite the supposed distinct roles of carrier proteins in their particular biosynthetic machinery, their structures are almost identical. The difference most observed between PCPs and ACPs is the overall charge of the protein. While PCPs surface is much less polar, the ACPs have mainly acidic side chains on their surface.[53]

1.5.2.3 Condensation domain

The condensation domain (C-domain) is the main entity of NRPS elongation, because it catalyzes the peptide bond formation between amino acyl substrates bound to PCPs of close modules. The C-domain contains a donor site and an acceptor site.[54] The C-domain catalyzes the nucleophilic attack of the α-amino group of the activated amino acid onto the carbonyl group of the thioester bound of the peptidyl-*S*-PCP.[55] The C-domain contains ~450 amino acids and is composed of two large similar subdomains arranged in a V-shaped canyon-like structure, of which the N-terminal subdomain shares high sequence and structural homology with the chloramphenicol acetyltransferases.[56–58] This characteristic V-shaped structure allows the correct positioning of the up- and downstream PCP-domains at each opening (acceptor and donor-site), with respect to the highly conserved catalytic His-residue of the HHxxxDG motif, which remains at the bottom of the canyon. Although the exact reaction mechanism has not yet been elucidated, it is suggested that the second His residue takes part in the deprotonation of the α-amino group of the aminoacyl-*S*-PCP

substrate, enhancing the electron-donor character of the nucleophilic PCP-bound substrate and, therefore, facilitating the reaction.

1.5.2.4 Thioesterase domain

The thioesterase domain (TE-domain) contains ~280 amino acids and is an important domain for releasing the product from the NRPS elongation chain. It is always found in the last modules or the termination modules.[59] Product release is catalyzed by two steps that involve an acyl-*O*-TE intermediate formation that is subsequently hydrolyzed by water or attacked by a peptide-internal-nucleophile. Some TE-domains catalyze product release either by generation of cyclic or branched-cyclic products.[46] Macrocyclization by TE-domain are essential mechanisms to release the product in NRPS.

1.5.3 Auxiliary domains

In addition to the fundamental domains A, PCP, C and TE, many additional domains are required to build up a peptide. These domains are classified into two types: some are an integral part of NRPS and act in *cis* and others act in *trans* on the way to mature NRPS peptide.[60,61]

1.5.3.1 Epimerization domain

Almost of nonribosomal peptides contain D-amino acid. In fact, NRPSs use two different mechanisms to incorporate D-amino acid into the peptide.[62] This latter action may be fixed by the specificity of the A-domain, which is predominantly observed in cyclosporin and microcystin biosynthesis.[63] The second mechanism utilizes the epimerization domain (E-domain), which contains ~450 amino acids and is located downstream of the PCP-domain. It catalyzes the racemization of the C-terminal amino acid of the peptide or the PCP-bound amino acid.[64] These processes are catalyzed by two various classes of the E-domain: aminoacyl epimerase, which could be a phase of initiation modules, and the peptidyl epimerase, which is a phase of an elongation module.[65]

1.5.3.2 *N*-methyltransferase domain

Many NRP have *N*-methylated peptide bonds, especially in a fungal origin such as cyclosporine, which has seven amino acids which are *N*-methylated.[63] The importance

of this modification is protection of the peptide against the proteolytic degradation, and support of the structural stability and the biological activity of the peptide.[59] This modification is introduced by an N-methylation domain (N-Mt-domain), containing ~420 amino acids,[48] which catalyzes the transfer of the *S*-methyl group of *S*-adenosylmethionine (SAM), which is the cofactor of the M-domain at the aminoacyl stage to peptide bond formation.[66]

1.5.3.3 Formylation domain

The formylation of the N-terminal of the α-amino group is catalyzed by the formylation domain (F-domain) in NRP. During catalyzation, the transfer of a formyl group from the N^{10}-fH_4F or N^5-FH_4F cofactor on the α-amino group of the amino acids takes place. It was reported in gramicidin biosynthesis that formylation of the initiation domain is important for the elongation of the NRPS chain, which catalyzes the α-*N*-formylation of PCP-bound L-Val.[67]

1.5.3.4 Cyclization domain

Heterocycles, such as thiazoline, oxazoline or methyloxazoline, are found in many NRPs. These structural features result from the heterocyclization of cysteine, serine or threonine side chains catalyzed by the cyclization domain (Cy-domain), which is responsible for the variants and structural modification of C-domains. Firstly, Cy- domains catalyze the usual peptide bond formation and then carry out cyclization of the nucleophilic side chain of cysteine or the hydroxyl side chain of serine or threonine onto the newly formed peptide bond. The newly formed heterocycles are often associated with oxidation domains (Ox-domains) which catalyze the FMN- dependent two-electron oxidation of the thiazoline or oxazoline ring structures to the thermodynamically more stable corresponding thiazoles or oxazoles.[73,77] Conversely, the reduction of thiazoline or oxazolines structures is mediated by *in trans* operating NAD(P)H-dependent reductases that recognize and directly reduce the PCP-bound substrate.

1.5.3.5 Hydroxylation

Many different classes of enzymes catalyze hydroxylation in microorganisms, such as heme $Fe^{(III)}$-oxygenase and FAD-dependent monooxygenase, which belong to microbial NMOs and catalyze the *N*-hydroxylation of long-chain primary amines.

The NMOs play an important role in the biosynthesis of the iron-coordinating hydroxymate group in many bacterial and fungal siderophores. The mechanism of using hydroxymate groups as iron-coordinating moieties usually requires the hydroxylation of the amino group of lysine or ornithine in the presence of molecular oxygene and NADPH, then the transfer of an acetyl or formyl group to the secondary amine intermediate. Most flavoprotein monooxygenase are able to use molecular oxygen (O_2) as an oxygen donor (the oxygen atom comes from water) to oxygenate an organic compound and this enzyme reduces the coenzyme NADPH or NADH as a source of reducing power for the flavine.[68,69,70]

1.5.3.6 Acetylation and formylation

Depending on the proposed biosynthesis of the erythrochelin siderophore bulding block L-haOrn isolated from *Saccharopolyspore erythraea*,[71] two pathways are suggested. The first displays the so-called "hydroxylation-first" pathway, in which hydroxylation of L-ornithine (L-Orn) by the FAD-dependent monooxygenase EtcB precedes acetylation by Mcd. On the other hand, the second is the "acetylation-first" pathway, where L-Orn is acetylated by the enzyme *N*-acetyl-transferase Mcd, and the second tailoring enzyme EtcB uses *δ-N*-acetyl-L-ornithine as substrate (Figure 1.5)[72]. In the pyoverdine biosynthesis pathway, the N^5-formyl-N^5-hydroxyornithine residues present in pyoverdine are formed from ornithine by the sequential action of *PvdA* (forming N^5-hydroxyornithine) and *PvdF* (forming N^5-formyl-N^5 hydroxyornithine),[73] and the *pvd Y*II is required for biosynthesis of pyoverdine and catalyzes acetylation of hydroxyornithine.[74] The *Rmo* and *Rft* genes in *R. Jostii* (RHA1) are required for the tailoring of the L-Orn precursor. Rmo monooxygenase was able to convert L-Orn into L-*δ-N*-hydroxyornithine (L-hOrn). As confirmed in a coupled reaction assay, this hydroxylated intermediate serves as a substrate for the subsequent N^{10}-formyl-tetrahydrofolate-dependent (N^{10}-fH_4F) Rft-catalyzed formylation reaction, establishing a route for the L-fhOrn biosynthesis prior to its incorporation by the NRPS assembly line.[75]

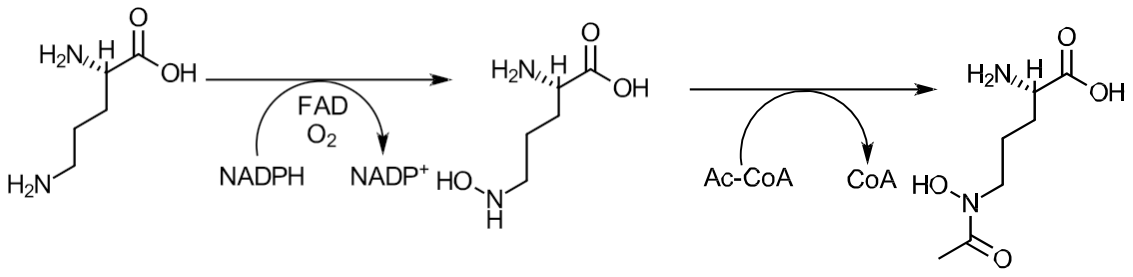

L-ornithine L-**δ**-*N*-hydroxyornithine L-**δ**-*N*-acetyl- **δ**-*N* -hydroxyornithine

Figure 1.5 Coupled enzymatic biosynthesis of the L-haOrn building block.[72] EtcB converts L-Orn into L-hOrn and the hydroxylated intermediate serves as a substrate for the subsequent Mcd-dependent acetylation reaction, giving rise to the iron-coordinating L-haOrn.

1.5.3.7 The type II thiosterase

A second type of TE-domain (TE II) was found in the NRPS gene cluster that ensures the deacylation of the misprimed PCP-domains, because about 80 % of CoA, the precursor of the Ppan cofactor required during the priming of the PCP-domain, is acylated in bacteria, which could lead to possible misacylation of the holo-ACPs and holo-PCP and block the substrate loading[76–78].TE-domain (TE II) can not hydrolyse the correct peptidyl-*S*-PCP bound substrate.[79]

1.5.3.8 Sulfontion (sulfation) modification

Sulfontion is an important molecular modification found in all kingdoms of life including microorganisms.[80] There are two classes of enzymes that catalyze this reaction in living organisms.[81] The first are the sulfotranferases, which catalyze the transferase for a sulfuryl moiety (SO_3^-) from 3 -phosphoadenosine-5 -phosphosulfate (PAPS) to the hydroxyl and primary amine groups of a variety of acceptors, such as phenolic compounds (catecholate). The second are the PAPS-independent aryl sulfotransferases (ASSTs), which catalyze sulfotransfer from phenolic sulfate ester to another phenol moiety.[82,83] On the other hand, there are other classes of sulfonation enzymes which are used by microorganisms to survive under nutrient limitation.[84] This class of enzymes is called sulfate starvation induced (SSI) proteins and they are synthesized only during S starvation.[85]There are three classes belonging to the (SSI)

proteins: class (I) transports and degrades organic S, such as a sulfate ester, alkylsulfates and myrosulfates, from the environment. Class (II) conserves S through the production of decreased S content proteins. Finally, class (III) remobilizes intracellular organic S. Aryl sulfatase enzymes (ARS) are one of the SSI proteins produced by microorganisms during S starvation. Aryl sulfatase hydrolyzes arylsulfate esters to the corresponding phenols and in organic sulfate.[84]

1.5.4 Classification of nonribosomal biosynthetic strategies

1.5.4.1 Linear NRPS (Type A)

The strategy used most in NRPSs assembles the peptide chain by a linear pathway (type A). Many linear NRPS are found, such as bacitracin,[86] surfactin,[87] tyrocidin,[88] cyclosporin,[63] pristinmycin,[89,90] fengycin[91,92] and ergotamine.[93] In linear NRPSs, the three essential domains are coordinated in the order (C-A-PCP) in the elongation module, while the initiation module, which starts the NRPS, lacks a C-domain. The TE-domain is found in the terminal module and, in most cases, releases the peptide product from the NRPS by hydrolysis or macrocyclization.[94] The biosynthesis of tripeptide (ACV), the backbone of all penicillins and cephalosporins, follows the type A route (Figure 1.6). Three amino acids are condensed together, and an E-domain in the last module accomplishes the conversion of the final amino acid from the L- to the D-isomer. Formation of the tripeptide on the final T-domain is by hydrolysis of the linear tripeptide from NRPS.[95–98]

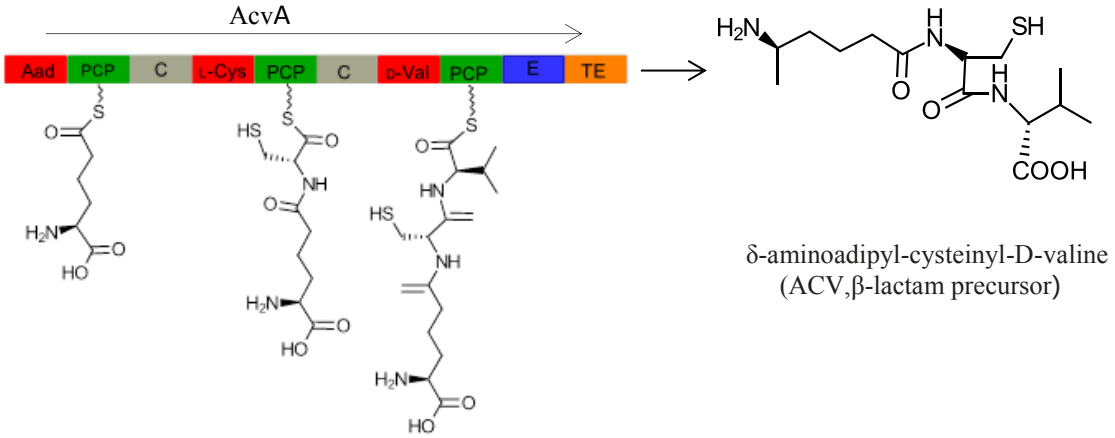

Figure 1.6 Schematic representation of the NRPS, ACV synthetase, that assembles the ACV tripeptide, the precursor for the formation of penicillin G and cephalosporin C.

1.5.4.2 Iterative NRPSs (Type B)

Type B iterative NRPSs use all of their modules more than once during the biosynthesis of a single NRP;[98] the enterobactin siderophore which is isolated from *E.coli* and is a cyclic trimer of dihydroxybenzoyl-serine units, is an example of this type B NRPS assembly (Figure 1.7). The NRPSs involved in the biosynthesis of this compound comprise a reduced number of modules that corresponds to only one set of the iterative sequences which is subsequently assembled to produce the final NRPS on the terminal PCP- or TE-domain. The monomer chains bound to its cognate PCP- domain are subsequently transferred onto the active site Ser residue of the terminal TE-domain, that way deacyling the last PCP so that the next monomer chain can be assembled in the TE-domain until the final NRPS is released from the enzymatic machinery by cyclization.[99]

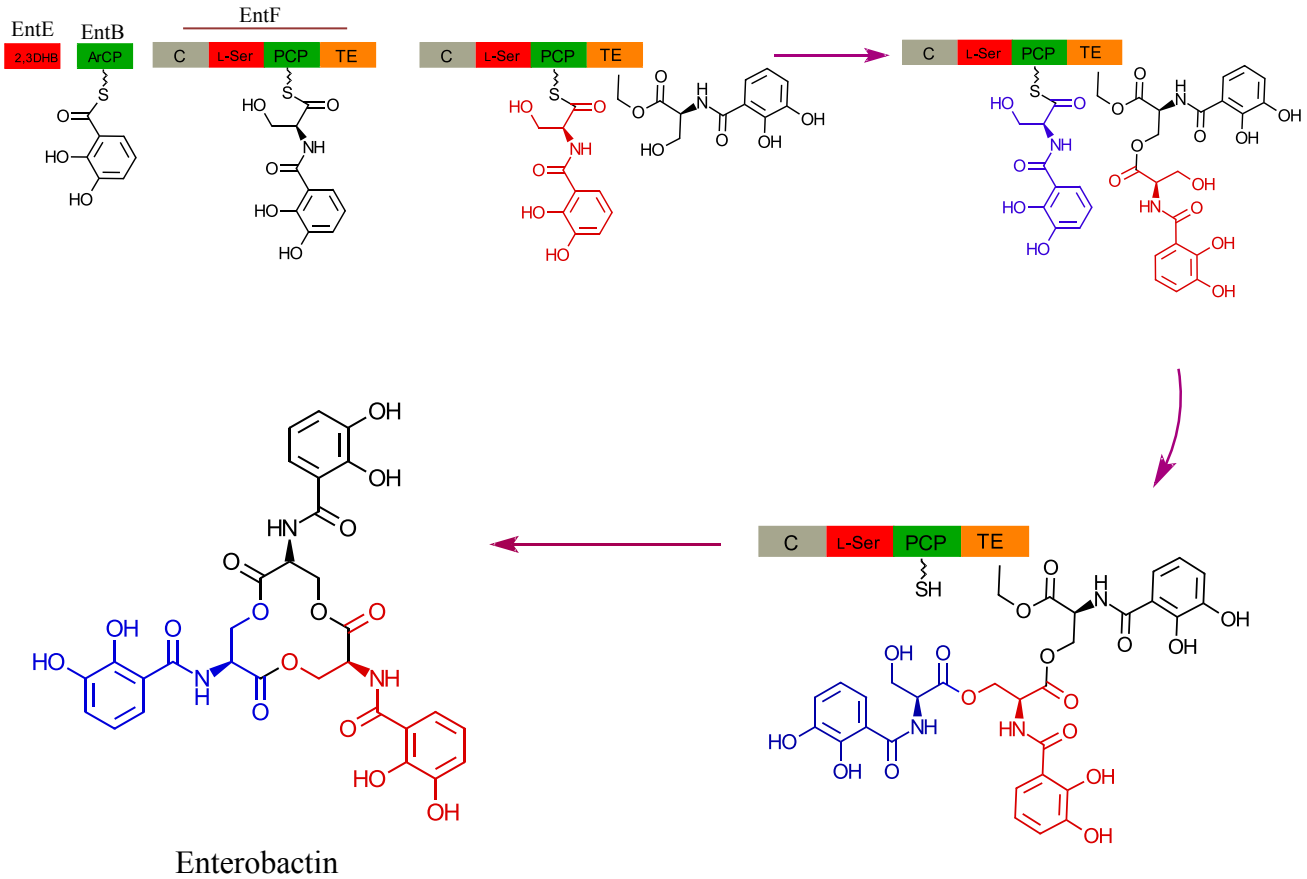

Figure 1.7 Enterobactin NRPS as an example of iterative NRPS type B. Three Dhb-Ser-S-Ppant intermediates are generated on the two modules of the enterobactin NRPS and are oligomerized and cyclized on the TE-domain.

1.5.4.3 Nonlinear NRPSs (Type C)

In contrast to type A and type B, nonlinear NRPSs contain at least one unusual arrangement of the core domains and it is very difficult to predict their possible products. There are many NRPSs that belong in this group, such as yersinibactin, vibrobactin, bleomycin, syringomycin and maycobactin. The reason for this different arrangement is the unusual internal cyclizations, such as bleomycin, or branch-point synthesis, such as vibrobactin and mycobactin. In myxochelin siderophore isolation from *stigmatella aurantiaca*, the C-domaine catalyzed formation of two amide bound during the biosynthesis pathway. In addition, the C-domain of the four-domain NRPS MxcG is responsible for acylation of both the α- and ε-side chain amino groups of the activated lysine residue with dihydroxybenzoyl groups, which are transferred from the PCP of MxcF (Figure 1.8).[99]

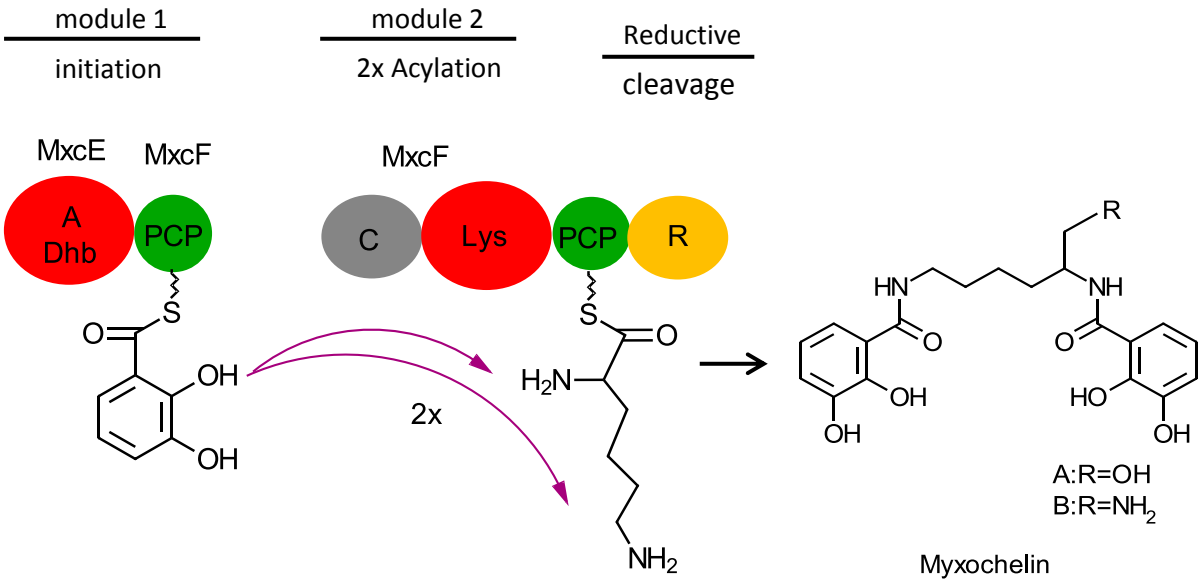

Figure 1.8 Myxochelin NRPS is a nonlinear NRPS type C. The proposed biosynthesis of the siderophore myxochelin involves two acylations of the lysine residue bound to MxcG with Dhb provided by MxcE and MxcF. The C domain of MxcG would carry out both reactions with the α-amino group and the ε-side-chain amino moiety of Lys-S-Pant-MxcG serving as nucleophiles.[99]

1.6 Iron uptake in bacteria

Under iron-limited conditions, bacteria use a variety of elaborate mechanisms to scavenge iron from various iron sources, which include the host proteins transferrin and lactoferrin, heme, and siderophores.[100] There is difference between iron uptake in Gram-negative and Gram-positive bacteria. Gram-negative bacteria possess a cell wall consisting of an outer membrane and peptidoglycan; this cell wall protects the bacteria from degradative enzymes.The space between these two layers is called periplasmic space. The outer membrane consists of a lipid bilayer with lipopolysaccharide and porins. This structure of the bacterial cell wall creates problems for the transport of nutrients into the cytoplasm of the cell. The small hydrophilic molecules, such as glucose, amino acids and phosphate, are small enough to pass directly through the porin proteins in the bacterial outer membrane. However, the iron-siderophore complex usually possesses molecular weight > 600 kd and this is too large to pass through the porin. To overcome this problem, the specific energy-dependent carrier proteins (outer membrane transporter) are important.[101] All outer membrane transporters (OMTs), such as FecA, FepA, FhuA (*E.coli*) and FpvA (*Pseudomonas* sp.), that are involved in the iron uptake have structures consisting of a 22-strand β-barrel that possesses a large proportion of hydrophobic aromatic amino acids on the external surface. The iron-siderophore complexes are transported to the periplasmic space through specific outer membrane receptors. In order the iron- siderophore complex holded by periplasmic binding proteins that tightly interact with the receptor-related TonB component, which provided the energy for this process. The TonB in *E.coli* possesses 239 amino acids with a molecular weight of 26 kDa, and is located in the outer membrane and cytoplasmic membrane. Gram-positive bacteria do not have an outer membrane and, thus, lack a periplasmic membrane. They also do not have the genes for the proteins of the TonB as expected[102]. The iron-siderophore binding proteins are anchored directly to the cytoplasmic membrane through the lipoprotein receptors that have high affinity for iron-siderophores and are covalently attached to a cysteine residue located in the lipobox of their signal peptides.[103] (Figures 1.9 and 1.10) show the schematic view of the uptake of iron-siderophores by Gram- negative and Gram-positive bacteria. In both Gram-negative and Gram positive bacteria, the iron-siderophore binding proteins transfer their complexes to cytoplasmic membrane ABC-transporters (ATP-binding-cassette transporters).

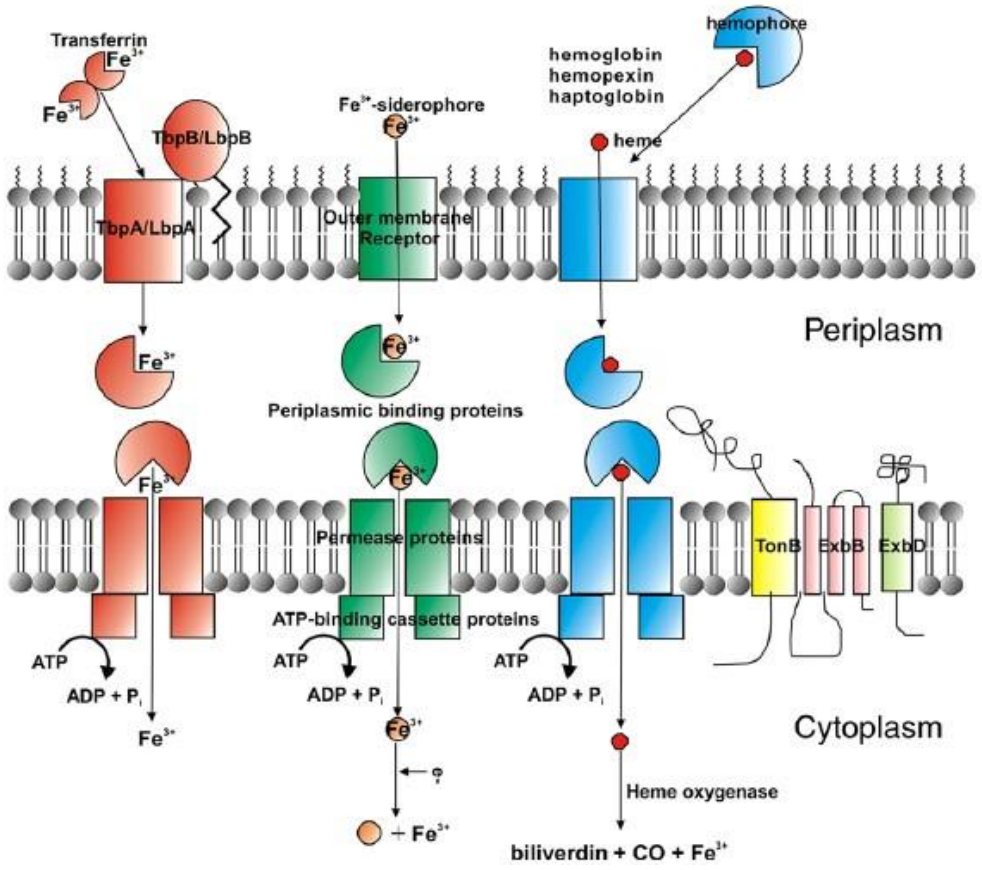

Figure 1.9 Schematic representation of iron uptake in Gram-negative bacteria. There are numerous iron uptake pathways in Gram-negative bacteria which include iron uptake from transferrin, siderophores, or heme. All of these uptake pathways require an outermembrane receptor, a PBP, and an inner-membrane ABC transporter. Not all bacteria have all three systems; but some have more than one type. Transport through the outer membrane receptor requires the action of the TonB system (TonB, ExbB, ExbD).[100]

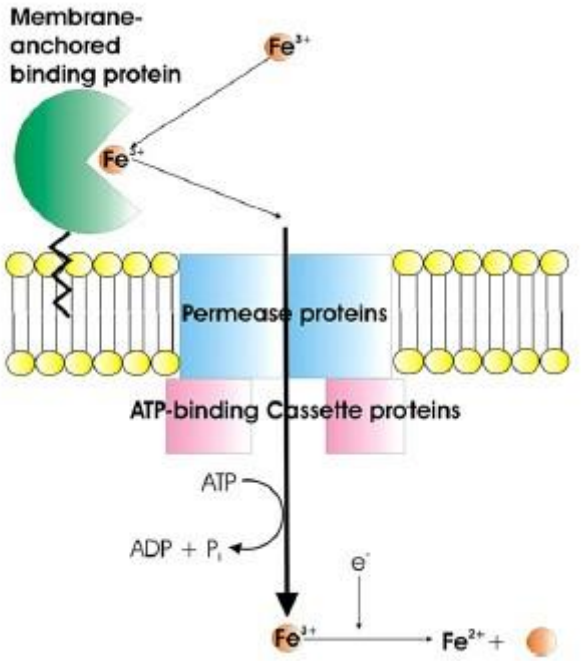

Figure 1.10 Schematic representation of iron uptake in Gram-positive bacteria, which unlike Gram-negative bacteria, lack an outer membrane. Therefore, the uptake of iron from heme, siderophore, or transferrin, involves a membrane anchored binding protein and a membrane-associated ABC transporter.[100]

1.6.1 Siderophore binding protein

Siderophore binding proteins play a key role in the uptake of iron in many Gram-positive and Gram-negative bacteria. Many periplasmic binding proteins have been studied in great detail, such as FhuD, FeuA, FepB and FecB.

1.6.1.1 FhuD hydroxamate binding protein

FhuD is a periplasmic binding protein that transports hydroxamate siderophores to the cytoplasm via the inner membrane-associated proteins FhuB and FhuC.[104–106] Generally, the similar structural units (δ-*N*-hydroxy-ornithine, trans-anhydromevalonic acid, and acetic acid) share the fungal hydroxamate siderophores.[107] In Gram-positive bacteria, FhuD is tethered to the cytoplasmic membrane by a lipid-modified N- terminal cysteine to compensate for the lack of a periplasm. Many of Gram-positive FhuD proteins have been characterized, such as FhuD from *Staphlococcus aureus*,[108–110] *Listeria monocytogenes*[111] and *Bacillus subtilus*.[112] FhuD from *E.coli* k_{12} is about

30 kDa. The crystal structure of FhuD in a complex with the ferrichrome homolog galichrome has been determined at 1.9 Å resolution, the first structure of a periplasmic binding protein involved in the uptake of siderophores. Gallichrome is held in a shallow pocket lined with aromatic groups; Arg and Tyr side chains interact directly with the hydroxamate moieties of the siderophore. FhuD possesses a novel fold, suggesting that its mechanisms of ligand binding and release are different from other structurally characterized periplasmic ligand binding proteins (Figure1.11).[106]

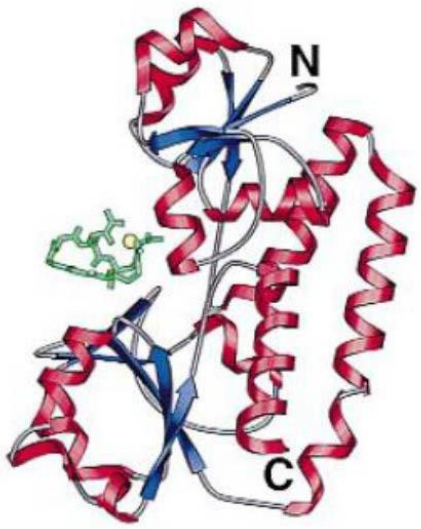

Figure 1.11 Stereo ribbon diagram showing the overall tertiary structure and secondary structure elements in the complex. The N-terminal domain is at the top of the figure. The gallichrome is green, with the gallium ion in yellow. Helices are colored red, b-strands blue and random coil regions gray. The binding cleft is a shallow pocket between the N-terminal and C-terminal domains.[106]

1.6.1.2 FeuA catecholate binding protein

The crystal structure of iron-siderophore binding protein FeuA from *B.subtilis* (297 amino acids without a lipoprotein signal peptide) has been determined at 1.7 Å in a complex with $[Fe^{III}(BB)]^{3-}$. FeuA is composed of two domains which show a Rossmann-like fold and are connected by a helix 22 amino acids long (Figure 1.12).[13]These structural elements are indicative of siderophore binding proteins of the"helical-backbone" metal-receptor superfamily, such as FhuD and CeuE.[13,106,113,114]

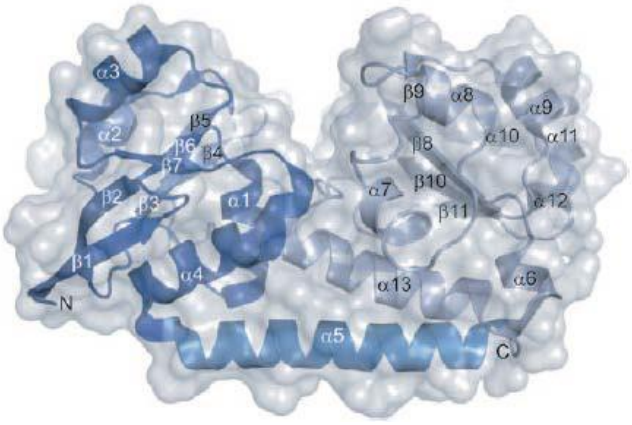

Figure 1.12 Overall structure of FeuA. The two asymmetric lobes and the connecting helix are shown in different color shades (N-terminal domain: dark blue, connecting helix: medium blue, C-terminal domain: light blue). The protein surface is shown in gray.[13]

1.6.1.3 FepB catecholate binding protein

The preplasmic binding protein FepB plays a key role in transporting the catecholate siderophore ferric enterobactin or enterochelin from the outer membrane in Gram-negative bacteria, such as enteric bacteria, including *E.coli*.[115,116] Enterobactin is able to scavenge Fe^{3+} to form $[Fe^{III}(Ent)]^{3-}$, which can be taken up via the ferric enterobactin (Fep) transport system.[117] This mechanisn contains proteins FepA, FepB, and FepCD, which are a TonB-dependent outer membrane transporter, a periplasmic binding protein (PBP) and the inner membrane ABC-dependent transporter, respectively.[100] The pro-FepB with 318 amino acids contains a signal peptide sequence, has a calculated molecular mass of 34.3 kDa and associates with the cytoplasmic membrane. The mature FepB protein with 292 amino acids has been calculated to have a molecular mass of 31.6 kDa and exists in the periplasm (Figure 1.13).[118]

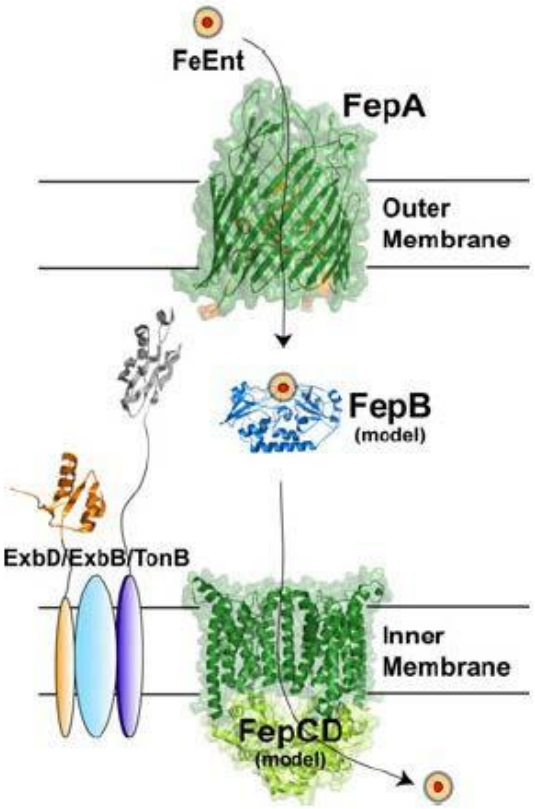

Figure 1.13 A representation of the Enterobactin siderophore uptake pathway in *E. coli* using ferric-enterobactin (FeEnt) transport (Fep)transport system.[101]

1.7 Aim of the work

Species belonging to the *Rhodococcus* genus are extensively studied as biocatalysts for steroid production and as tools for bioremediation purposes.[119,120] Whole genome sequencing information revealed the *Rhodococcus* genus possesses a vast potential for secondary metabolite production; however, very few natural products have been isolated so far. In particular, within the *Rhodococcus* genus, substantial chemical diversity has been observed among different siderophores through the structure elucidation of rhodochelin,[121] rhodobactin[122] (Figure 1.14), and heterobactin A1[123] and the suggestion of the structures of rhequichelin[124] and rhequibactin.[125] They belong to the hydroxamate-catecholate mixed type family, with the common presence of 2,3- dihydroxybenzoic acid (2,3-DHB) and differently modified ornithine residues within their structures. Therefore, the focus of this work was towards the isolation of new structures that may further highlight the diversity of siderophores from this genus.

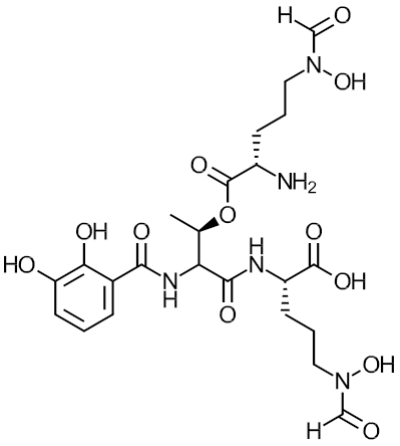

Rhodochelin

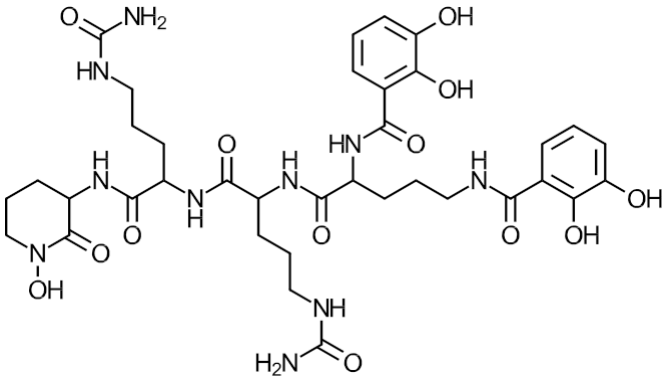

Rhodobactin

Figure 1.14 Chemical structures of representative siderophores isolated from *Rhodococcus*strains: rhodochelin and rhodobactin were isolated from *R. jostti RHA* and *R.rhodochrous* OFS, respectively.

In this study, the isolation and the structural characterization of the endogenous siderophores of *Rhodococcus erythropolis* PR4 confirm the metabolic capacity of the

strain to produce secondary metabolites. The genome mining identification of the NRPS-containing gene cluster responsible for the biosynthesis of the molecule permits the rational construction of isogenic deletion mutant strains. Subsequently, the metabolic profile comparison between the wild-type and the mutant strains undoubtedly connects the biosynthesis of the natural product with the corresponding genes. Finally, the biochemical characterization of the recombinantly produced enzymes associated with the biosynthesis of the siderophore, integrates the genetic results and allows the postulation of a model for the biosynthesis of the newly discovered iron scavenging compound.

Chapter 2

Material

2.1 Equipment

Table 2.1 List of the devices used in this study.

Device	Manufacture and type
Autoclave	Tuttnauer 5075 ELV, Fedgari Autoclavi SPA FV A3/A1
CD-Spectrometer	J-810 (*Jasco*)
Centrifuages	Sorvall RC 5B Plus and RC6+ (SS-34, SLC-300, SLC-4000 rotor Heraeus Minifugue RF and Megafugue 1.0R, Eppendorf 5415 D, 5415 R and 5702 R
Clean bench	Antair BSK
Documentation system for DNA-electrophoresis gels	Cybertech CS1 camera, Mitsubishi video copy thermo printer
Electrophoresis chamber	Agarose gel chambers manufactured in-house (PUMa, Marburg), Bio-Rad Mini-PROTEAN 3 gel chamber
Electroporation	Bio-Rad Gene-Pulser II
Fast protein liquid chromatography (FPLC)	Amersham Pharmacia Biotech Äktaprime and Äktapurifier: (pH/C-900, UV-900, P-900 and Frac-900 modules
French-press	SLM Aminco French-Pressure Cell Press 5.1, Thermo Spectronic Standard Cell 40 KP
HPLC-systems	Agilent series 1100 (HPLC-system with DAD- and ESI-Quad-MS-detection, vacuum degasser, quarternary pump, auto sampler, Preparative fraction collector, column thermostat, HP-ChemStation Software) Thermo Scientific LTQ-FT Applied Biosystems API QStar Pulsar i
Incubators	New Brunswick Scientific Series 25, Innova 4300 Shaker, Infors HT Multitron II and Unitron
Lyophilizer	Christ Alpha 2-4 LSC
NMR-spectrometer	Bruker AV600
pH meter	Schott CG 840/ Seven easy mettler Tolledo
Pipettes	Eppendorf Research series
Rotary Evaporator	Heidolph Laborota 4000
Scintillation counter	Packard Tri-Carb 2100-TR
Spectrofluorometer	FP-6500 (*Jasco*)
Spectrophotometer	PEQLab Nanodrop ND-1000; Pharmacia Ultrospec 3000
Speed-Vac	Uniequip Univapo 150H
Thermal cycler	Eppendorf Mastercycler Personal
Thermomixer	Eppendorf Thermomixer comfort
Vortexer	Scientific Industries VortexGenie2
Water deionizer	Seral Seralpur Pro90CN

2.2 Chemicals and enzymes

All chemicals not listed in table 2.2 were purchased from Sigma-Aldrich (Steinheim, Germany), Fulka (Steinheim, Germany) or Merck (Darmstadt, Germany) in p.a.quality and were used without further purification.

Table 2.2 Chemicals, enzymes and general materials.

Manufacture	Product
Applichem (Darmstadt, Germany)	ampicillin, kanamycin, media components
Biomol (Ilvesheim, Germany)	DTT
Brand (Wertheim, Germany)	Plastbrand PS cuvettes
Eppendorf (Hamburg, Germany)	1.5 and 2.0 mL reaction tubes
Eurogentech (Seraing, Belgium)	agarose, electroporation cuvettes
GE Healthcare (Freiburg, Germany)	IPTG, FPLC Ni-NTA and Superdex 200 5/150 GL SEC columns, yeast extract, aldolase, ovalbumin, ribonuclease, aprotinin protein standards
Invitrogen (Karlsruhe, Germany)	*E. coli* strains (BL21, TOP10)
Macherey & Nagel (Düren (Germany	C8- and C18-HPLC columns (Nucleosil, Nucleodur)
Merck4Biosciences – Novagen (Nottingham, UK)	pET28a(+),pET41a(+)
Millipore (Schwalbach, Germany)	Dialysis membranes (pore size: 0.025 μM), Amicon Ultra-15 concentrators
MP Biomedicals (Illkirch, France)	coenzyme A trilithium salt
New England Biolabs (Frankfurt Germany)	desoxyribonucleotides (dATP, dTTP, dGTP, dCTP), DNA ladders, protein size markers, restriction endonucleases, Phusion Hi-Fidelity DNA polymerase, T4 DNA ligase
Oxoid (Cambridge, UK)	agar nr. 1, tryptone
Perkin Elmer (Waltham, USA)	$Na_4{}^{32}P_2O_7$
Phenomenex (Torrance, USA)	Synergi Fusion RP-80 HPLC column
QIAgen (Hilden, Germany)	QIAquick Gel Extraction kit, Ni-NTA IMAC resin
Roth (Karlsruhe, Germany)	acrylamide solution, β-mercaptoethanol, ethidium bromide, scintillation fluid
Sarstedt (Nümbrecht, Germany)	Pipette tips, Falcon tubes (15 and 50 mL)
Schleicher & Schüll (Dassel, (Germany	Sterile filters (0.20 and 0.45 μm), Whatmann-3MM paper
Serva (Heidelberg, Germany)	bromophenol blue, Triton X-10
Thermo Scientific (Waltham, USA)	Hypercarb HPLC column

2.3 Primers

All primers listed below in table 2.3 were purchased from Sigma-Aldrich (Steinheim, Germany) in HPLC grade and were used for PCR amplification of the targeted genes.

Table 2.3 List of primers used in this work. Restriction sites inserted for cloning are underlined.

Primer name	sequence(5'-3')	Restriction site	plasmid	Target gene
htbE F	CGGAATTCCATATGACATCGAGGATCGCTCGC	NdeI	pET28a(+)	htbE
htbE R	CCCAAGCTTTCAACTCGACAGAGTCTGTGCG	Hind(III)	pET28a(+)	htbE
htbD F	CGCGATTCCATATGAGCAACACCGTGGACCGT	NdeI	pET28a(+)	htbD
htbD R	CCCAAGCTTCTGCGGGCACAGGACCTGAAC	Hind(III)	pET28a(+)	htbD
htbGCAT1F	CGCGATTCCATATGTCCACAGACGAGGGGATC	NdeI	pET41a(+)	htbGCAT1
htbGCAT1R	CCCAAGCTTCGGCTCGGAGGTGTCGGA	Hind(III)	pET41a(+)	htbGCAT1
mbtH F	CGGGGTACCTCAGCTCTCGACTGCGTGCTTTC	KpnI	pACYC	mbtH
mbtH R	ATAAGAATGCGGCCGCTCAGCTCTCGACTGCG TGCTTTC	NotI	pACYC	mbtH
htbGP1	CCGGAATTCCAGCAGTGCGATACGAGATGCCC ACC			
htbGP2	GTGGTTTTCAAACTATGTGGCCGTGCGTTTCGA GTCTGTGGACACACGTCACCCAAGGGT			
htbGP3	ACCCTTGGGTGACGTGTGTCCACAGACTCGAA AC GCACGGCCACATAGTTTGAAAACCAC			
htbGP4	GCTCTAGAGCTGCCGCGACGTAGATGACCCAC			
EXT1F	CGGATCGAGTGGAGTTCGTGACCGAG			
INT1R	CGCTCGTCACGGACGTCGGTGATC			
INT2F	CGACCGACACAACCTACGACGGACCG			
EXT2R	CAACGTCGGCATCAAAGCCATCAAGGCCG			
CTA2F	CGCGATTCCATATGTCCGATTGCTCGGCGACGA			
CTA2R	CCCAAGCTTCTGCATGTGATAGACATCCGTACC			
KANR	CGATAGAAGGCGATGCGCT			
htbH F	GGCCTTCCATATGAGTAGCGATTCGAACGACG	Nde I	pET28a(+)	htbH
htbH R	CCCAAGCTTTCATGCGAAGGTCTGGCCG	Hind III	pET28a(+)	htbH
HMO F	GGAATTCCATATGAGTGAATCACCGAGAGACT	Nde I	pET28a(+)	HMO
HMO R	CCCAAGCTTTCATCTCGCCTCACTCGTT	Hind III	pET28a(+)	HMO

2.4 Plasmids

2.4.1 pET28a (+) and pET41a(+)

The pET28a (+) and pET41a(+) expression vectors system were employed for the production of recombinant proteins in *E. coli* (Figure 2.1). The pET28a (+)vector adds a hexahistidine (6xHis) fusion tag at the N- or C-termini of the recombinant protein, to allow subsequent Ni-NTA affinity chromatography purification. Similarly the pET41a(+) in addition it has GTS Tag and S-Tag. Transcription of the cloned genes is dependent on both T7 RNA polymerase activity and dissociation of the LacI repressor from its corresponding operator, upon IPTG induction. Plasmid selection and maintenance is permitted by the kan^R gene, which confers resistance to kanamycin.

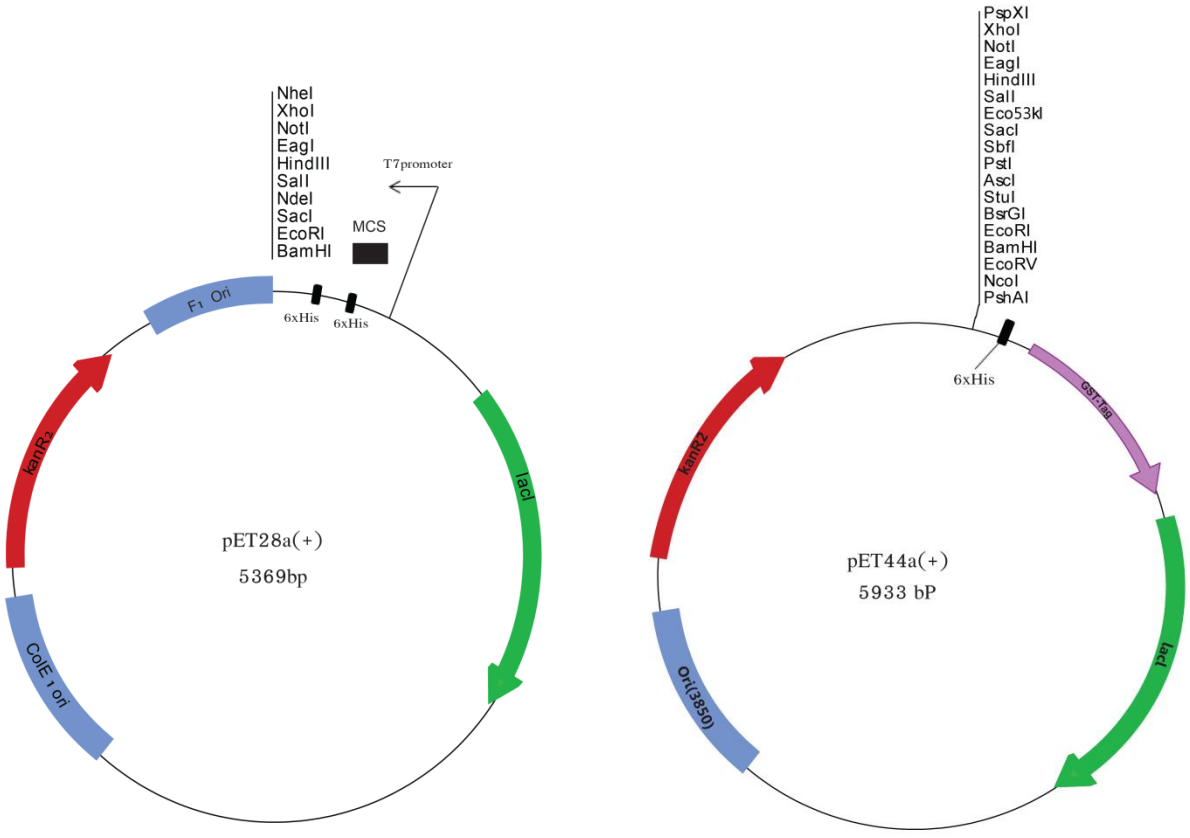

Figure 2.1 Physical map of pET28a(+) and pET41a(+).

2.4.2 pK18mobsacB

The pK18mobsacB plasmid is a mobilizing cloning vector for the conjugative transfer of DNA into a recipient host.[126] Deriving from the *E. coli* pK18 plasmid,[127] it features the *lacZα* fragment inserted within the MCS and the kan_R gene for selection and maintenance (Figure 2.2). The mobilizing machinery of the RP4 plasmid[128] confers broad host-specificity between different Gram-negative and Gram-positive species.[129,130] The *sac*B gene encodes for the *B. subtilis* levansucrase, which renders the recipient strain sensitive to sucrose, and thus is applicable as a negativeselection marker.[131,132] The plasmid was kindly provided by Dr. Robert van der Geize, University of Groningen, The Netherlands.

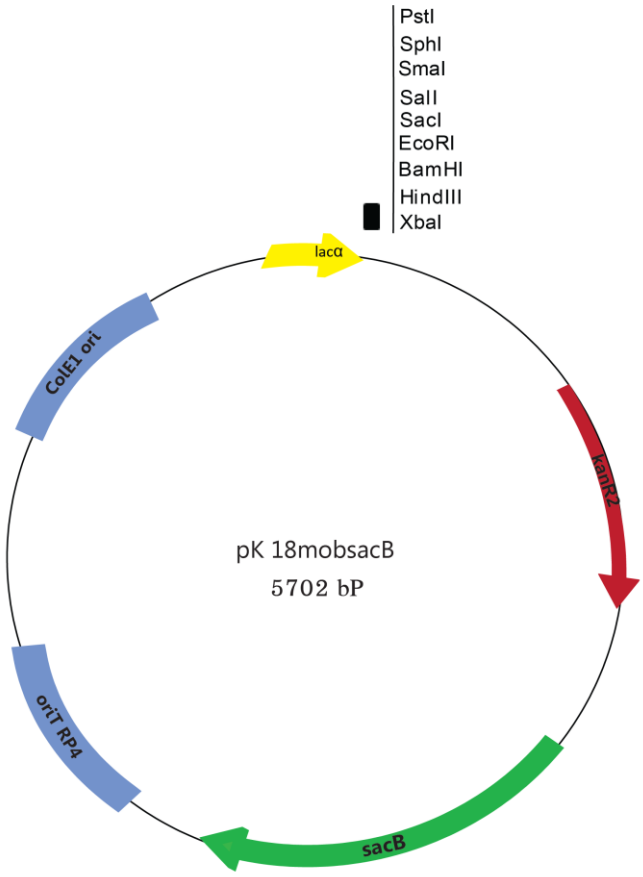

Figure 2.2 Physical map of pk18mobsacB.

2.5 Bacterial strains

2.5.1 *Rhodococcus erythropolis* PR4

Rhodococcus erythropolis PR4 has been isolated from the deep sea at a depth of 1,000 m in south of Okinawa Island, Japan (the Pacific Ocean). This strain can utilize *n*-alkanes of C_8 to C_{20}, alkylbenzenes, and pristine (2,6,10,14,tetramethylpentadecane) as sources of carbon and energy. It can also produce a large quantity of extracellular polysaccharides **(EPSs)**, which are assumed to play a crucial role in its tolerance to a variety of organic solvents.The complete genome consisted of one circular chromosome (6,516,310 bp) GC content 62.31%), one linear plasmid (pREL1: 271,577 bp), and two circular plasmids (pREC1: 104,014 bp, and pREC2: 3,637 bp) all with some sequence similarities to other *Rhodococcus* plasmids . A total of 6,437 ORFs were predicted on the chromosome and three plasmids. The chromosome and linear plasmid encode many genes involved in the degradation of alkanes. In addition, genes responsible for the degradation of intermediates in the catabolism of aromatic compounds, such as protocatechuic acid and catechol, are clustered on the chromosome. The genome also contains a number of genes for secondary metabolism such as NRPS and EPS biosynthesis.[1,2]

2.5.2 *Rhodococcus erythropolis* IGTS8

Rhodococcus erythropolis IGTS8 is the most extensively studied microorganism on researching of biological desulfurization systems. This Gram-positive bacterium is able to extract sulfur from DBT(dibenzothiphene), it has larg plasmid (150 kb).[120,133]

2.5.3 *Escherichia coli* TOP10

E. coli TOP10 strain are provided at a transformation efficiency of 1 x 10^9 cfu/µg supercoiled DNA and are ideal for high-efficiency cloning and plasmid propagation. They allow stable replication of high-copy number plasmids. The genotype is: F^- *mcr*A Δ(*mrr-hsd*RMS-*mcr*BC) φ80*lac*ZΔM15 ΔlacX74 *rec*A1 *ara*D139 Δ(*ara-leu*)7697 *gal*U *gal*K *rps*L (StrR) *end*A1*nup*G.

2.5.4 *Escherichia coli* BL21 (DE3)

Escherichia coli BL21 (DE3) is one of the most widely used host for expression of plasmid DNA of recombinant proteins using T7-promoter. This strain has the genotype: F– *ompT* *hsd*S_B(r_B^-, m_B^-) *gal dcm* λ(DE3) and is deficient both I Ion protease and ompT outermembraane protease, which reduces the proteolytic degradation and thus increase the expression level of the target protein. Furthermore this strain contains IPTG inducible T7 RNA polymerase gene, which is essential for the IPTG induction of genes under T7- promoter control.[134]

2.5.5 *Escherichia coli* S17-1

The *E. coli* S17-1 strain (genotype recA pro hsdR RP4-2-Tc::Mu-Km::Tn7) was used as mobilizing strain for the transfer of the pK18mobsacB plasmid into the recipient *R.erythropolis* PR4, through bacterial conjugation. The mobilizing elements of the RP4 plasmid are stably integrated within the chromosome, in order to avoid self transfer of the original conjugating vector.[135] The strain was kindly provided by Dr. Robert van der Geize, University of Groningen, The Netherlands.

2.6 Culture media

The media listed below were used for the cultivation and fermentation of the bacterial strains. If solid agar plates were required for the cultivation of the microorganism , agar nr. 1 was added to a final concentration of 1.5 % (m/w). All media were sterilized by autoclavation, (121 °C, 1.5bar, 30min). After cooling down to 55°C, antibiotics and other additional labile components were added after sterile-filtration, prior to use.

2.6.1 Lysogeny broth (LB-Miller)

LB broth (buffered at pH 7) has been routinely used for the cultivation and the maintenance of *R.erythropolis* PR4 and *E.coli* strains.

Yeast-extract	5g/L
Tryptone	10g/L
NaCl	5g/L

2.6.2 M9 minimal medium

M9 minimal medium was used for the isolation and the fermentative production of Heterobactin.

$Na_2HPO_4 \cdot 2\ H_2O$	8.5g/L
KH_2PO_4	10 g/L
NH_4Cl	1 g/L
NaCl	0.5g/L

Prior to use, a concentrated trace element mix (100xMg/Ca/B1/Goodies) was prepared as follows and added to a final 1x concentration. Sterile glucose solution was used as a carbon source (final concentration: 4 g/L). Where required, Fe^{3+} was added from a sterile-filtered $FeCl_3$ solution.

100x Mg/Ca/B1/Goodies (100 mL)

MgSO4 1M	20 mL
CaCl2 1M	1mL
thiamine 10 mM	1mL
Conc. goodies	25 mM
ddH2O	top up to volume

Concentrated goodies (100mL)

Stock salts sol.	50 mL
$MgSO_4 \cdot 7\ H_2O$	3 g
ddH_2O	top up to volume

Stock salts solution (1L)

$MgCl_2 \cdot 6\ H_2O$	22.94 g
$CaCO_3$	2.0 g
$ZnSO_4 \cdot 7\ H_2O$	1.44 g
$MnSO_4 \cdot H_2O$	0.85 g
$CuSO_4 \cdot 5\ H_2O$	0.25 g
$CoCl_2 \cdot 6\ H_2O$	0.24 g
H_3BO_3	0.06 g
HCl (conc.)	51.3 mL
ddH_2O	top up to volume

Chapter 3

Methods

3.1 Molecular biology techniques

The general molecular biology methods are used in this work such as DNA agarose-gel electrophoresis, PCR , protein SDS-PAGE and their solutions and buffers.

3.1.1 General strains maintenance

All *E. coli* strains were maintained on LB-agar plates and incubated at 37 °C. *Rhodococcus erythropolis* PR4 and derivative strains were maintained on LB-agar plates at 30 °C. Liquid cultures were incubated under continuous shaking at 180 rpm. Antibiotics were added where required. For long-period storage, sterile glycerol was added to a liquid culture [final concentration: 20% (v/v)] and the resulting stocks were stored at -80 °C.

3.1.2 Genomic DNA preparation

Inoculate a 5 mL liquid culture, grow in conditions appropriate for that strain until the culture is saturated (generally overnight culture), the cells were harvested by centrifugation at 13,000 rpm for 5 min. The cell pellet was washed with 1 mL of water and resuspended in 500 µL lysis buffer [100 mM TRIS, 50 mM EDTA, 1% (w/v) SDS, pH 8]. Glass beads were added to a final volume of 1.25 mL. The mixture was vortexed for 2 minutes and the liquid was transferred into a new microfuge tube. 275 µL of 7 M ammonium acetate pH 7 was added and the solution was incubated for 5 min at 65 °C, and subsequently 5 min on ice. 500 µL of chloroform were added and the mixture was vortexed for 2 min. Following a centrifugation step at 13,000 rpm for 5 min, the recovered aqueous phase was added to 800 µL of ice-cold isopropanol. The genomic DNA was precipitated by centrifugation (5 min, 13,000 rpm), prior to 5 min incubation on ice. Subsequently, the pellet was washed with 500 µL of ice-cold 70% ethanol solution, dried and resuspended in 50 µL of EB buffer (10 mM TRIS, pH 8.5).

3.1.3 Plasmid preparation

Plasmid preparation was done by the (Plasmid Miniprep Kit-Sigma-Aldrich), 1-5 mL liquid cell (overnight culture) was centrifuged at 13,000 for 1 minute. After resuspension of the cell pellet in 200 µL resuspension buffer, 200 µL lysis buffer was added. The mixture was gently inverted 6 to 8 times (do not vortex), and incubated for 5 min (allow to clear) at room temperature (RT). The cell after lysis was precipitated

by adding 350 µL neutralization buffer. The mixture was gently inverted 6 to 8 times. After centrifugation at 13,000 rpm for 10 min, the cleared lysate was transferred into a new binding column and mixed with 750 µL wash buffer (10 mM Tris HCl (pH 7.5), 100 mM NaCl, 2.5 mM EDTA). After centrifugation at 13,000 rpm for 1 minute the flow-through was discarded then spin for 1 minute to dry the column. The plasmid DNA was eluted in 50 µ L H_2O and stored at-20°C.

3.1.4 Gene amplification via PCR technique

Target gene were amplified from genomic DNA of the *R.erythropolis* PR4 using the primers listed in table 2.3, PCR mixtures consisted of Phusion High-Fidelity DNA Polymerase (NEB), GC-rich DNA template, 5% DMSO with (d-NTP) deoxynucleoside triphosphate. PCR fragments were purified with QIAgen gel extraction purification kit instructions. Digested with corresponding restriction enzymes (NEB), the amplified gene was ligated into pET28a (+) (Novagen) with T4 ligase (NEB). *E.coli* TOP10 competent cells were used for transform the construct. The correct sequence was confirmed by DNA sequencing (GATC Biotech), and the construct was transformed into *E.coli* BL21 (DE3) for protein expression.

3.1.5 Construction of the *Rhodococcus* Deletion Mutant Δ*htbG*.

The *Rhodococcus* "markerless" gene deletion mutant was generated as previously described.[121,136] *R. erythropolis* PR4 cells were grown on LB plates supplemented with nalidixic acid for five days, harvested, and resuspended in 2 mL of fresh LB broth. The same procedure was repeated with an overnight plate of *E. coli* S17-1 strain carrying the derivative mutagenic construct pk18mobsacB::PR4ΔhtbG,[126, 135]additionally grown at room temperature (RT) for a further 24 h. Each cell suspension (750 µL) was mixed, incubated briefly at RT, pelleted, and resuspended in 2 mL of LB broth. Of this suspension, 200 µL was spread on LB and incubated overnight at 30 °C. The following day, cells were harvested and resuspended in 2 mL of LB broth. Aliquots (150 µL each) were successively spread on LB plates supplemented with nalidixic acid and kanamycin and incubated at 30 °C for three days, until only *Rhodococcus* colonies appeared. Transconjugants were grown in liquid medium, and vector integration was checked by PCR of the kanamycin cassette

and by replica plating on LB supplemented with kanamycin, or kanamycin and 10% sucrose. To force plasmid excision, single integrant colonies were inoculated in LB broth and subsequently plated on LB supplemented with 10% sucrose and grown at 30 °C until new colonies appeared. To confirm correct plasmid excision, single clones were tested for kanamycin sensitivity by replica plating and by PCR using different primer pairs: for the kanamycin cassette (KANF and KANR), for the deleted gene (CTA2F and CTA2R) and for a flanking region spanning the deletion (upstream EXT1F and INT1F, downstream INT2F and EXT2R, Figure S10).

3.2 Recombinant proteins expression and purification

3.2.1 Protein expression

25-30 mL of an overnight culture of *E. coli* BL21 (DE3) and BL21Δ *ybdz* cells (for *htbE* and *htbG*-CAT1) carrying the desired expression construct was diluted inside a 2 L baffled flask containing 500 mL of fresh LB medium supplemented with 50 µg/mL kanamycin. The cells were incubated at 25°C and 230 rpm shaking, until the OD_{600} ~ 0.6 was reached. Protein expression was induced with IPTG (50 µM), followed by incubation at 25°C and 230 rpm for 4 h. The cells were harvested by centrifugation at 4°C and 6,000 rpm for 20 min, resuspended in appropriate buffer and stored at -20°C.

3.2.2 Protein purification

For purification of His_6-tagged recombinant protein, the cells were disrupted by French press after the cell pellet was thawed on ice and lysed with tip of lysozyme, 5 µL benzonase nuclease to decrease the viscosity of the solution and 30 µL $MgSO_4$ for the benzonase nuclease to act. After the centrifugation step (17,000 rpm,4°C,30 min), the cleared lysate was sterile-filtered and applied to a Ni-NTA affinity chromatography using FPLC ÄktaPrime system with a flow rate of 0.8 mL/min. The elution was carried out using a linear gradient from 3 to 50% HEPES B buffer (50 mM HEPES, 250 mM imidazole, 300 mM NaCl, pH 8) over 30 min, followed by a linear increase to 100% B in 10 min with a flow rate of 1 mL/min, harvesting 2 mL fractions. Elution was monitored at 280 nm and protein-containing fractions were checked by qualitative Bradford assay[137] and further analyzed by SDS-PAGE. Pooled fractions were dialyzed against 25 mM HEPES, 100 mM NaCl, pH 7.5 buffer, and concentrated with Amicon Ultra-15 concentrators (30,000 and 50,000 size).

3.2.3 Protein determination

The concentration of the recombinant proteins were determined by Bradford colorimetric assay using a BSA calibration curve.

3.3 Analytical methods

3.3.1 HPLC-MS

High performance liquid chromatography (HPLC) was used as a standard methodology for the characterization of compounds based on the retention time on a chromatography column. Reversed-phase (RP) chromatography relies on the hydrophobic interaction between compounds and the non-polar stationary phase of the column (porous graphitic carbon or C8 or C18 coated silica gel). The elution of the compounds is mediated employing a gradient with methanol or acetonitrile, which shifts the interaction of the analyte for the column towards the mobile phase. The retention time of the compounds is monitored by UV-vis detection. The mobile phases were routinely supplied with either 0.1% TFA, or 0.05% formic acid, or 20 mM NFPA as ion pairing reagents to improve chromatographic separation and electrospray mass ionization (ESI-MS) of the liquid compounds at atmospheric pressure. Routine mass-spectrometry (MS) analysis were carried out on an Agilent 1100 MSD system.

3.3.2 High resolution –MS

HR-MS measurements were performed on either an Orbitrap Velos Pro or an LTQ-FT instrument (Thermo Fisher Scientific). RP-HPLC-MS experiments were carried out on an Agilent 1100 HPLC system equipped with a Machery-Nagel Nucleoshell RP18 column, 125 × 2 mm, 2.7 μm particle size, and coupled to an Agilent 6100 ESI-MS detector (drying gas flow 12 L/min, drying gas temperature 350 °C, nebulizer pressure 35 psig, capillary voltage 3000 V, positive mode).

3.3.3 HPLC-CID-LTQ-MS

Heterobactin MS fragmentation experiments were carried out on an Orbitrap Velos Pro (Thermo Fisher Scientific) by collision-induced dissociation (CID).

3.3.4 Protein identification via mass spectrometry

Identification of the peptide molecular weight was verified via mass spectrometry data with the MASCOT database[138]. The corresponding gel bands of the protein were stained with coomassie Berilliant Blue excised from SDS-PAGE gel and incubated with 200 µL of wash solution [200 mM NH4HCO3, 50% (v/v) acetonitrile] for 30 min at 37 °C. The solvent was subsequently removed in a speed-vac manifold to complete dryness (37 °C, 30 min). *In-band* tryptic digestion was carried out by addition of 20 µL of a trypsin solution (0.02 µg/µL trypsin, 10% $NH4HCO_3$, 10% acetonitrile, pH 8.1) at 37 °C for 45 min. The excess of trypsin was removed, followed by an additional incubation period of 16 h. Peptide fragments were eluted with 25 µL of a diffusion solution [1% (v/v) TFA, 10% acetonitrile, pH 8.1] and sonicated at RT for 45 min. The samples were analyzed on a nanospray-ESI-qTOFMS system and the subsequent comparison of the peptide mass fingerprint with the MASCOT database allowed the correct protein identification.[139]

3.3.5 Heterobactin isolation

For the isolation of heterobactins, *R. erythropolis* PR4 was grown for two days in LB medium. Cells were harvested, washed and resuspended in an equal amount of M9 medium. A 1/100 aliquot was used to inoculate polycarbonate flasks containing fresh minimal medium supplemented with trace elements and 4 g/L glucose. Cultures were grown for 5-7 days until a CAS (Chrome azurol sulfonate) positive reaction of the supernatant was observed.[140] The culture supernatant was extracted with 5 g/L of XAD-16 resin (Sigma-Aldrich) for 1 h at 4 °C, filtrated and following a water washing step, the adsorbed compounds were eluted with methanol and immediately concentrated under reduced pressure at 30 °C to dryness. The eluate was resuspended in 2 mL of water and analyzed by RP-LCMS, utilizing the solvent gradient water + 0.1% TFA (solvent A) and acetonitrile + 0.1% TFA (solvent B), with a linear gradient from 8% to 25% B within 30 min, followed by a linear increase to 95% B in 3 min and holding B for additional 5 min. The flow rate was set to 0.2 mL/min and the column temperature to 25 °C. Large-scale purification via preparative RP-HPLC was performed utilizing the solvent gradient water + 0.1% TFA (solvent A) and acetonitrile + 0.1% TFA (solvent B), with a linear gradient from 8% to 25% B within

45 min, followed by a linear increase to 95% B in 5 min and holding B for additional 5 min, using 215 nm as wavelength for detection and a flow rate of 18 mL/min. Siderophore-containing fractions were identified via CAS assay and ESI-MS. Positive fractions were pooled according to their respective *m/z*, lyophilized, and subjected to further analysis.

3.3.6 Heterobactin purification

For large-scale heterbactin purification the preparative RP-HPLC was used and performed utilizing the solvent gradient water + 0.1% TFA (solvent A) and acetonitrile + 0.1% TFA (solvent B), with a linear gradient from 8% to 25% B within 45 min, followed by a linear increase to 95% B in 5 min and holding B for additional 5 min, using 215 nm as wavelength for detection and a flow rate of 18 mL/min. Siderophore-containing fractions were identified via CAS assay and ESI-MS. Positive fractions were pooled according to their respective *m/z*, lyophilized, and subjected to further analysis. Preparative RP-HPLC was accomplished on a Machery-Nagel Nucleodur C18 Htec 250 × 21 mm column, 5 µm particle size, combined with an Agilent 1100 preparative HPLC system.

3.3.7 UV-vis spectroscopy

UV-vis spectra were recorded on an Ultrospec 3000 (Pharmacia) spectrophotometer. Wavescan measurements were performed within a wavelength range of 250-800 nm and a scan rate of 750 nm/min. Absorption spectra of heterobactin A and S2 and *holo*-heterobactin A and S2 were recorded in water at a final concentration of 400 µM. *Holo*-complexes were obtained by incubating 400 µM heterobactin A and S2 with equimolar aqueous $FeCl_3$ (400 µM) for 5 min at RT prior to the scan. Extinction coefficients were calculated from the UV-vis spectra.

3.3.8 ATR-IR spectroscopy

ATR-IR spectra were performed on a Tensor 37 spectrometer (Bruker Optics) with dried purified heterobactin A and S2.

3.3.9 Assignment of heterobactin A amino acid stereoconfiguration via FDAA-derivatization

Determination of the amino acid configurations was achieved through total acid hydrolysis of heterobactin A followed by derivatization with Marfey's reagent (Nα-(2,4-dinitro-5-fluorophenyl)-L-alaninamide, FDAA)[141]. Purified heterobactin A (0.9 mg) was hydrolyzed in 400 µL of 6 M HCl at 99°C for 24 h. The lyophilized hydrolysate was resuspended in 60 µL of 1 M $NaHCO_3$, and 50 µL of this solution was added to 180 µL of 1% FDAA solution in acetone. The derivatization reaction was carried out for 1 h at 37 °C and terminated by the addition of 20 µL of 1 M HCl. FDAA standard derivatives of amino acids (L/D-Arg, Gly, L-hOrn) were prepared by incubation of 25 µL of 50 mM amino acid solution with 50 µL of 1% FDAA solution and 10 µL of 1 M $NaHCO_3$ for 1 h. After lyophilization, all of the products were resuspended in 200 µL of 1:1 H_2O−CH_3CN solution prior to the injection of 10 µL a 1/10 dilution in H_2O into a HPLC-MS system equipped with a Nucleoshell RP18 column utilizing the following solvent gradient: 0−30 min, 0−30% buffer A (10 mM ammonium formate, 1% MeOH, 5% CH_3CN, pH 5.2) into buffer B (10 mM ammonium formate, 1% MeOH, 60% CH_3CN, pH 5.2), followed by a linear increase to 95% buffer B in 2 min and holding 95% buffer B for an additional 5 min. The flow rate was set at 0.2 mL/min, and the column temperature at 25 °C. Elution was monitored in single-ion mode.

3.3.10 The optical rotation of heterobactin A

Determination of the optical rotation of heterobactin A was performed on a Jasco DIP-370 digital polarimeter. The measurement was carried out at 20°C at 589 nm (sodium D line), using a 1 dm cuvette. About 7.5 mg of heterobactin A was dissolved in 2 mL absolute MeOH, [α] value was clculated using equation (1).

$$[\alpha]_{\lambda}^{T} = \frac{\alpha}{c.l} \qquad (1)$$

[α] = specific rotation, T = temperature, λ = wavelength, α = optical rotation,
c = concentration in g/100ml, l = optical path length in dm.

3.3.11 NMR-spectroscopy

NMR-spectroscopic structure elucidation of heterobactin A and S2 was carried out with Dr.Xiulan Xie (Chemistry department-NMR facility,Philipps-Univertät Marburg). NMR experiments were done on two samples. About 9.5 mg of heterobactin A and 2.5 mg of heterobactin S2 was dissolved in 0.10 ml DMSO-d_6 in a 3 mm Shigemi tube matched to DMSO. Measurements were carried out on a Bruker AV500 or AV600 spectrometer with a BBFO or a TXI ($^{1}H–^{13}C/^{15}N$) probe installed with z gradient. The one-dimensional spectra ^{1}H and ^{13}C, the homonuclear two-dimensional spectra DQF-COSY, TOCSY, NOESY and ROESY, HSQC, and HMBC spectra were obtained for both samples, while the $^{1}H–^{15}N$ HSQC and HMBC spectra were recorded on heterobactin A with standard pulse programs at 296 and 290 K.The TOCSY spectrum was recorded with a mixing time of 80 ms, while NOESY and ROESY spectra were taken at 500 and 300 ms mixing time, respectively. The 1D spectra were acquired with 65 536 data points, whereas 2D spectra were collected using 4096 points in the F2 dimension and 512 increments in the F1 dimension. For 2D spectra 16−128 transients were used, while the ^{13}C spectrum was recorded with 48 K scans. The relaxation delay was 2.5 s. The ^{1}H and ^{13}C chemical shifts were referenced to the solvent signals, whereas those of ^{15}N were assigned with the spectrometer default calibration. The spectra were processed by Bruker Topspin 3.1.

3.3.12 Circular dichroism spectroscopy

CD spectroscopy was carried out using a J-810 Spectropolarimeter (JASCO) in 0.2 cm path length cuvettes in 5 mM K_2HPO_4/KH_2PO_4 buffer pH 7.0 . If necessary, buffer exchange was done with Hi-Trap Desalting column (GE Healthcare) prior to analysis. Secondary structure analysis was done by scans in the far-UV region between 190 and 300 nm with protein concentrations of 10 µM at 5 °C. Three spectral accumulations were performed by using a bandwidth of 1 nm, a response of 1 s, and a data pitch of 0.2 nm. For the recording of denaturation curves, 10 µM of ferric siderophores were added to the protein solutions, which were incubated for 10 min and then measured in a range from 5 to 95 °C by using a temperature slope of 1°C min^{-1} and a data pitch of 0.2°C. The monitored wavelength was 209 nm with a bandwidth of 1 nm and a response of 1s.

3.3.13 Fluorescence spectroscopy

For the measurement of intrinsic tryptophan/tyrosine fluorescence a FP-6500 spectrofluorometer (JASCO) was used. Experiments were carried out at 20°C (constant temperature), using an excitation and emission bandwidth of 5 nm each, and a response of 0.5 s. For each measurement series, a protein solution of 1 μM for HtbH in 50 mM Tris– HCl, pH 8.0, 100 mM NaCl was placed in a 1x1 cm^2 cuvette, and titrated stepwise with a freshly prepared ligand stock solution. Measurment started with a Solution A (50 mM HEPES, 100 mM NaCl; pH 7.0) containaing 50 nM His-HtbH without any ligands and was pursued by adding defined quantities of Solution B containing 50 nM His-HtbH and the ligand at high concentration in the same buffer. The soloution was mixed by magnetic stirring in the cuvette for 5 min. Fluorescence was measured upon sample excitation at 280 nm with a data pitch of 0.5 nm. Quenching data of normalized fluorescence emission maxima were used for plotting and binding constant calculation according to the Law of Mass Action.[142]

3.3.14 Gel filtration Chromatography

2 ml of a 10 mg/ml protein was analyzed by a superdex 200-5/150 GL column combined with an ÄKTA purifier (Amersham Pharmacia biotech) equilibrated with (pH 8, 25mM TRIS, 150 mM NaCl) buffer. The pooled fractions were dialyzed and concentrated as described before and stored at -80°C for use in further assays.

3.4 Biochemical methods

3.4.1 A domain Activity and Selectivity ATP/PP_i exchange assay

Several amino acids and two aryl acids were used to analyze the substrate specificity of the enzyme in a typical radioactive ATP/$^{32}PP_i$ exchange assay. A domains selectively recognize and activate amino and carboxy acids as (amino) acyladenylates under the consumption of ATP and release of PP_i. This reversible reaction is a fast qualitative assay for A domain activity and selectivity.[143,144]

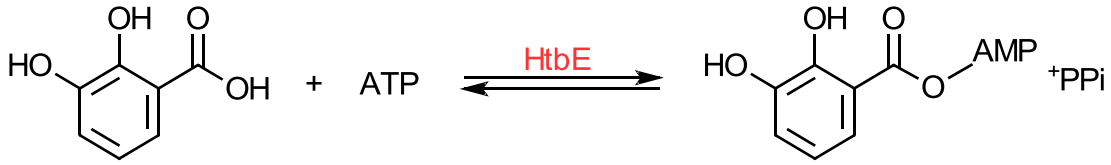

Figure 3.1 The reversible adenylation reaction to investigate the substrate specificity of the adenylation domain HtbE.

Adding ^{32}P-labeled inorganic PP_i to the reaction mixture therefore leads to the formation of ^{32}P-ATP if the amino acid(s), which is present in the assay, is activated by the A domain. The ^{32}P-ATP can be separated easily by adding activated charcoal to the reaction mixture. A 100 µL reaction was composed of the following: 50 mM Tris HCl pH 7.5 buffer, 10 mM $MgCl_2$, 1 mM DTT, 1 mM ATP, 5 mM $Na_4P_2O_7$, 10 mM amino acid. Prior to initiation of the reaction with 2 µM recombinant protein, 20 µL of a Na_4 $^{32}P_2O_7$ solution (approx 100,000 counts) was added. The reaction was incubated at 25°C for 30 min and subsequently quenched with 750 µL of charcoal suspension [100 mM $Na_4P_2O_7$, 600 mM $HClO_4$, 1.6% (w/v) charcoal]. After a washing step with water, the resuspended charcoal was combined with 3 mL of scintillation fluid, prior to counting with a Packard Tri-carb 2100TR liquid scintillation analyzer. All reactions were performed in triplicate.

3.4.2 Hydroxylation assay

The FAD- dependent monooxygenase HMO catalyzed the hydroxylation of the L-Orn in precense of the cosupstrate NADPH and molecular oxygen. Hydroxylation assay 50µL reaction contained: 100mM Tris PH8, 2 mM cosubstrate NADPH, 25 µM cofactor FAD, 1mM L-Orn, and 20 µM HMO recombinant protein with final volume

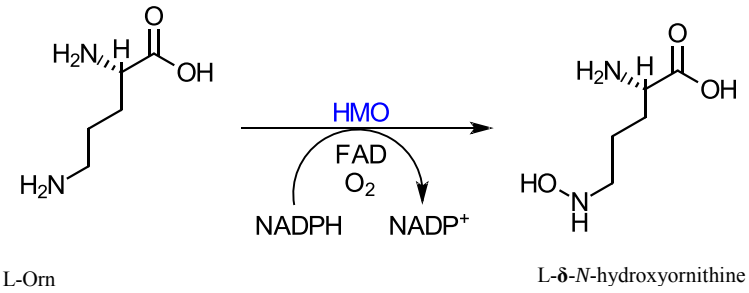

L-Orn L-**δ**-*N*-hydroxyornithine

Figure 3.2 Reaction schem of the HMO-catalyzed FAD/NADPH-dependent δ – amino L-Orn hydroxylation.

50µL, incubated for 4 hours at 30°C and stopped by addition of 2 µL formic acid. Hydroxylation assays were analyzed on a hypercarb column 100x2.1 mm (Thermo Fisher) by reversed phase (RP) HPLC-MS (Aglient 1100) system connected with an ESI-MS detector (Aglient 1100 MSD). Utilizing 20 mm NFPA (solvent A) and acetonitrile (solvent B), the flow rate was set to 0.2 mL/min and the column temperature 20°C, linear increase from 0% to 15%B in 25 min followed by a linear increase to 100%B in 2 min, holding B for an additional 3 min. The elution was observed in single-ion mode (SIM).

3.4.3 Substrate Specificity assay of HMO

The specificity of HMO was determined with a variant of amino acid L-Orn, D-Orn, L-Val, L-Gln, L-Glu, L-Lys, and L-Arg. The hydroxylation assay did as describe before.

3.4.4 Determination of the kinetic parameters of HMO

Reaction kinetics were performed spectrophotometrically on an Ultrospec 3100 pro spectrophotometer (Amersham Biosciences). Concentrations of cosubstrate NADPH and cofactor FAD were 0.5 mM and 20 µM, respectively and L-Orn concentration varied between 0.1 and 20 mM. Calculation of initial rates was based on decrease of NADPH absorbance (ε = 6300 M^{-1} cm^{-1}), and the determination of kinetic parameters were carried out with Enzyme Kinetics Michaelis-Menten equation plot (GraphPad Prism 6).

$$V_\circ = \frac{V_{max}[S]}{K_m + [S]} \qquad (2)$$

V_0 is the velocity of the reaction. V_{max} is the maximal rate of the reaction. **[S]** is the concentration of the substrate. K_m is the Michaelis-Menten constant.

3.5 Bioinformatic methods

Many web sites and data basses programs were used in this study to analyze nucleic acids sequences (GATC Biotech), proteins sequences, antiSMASH web-site allowed identification of the major known secondary metabolites gene clusters.[145] The prediction of the adenylation domain substrate specificity was carried out with NRPSpredictor and its updated version NRPSpredictor2.[146,147] Sequence-homology searches were executed using the BLAST algorithm. Multiple sequence alignment carried out by using the Clustal Omega algorithm and Emboss Needle [150]. Oligo Calc: Oligonucleotide Properties Calculator for designed the primers, ExPASy (Bioonformatics Resource portal) for protein sequence calculation, protein molecular weight calculation, in *silico* Molecular Biololgy tools. All sequences were retrieved from the NCBI database (http://www.ncbi.nlm.nih.gov/).

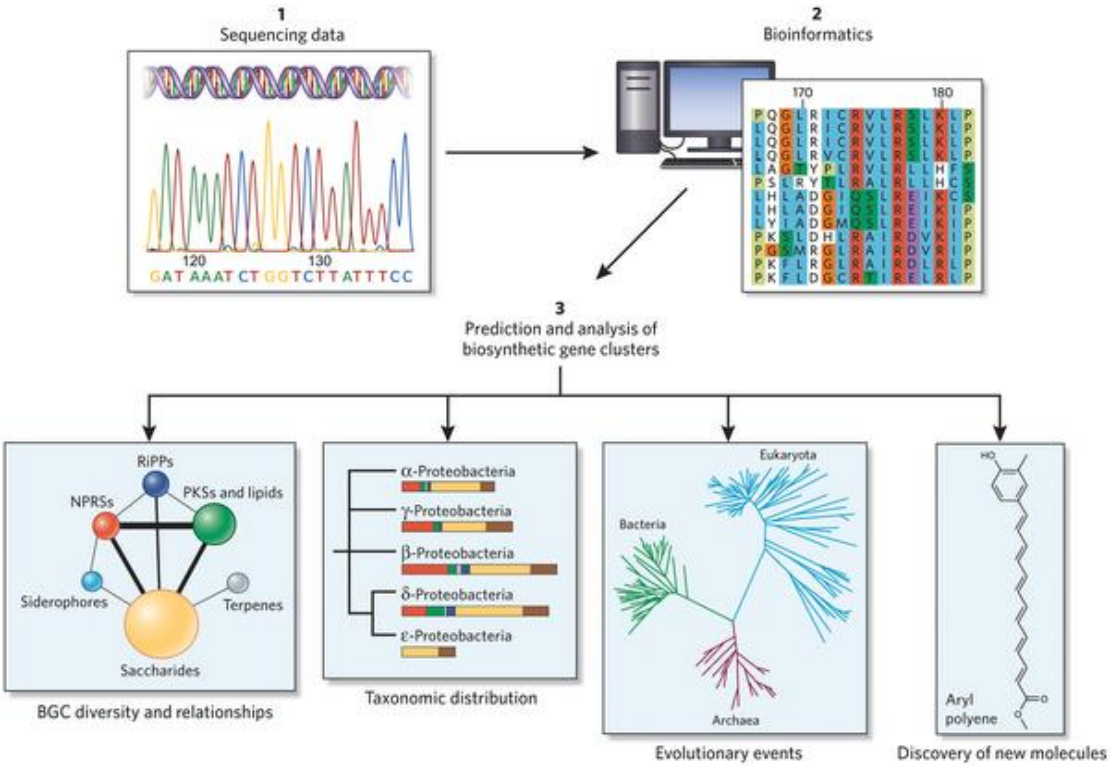

Figure 3.3 Sequencing data as a renaissance in secondary metabolite research.[148]

Chapter 4

Results

4 .1 Heterobactin Isolation and Structural Elucidation

4.1.1 Isolation and purification of heterobactin

Microorganisms have a tightly regulated system concerning the biosynthesis of siderophores. In order to elicit the production of a siderophore, *R. erythropolis* PR4 was cultivated in M9 minimal medium under iron-depleted conditions until the formation of an iron-scavenging compound was confirmed by chrome azurol sulfonate (CAS) liquid assay.[140] After treatment of the culture supernatant with XAD-16 resin, the compounds adsorbed were eluted with MeOH and subjected to HPLC-MS analysis. The resulting chromatogram showed that, under the conditions employed, three major metabolites were found (Figure 4.1A, blue line). The two most hydrophilic compounds displayed *m/z* ratios of 696.19354 and 696.19384 ($[M + H]^+$), respectively, indicating two molecules with the same molecular formula. On the other hand, the most lipophilic compound displayed an *m/z* of 616.23636 ($[M + H]^+$; (Figure 4.1B). The mass differences observed of *m/z* 79.95718 and *m/z* 79.95748 between the first two and the latter compound suggested a sulfonation modification (*m/z* 79.95681, calculated). In order to determine if this modification is affected by the presence of sulfate (from $MgSO_4$) in the medium, the wild-type strain was grown in M9 minimal medium in the presence of an equimolar amount of $MgCl_2$. Under these conditions, the most lipophilic compound was the major metabolite (Figure 4.1A, green line), supporting the sulfonation of the first two compounds.

4.1.2 Comparison between the *R. erythropolis* PR4 and *R. erythropolis* IGTS8 HPLC-MS profile

The siderophore heterobactin A was previously characterized from *R. erythropolis* IGTS8.[123] In order to determine whether the compounds isolated from the culture supernatant of *R. erythropolis* PR4 were the same as from *R. erythropolis* IGTS8, the latter strain was grown under the same conditions. Surprisingly, HPLC-MS profile comparison revealed that both strains produced an identical chromatographic profile, with the presence of the two sulfonated forms and the nonmodified one (Figure 4.1A, orange line).

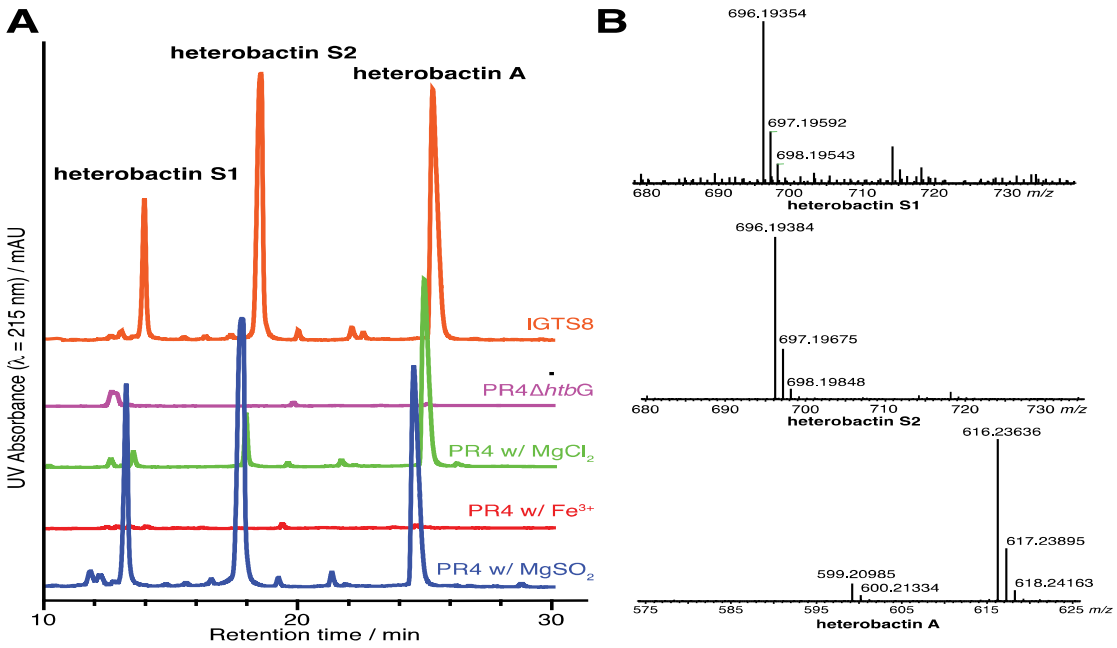

Figure 4.1 (A) HPLC traces of extracted culture supernatants. *R. erythropolis* PR4 was grown in M9 minimal medium in the absence (blue line) or presence (red line) of iron. Under the application of iron-limiting conditions, three major metabolites are secreted. Heterobactin S1 and S2 are sulfonated derivatives of heterobactin A and their production could be reduced by replacing $MgSO_4$ with $MgCl_2$ (green line). The assembly of the main scaffold of the siderophore is built up by an NRPS: the isogenic deletion mutant strain PR4Δ*htb*G is defective for siderophore assembly (purple line). The identical chromatographic profile of *R. erythropolis* IGTS8 grown under similar growing conditions leads to the conclusion that the two strains share the same siderophores (orange line). (B) HR-MS spectra of the isolated compounds.

In addition, HR-MS measurements of the nonsulfonated compound isolated from *R. erythropolis* IGTS8 revealed this compound to have an *m/z* of 616.2357 and not 599.20959 $(M+H]^+$), as previously reported. In conclusion, under iron-limiting conditions, both *R. erythropolis* PR4 and *R. erythropolis* IGTS8 produce three iron-scavenging compounds, whereas two of them are modified by sulfonation. On the basis of these results and in accordance with the compound known previously, the most lipophilic compound has been renamed “heterobactin A,” whereas the two sulfonated forms have been renamed “heterobactin S1” and “S2”.

4.1.3 Structure elucidation of heterobactin via MS^n

Collision-induced dissociation experiments were carried out in order to acquire information regarding the building block composition of the three heterobactin variants and their connectivity. Heterobactin A MS^2 and MS^3 fragmentation revealed the consecutive neutral loss of two 2,3-DHB (observed *m/z* 136.01609 for MS^2 and 136.01611 for MS^3, calculated *m/z* 136.01604, $[M+H]^+$). The following MS^4 fragmentation of the resulting peptide fragment (which is composed of a linear assembly of cyhOrn-Gly-Arg) showed a neutral loss of an NH_3 molecule (observed *m/z* 17.02645, calculated *m/z* 17.02655). Finally, MS^5 fragmentation of the aforementioned ion led to a specific ion fingerprint (Supporting Information Figure 1). The MS^n fragmentation studies of the sulfonated heterobactins S1 and S2 revealed a similar fragmentation pattern (Supporting Information Figures 2 and 3), suggesting that the modifications occur on the aromatic moieties in these compounds. Overall, the mass spectrometric analysis of the isolated siderophores heterobactin A, S1 and S2 share a common scaffold which is built up by two 2,3-DHB, an arginine, a glycine and a cyclo-δ-*N*-hydroxyornithine (cyhOrn).

4.1.4 Assignment of heterobactin A amino acid stereoconfiguration

A derivatization of the heterobactin A acid hydrolysate with FDAA (Marfey's reagent) was carried out in order to assign the stereoconfiguration of the amino acids. The resulting mixture was then subjected to HPLC-MS analysis and compared with derivatized amino acid standards (L/D-Arg, Gly, L-hOrn). The comparison of the HPLC-MS chromatograms and the MS spectra of the derivatized acid hydrolysate with the synthetic amino acid standards revealed the sole presence of D-Arg, Gly and L-hOrn as heterobactin A constituents (Figure 4.2).

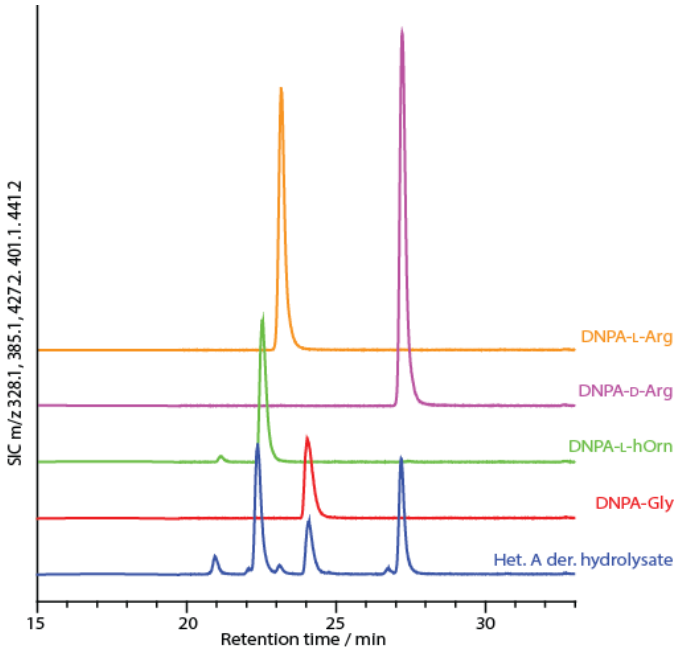

compound	t_R synthetic standard (min)	t_R het. A der. hydrolysate (min)
DNPA-Gly	24.0	24.1
DNPA-L-Arg	23.1	
DNPA-D-Arg	27.2	27.2
DNPA-L-hOrn	22.5	22.4

Figure 4.2 HPLC-MS profile of the FDAA-derivatized amino acid standards and of the products of heterobactin A acid hydrolysis. The corresponding retention times are given. Elution was monitored in SIM, corresponding *m/z* ($[M+H]^+$): ‹328.1 DNPA-Gly,385.1 DNPA-Orn, 427.2 DNPA-Arg, 401.1 DNPA-hOrn. The reaction of L-hOrn with FDAA in acetone resulted in the formation of a ($[M+H]^+$) compound known to be its nitrone derivative *m/z* 441.2, as previously reported during the synthesis of *ε-N*-acetyl-*ε-N*-hydroxylysine.

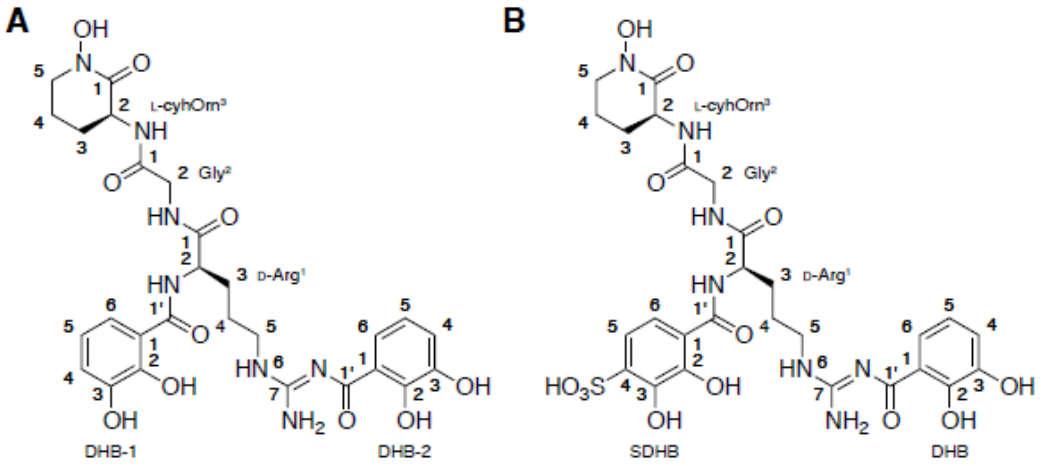

Figure 4.3 The structure of heterobactin A (left) and heterobactin S2 (right) showing the numbering of the building blocks.

4.1.5 The optical rotation of heterobactin A

The specific optical rotation value was determined via a polarimeter instrument to acquire additional information from the stereoconfiguration of the whole heterobactin A siderophore compound. The purified heterobactin A was dissolved in methanol. The optical rotation value in RT was [α] = −6.4 and when compared previously with heterobactin A, the optical rotation value was close at [α] = −7.5.

4.1.6 Structure elucidation of heterobactin via NMR

The final structures of heterobactins A and S2 were determined by NMR spectroscopy. The ^{1}H NMR spectrum of heterobactin A showed two doublets at 8.86 and 8.16 ppm for the amide proton of D-Arg^{1} and L-cyhOrn^{3}, respectively, while a triplet at 8.36 ppm was assigned to that of Gly^{2}. One broad triplet at 9.42 ppm was observed for the εNH of Arg^{1}, while a broad singlet at 11.86 ppm was assigned to the hydroxyl group at position 2 of DHB-1. In the aromatic region, two doublets and a triplet at 7.42, 6.94 and 6.71 ppm, respectively, were detected for DHB-1. Similarly, two doubles and a triplet at 7.25, 7.03 and 6.76 ppm, respectively, were detected for DHB-2. The ^{1}H NMR spectrum of heterobactin S2 showed close similarity to that of heterobactin A, with two additional features: (1) one additional sharp peak at 10.66 ppm was observed for the hydroxy group at position 3 of the SDHB; (2) in proximity to the signals of DHB-1, only two doublets at 7.38 and 6.97 ppm were detected for sulfonyl-DHB (SDHB). A further difference was observed in the change of the ^{13}C chemical shift of DHB at position 4, which is 118.85 ppm for DHB-1 of heterobactin A, but 132.96 ppm for SDHB due to sulfonation at this position. Therefore, the sulfonation in heterobactin S2 was determined to be in position 4 of the first DHB. Total correlation spectroscopy cross-peaks confirmed the presence of one arginine, one glycine and one ornithine in the compound for both samples. The NOE contacts between NH of Arg^{1} and H-6 of DHB-1, NH of Gly^{2} and Hα of Arg^{1}, and NH of cyhOrn^{3} and Hα of Gly^{2} were observed which confirm the sequential connections. Furthermore, long-range ^{1}H-^{13}C correlation was observed from Hα and Hδ to the carbonyl carbon of cyhOrn^{3}, which can only be due to the cyclization of cyhOrn^{3}.

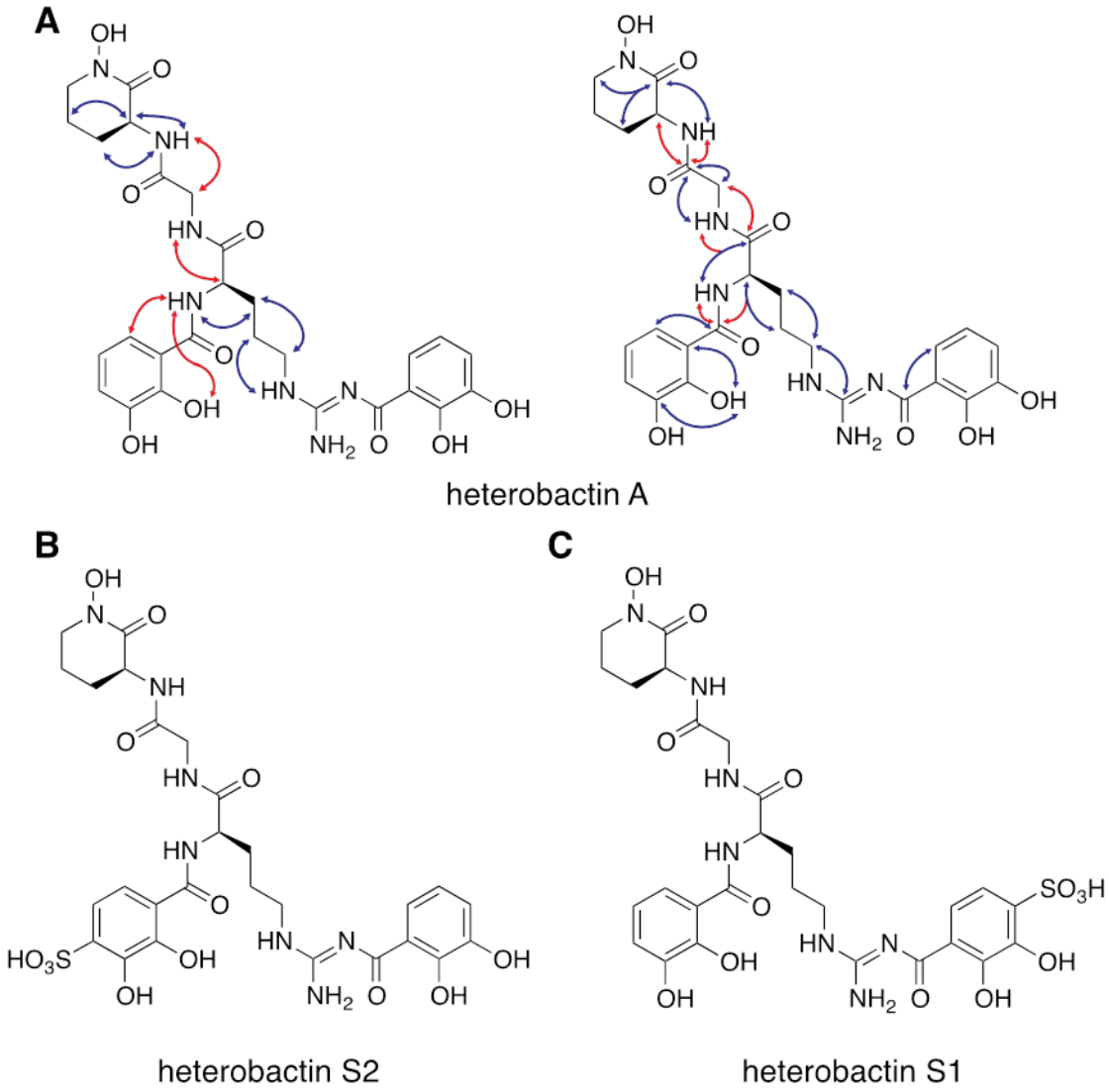

Figure 4.4 (A) NOE (left) and HMBC (right) contacts of heterobactin A in DMSO-d_6 at 296 K. Blue arrows indicate intraresidue correlations, while red arrows represents long-range interresidue correlations. (B) The structure of heterobactin S2 features a sulfonation modification on one 2,3-DHB moiety. (C) The structure of heterobactin S1 is presented on the basis of the hypothesis that the sulfonation modification occurs on the alternate 2,3-DHB residue. The naming and the atom numbering of the 2,3-DHB moieties have been highlighted for unequivocal identification.

An HMBC cross-peak at 3.31 and 154.31 ppm was observed for the correlation between Hδ and the guanidine quaternary carbon of Arg[1]. Therefore, putting all these long-range connections together, the structures of heterobactin A and heterobactin S2 are presented in (Figure 4.4) . The ^{1}H, ^{13}C and ^{15}N chemical shifts assigned are listed in Supporting Information Table S1.

4.1.7 Physicochemical properties of heterobactin A and S2

Ferric iron complexes of heterobactin A and S2 were analyzed via UV-vis spectroscopy, ATR-IR spectra and HR-MS in order to determine whether heterobactin A and S2 possess a physiological function as iron-chelating compounds. Both compounds retained the capacity to complex Fe^{3+}, which is reflected both in the UV-vis spectra, ATR-IR spectra and HR-MS. In particular, binding of the ferric ion altered the spectral properties of the siderophore, resulting in a shift of the absorption peak from 318 nm of *apo*-heterobactin A to 332 nm of *holo*-heterobactin A (corresponding to the $\pi \rightarrow \pi^*$ transition of the catechol group) and from 320 nm of *apo*-heterobactin S2 to 339 nm of *holo*-heterobactin S2. The occurrence of three new absorption peaks at 409, 560 and 580 nm, indicative of the *ferric*-hydroxamate and *ferric*-catecholate charge transfer, respectively. HR-MS analysis confirmed the identity and the 1:1 stoichiometry of the *apo*-heterobactin A which has an *m/z* of 616.2364 and calculated of 616.2367. The *holo*-heterobactin A complex, has an *m/z* of 669.1479 ($[M-H+Fe^{3+}3H]^+$, calculated 669.1476) and *apo*-heterobactin S2 complex has an *m/z* of 696.1938 (calculated 669.1476). The *holo*-Heterobactin S2 complex, has an *m/z* of 749.1053 ($[M-H+Fe^{3+}-3H]^+$, calculated 749.1050). The complete UV-vis and ATR-IR analysis of the *apo*- and *holo*-heterobactin A and S2 are shown in (Figure 4.5) and (Figure 12) in the Supporting Information.

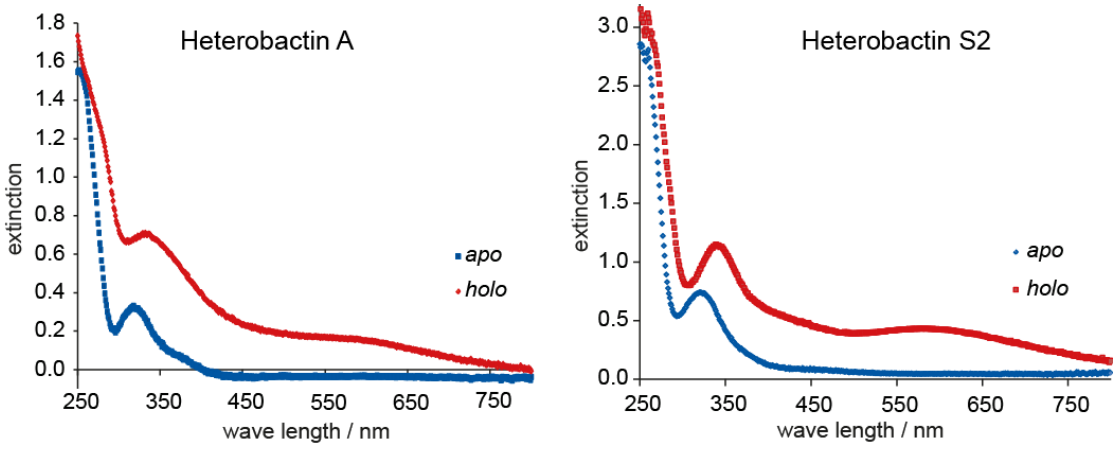

Figure 4.5. Left, UV-vis spectra of 400 µM *apo*-heterobactin A (blue line) and 400 µM *holo*-Fe^{3+}:heterobactin A (red line). Right, UV-vis spectra of 400 µM *apo* heterobactin S2 (blue line) and 400 µM *holo*-Fe^{3+}:heterobactin S2 (red line).

4.2 Bioinformatic Analysis of *R. erythropolis* PR4 Genome and Identification of the Heterobactin Gene Cluster

4.2.1 Identification of the heterobactin biosynthetic gene cluster via genome mining

In order to establish a connection between heterobactin A and the genes involved in its biosynthesis, the genome sequence of *R. erythropolis* PR4 was analyzed using the antiSMASH bioinformatic tool that allowed the identification of two putative siderophore gene clusters.

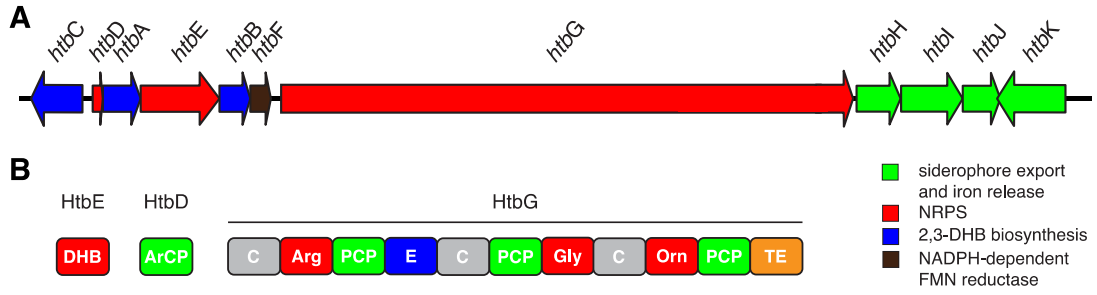

Figure 4.6 Bioinformatic overview of the heterobactin's biosynthetic gene cluster. (A) The arrangement of the *htb* gene cluster. (B) The domain's organization of the NRPSs HtbE, HtbD and HtbG. The second module of the HtbG NRPS features an unusual domain organization with a swapped C-PCP-A arrangement.

The first cluster is composed of 11 ORFs and covers a region of approximately 28 kbp located between the genes RER_09700 and RER_09800.The arrangement of the cluster resembles the organization of the genes responsible for the biosynthesis of the hydroxamate type siderophore requichelin (*R. equii*).[124] As previously reported, to some extent this arrangement is conserved among other *Rhodococcus* spp., despite the insertion of a variable number of additional genes within the different *Rhodococcus* isolates. The structure of requichelin has been postulated on the basis of the NRPS modular organization and the A-domain substrate specificities. It is predicted to consist of N^5-formyl-N^5-hydroxyornithine, serine, N^5-hydroxyornithine and N^5-acyl-N^5-hydroxyornithine, resembling the erythrochelin/foroxymithine-like cryptic siderophore previously proposed in *R. jostii* RHA1 and other actinomycetales strains (Figure S9). Therefore, on the basis of the evidence suggested, the first cluster was

excluded as the heterobactin biosynthetic gene cluster. The second cluster, composed of 11 genes, spans a region of approximately 23 kbp and is located between ORFs RER_26950 and ORFs RER_27050 (Figure 4.6A). The first five genes within the cluster (RER_26950−RER_26990) share homology with the ones responsible for 2,3-DHB biosynthesis from its chorismate precursor and, thus, have been renamed as htbC, htbD, htbA, htbE and htbB.[149] Similarly to those *Rhodoccocus* sequenced strains known, the genes for isochorismatase and the aryl carrier protein functions (HtbB and HtbD, respectively) are split into two separate ORFs. The following gene, RER_27000, has been renamed htbF and shows homology to Escherichia coli WrbA, a multimeric flavodoxin/FMN-dependent NAD(P)H:quinone oxidoreductase. The presence and the function of this gene within the siderophore cluster remain elusive. The largest gene within the cluster is RER_27010 (approximately 12.5 kbp) and encodes for the NRPS *HtbG* (Figure 4.6B). Superficially, *HtbG* resembles a typical NRPS, with three complete modules and the terminal thioesterase domain. Substrate specificity prediction for the adenylation (A) domains proposed a preference for arginine (A1), glycine (A2) and ornithine (A3, Table 4.1). In addition, the presence of an epimerization (E) domain within the first module is in accordance with the D-configured arginine detected in heterobactin A. Interestingly, the most prominent feature of the heterobactin NRP is the unusual domain organization within the second module. There, the prototypical NRPS modular organization C-A-PCP is swapped to C-PCP-A. A BLAST search revealed that this unprecedented domain arrangement is exclusive to a few *R. erythropolis* isolates and to *R. qingshengii*, which suggests that these strains could share the same siderophore. The remaining four ORFs of the gene cluster are probably involved in siderophore export (RER_27030 and RER_27050, htbI and htbK, respectively), the import of the iron-siderophore complex (RER_27020, htbH) and cytoplasmic reductive release (RER_27040, htbJ). A complete overview of the gene clusters and the ORFs found therein is presented in Table S1.

Table 4.1 Adenylation substrate specificity prediction of the htb cluster A-domains carried out with the NRPSpredictor2 bioinformatic tool[a].

A-domain	Active side residues	substrate
HtbE	DADDVGLVDK	DHB (80 %)
HtbG-A1	DADDVGLVDK	Arg (100 %)
HtbG-A2	DILQLGVVWK	Gly (90 %)
HtbG-A3	DMENMGLINK	Orn (90 %)

[a]Substrate specificity is given according to the nearest neighbor method.

4.2.2 Gene deletion studies in *R. erythropolis* PR4 and test for heterobactin activity

The construction of a "markerless" in-frame gene-deletion mutant strain was carried out in order to establish the connection between heterobactin A and the putative gene cluster responsible for its biosynthesis. The NRPS gene *htbG* was deleted from the wild-type strain, resulting in the new strain PR4Δ*htbG* (Figure S10). Under the application of iron-limiting conditions, the mutant strain grew similarly to the wild-type, although it was incapable of displaying a CAS-positive reaction. In addition, the extracted culture supernatant lacks the three heterobactin variants typical of the wild-type strain (Figure 4.1A, purple line). This result proves the involvement of the NRPS HtbG in the production of the heterobactins and links the biosynthetic gene cluster with the natural product.

4.3 Biochemical Characterization of Heterobactin NRPS Assembly Enzymes

4.3.1 ATP/PP_i exchange assay

In order to verify the substrate specificity of the stand-alone A-domain HtbE and of the A-domain from the dissected initiation module of the NRPS HtbG, the corresponding genes were cloned and heterologously produced in *E. coli*, and the resulting proteins were purified via affinity chromatography (Figure 4.7). In particular, a multiple sequence alignment revealed all the A-domains of the NRPS HtbG to be MbtH-dependent (Figure S11); therefore, the MbtH-like protein gene RER_09800 was cloned in the pACYC vector (without a purification tag) and coexpressed together with HtbG-CAT1. Several amino acids and two aryl acids were used to analyze the substrate specificity of the enzyme in a typical radioactive ATP/$^{32}PP_i$ exchange assay. The recombinant HtbE showed a distinct preference for 2,3-DHB, whereas the dissected HtbG-CAT1 showed a preference for L-Arg. In both cases, the results obtained validate the bioinformatic prediction and match the sequence of the product heterobactin A (Figure 4.8).

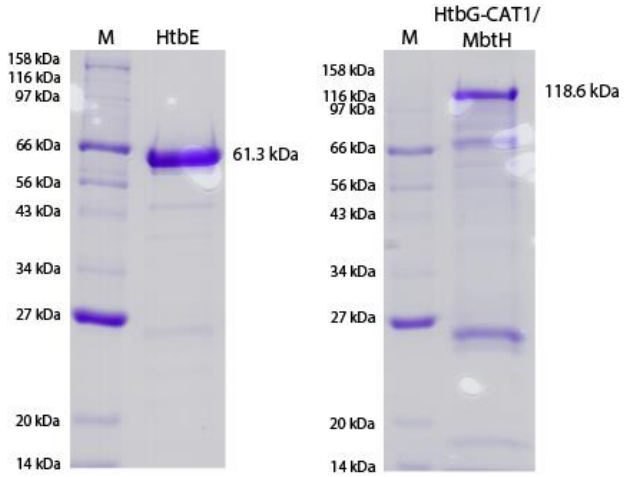

Figure 4.7 Coomassie blue staining of the SDS-PAGE of purified recombinant HtbE (left) and HtbG-CAT1 coexpressed with MbtH (right).

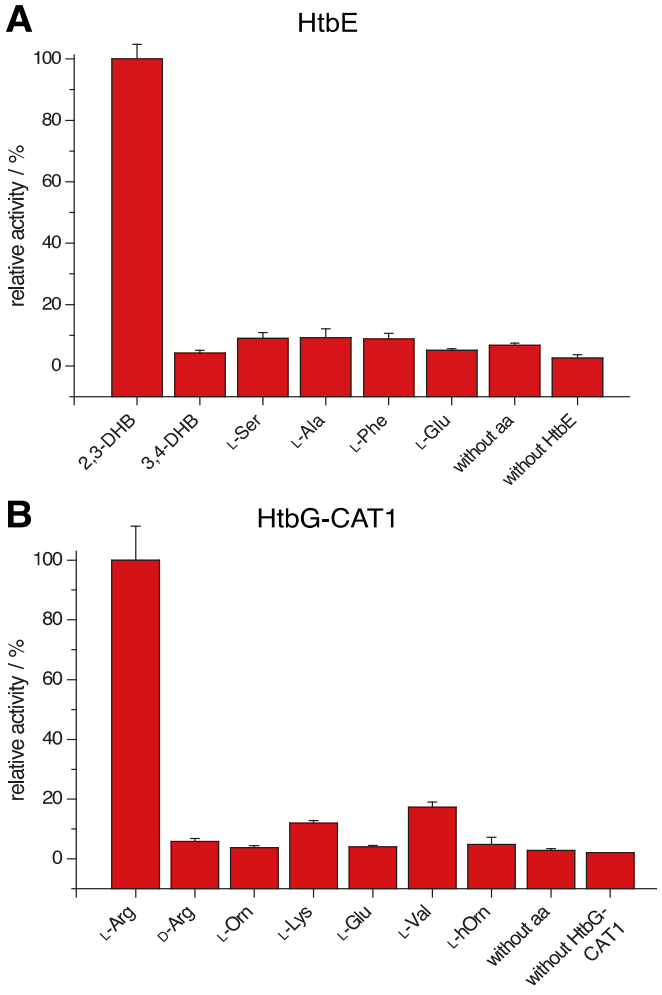

Figure 4.8 ATP/$^{32}PP_i$ exchange assay. Relative activities obtained from the ATP/PP_i exchange assay for HtbE (A) and the A-domain from the dissected initiation module of the HtbG (B). Error bars represent standard deviations calculated from three independent measurements.

4.4. Biochemical Characterization of HMO L-Orn Monooxygenase

4.4.1 Bioinformatic analysis of the *NMO hmo*

In the previous studies by Bosello et al. (2011) and Robbel et al. (2011),[72,75] it was shown that *NMO (N*-hydroxylating flavoprotein monooxygenase*)* encodes for a putative L-Orn *N*-hydroxylating flavoprotein monooxygenase which is involved in the biosynthesis of a hydroxamate siderophore. A bioinformatics analysis demonstrated that *hmo* belongs to the class of NAD(P)H/FAD dependent monooxygenases; it exhibits high similarity along the overall sequence when compared to homologues characterized already (*PvdA*, *Rmo, AmcK, CchB*, and EtcB). As depicted in the multiple sequence alignment shown in (Figure 4.9), each monomer of the enzyme contains three well-defined domains linked together by flexible loops. The FAD-binding domain is the largest of the three domains about (250 residues) and is folded into an α/β-nucleotide-binding architecture. The NADPH-binding domain contains 144 residues and folds into an α/β-nucleotide-binding fold. The smallest domain is the substrate (L-Orn)-binding domain containing 45 residues. The general structure is usually coordinated between these three domains with two Rossmann-like dinucleotide-binding domains, one each for FAD and NADPH binding.

4.4.2 Recombinant production and purification of active apo-HMO

The gene *hmo* was amplified from genomic DNA of *R. erythropolis* PR4 and cloned into the pET28a (+) expression vector. The monooxygenase was carried out using the Phusion High-Fidelity DNA Polymerase, following the manufacturer's instruction for GC-rich DNA templates. The amplicon was digested using a corresponding endonuclease and ligated into the vector pET28a(+). After verification of DNA-fidelity by sequencing (GATC-Biotech), *E.coli* BL21(DE3) were transformed with plasmids via electroporation of heterologous production of HMO and purified via Ni-NTA affinity chromatography without binding the cofactor FAD (in *apo* form). The final HMO protein yield after concentration and dialysis was 6.0 mg/L, and was then purified via gel filtration, (Figure 4.10).

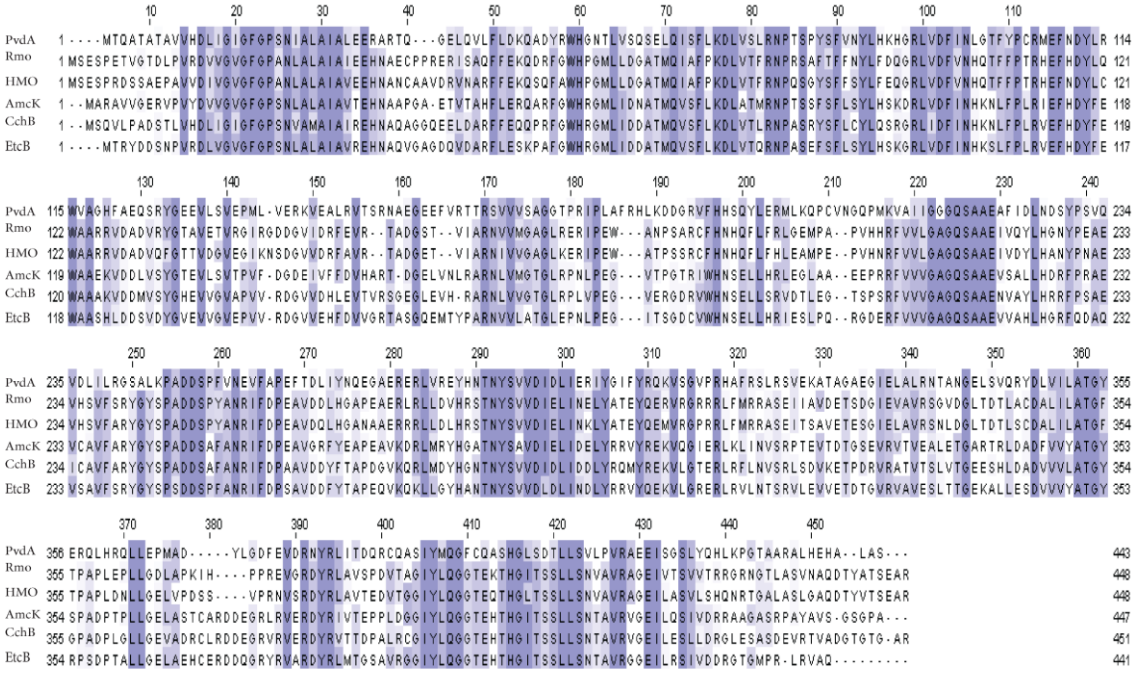

Figure 4.9 Multiple sequence alignment of different *NMO* homologous to HMO (*R. erythropolis PR4*) carried out by using the Clustal Omega algorithm.[150] The alignment includes: PvdA (*Pseudomonas aeruginosa*, 30.6 % sequence identity, 42.9 % sequence homology), Rmo (*R. jostii*, 77.5 %, 86.6 %), AmcK (*Amycolatopsis* sp.MJM2582 47.9%, 60.5%), CchB (*S.coelicolor*, 47.8 %, 61.68 %) and EtcB (*S.erythraea* 50%, 63.6%).

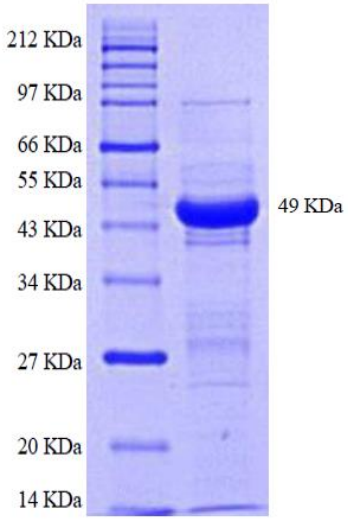

Figure 4.10 Coomassie blue staining of the SDS-PAGE of purified recombinant HMO.

4.4.3 Biochemical characterization of HMO

In order to investigate if HMO is catalyzing the *δ-N*-hydroxylation of L-Orn, it was incubated with reducing cosubstrate NADPH and cofactor FAD in the presence of molecular oxygene. RP-HPLC-MS analysis of the assay after 4 h revealed a 60 % conversion of L-Orn (t_R 6.2 min, *m\z* 133.1$[M+H]^+$ observed, *m\z* =133.1$[M+H]^+$ calculated) to L-hOrn (t_R15.5 min, *m\z* 149.1$[M+H]^+$ observed, *m\z* =149.1$[M+H]^+$ calculated) in the presence of HMO and molecular oxygen. During the conversion of L-Orn to L-hOrn, it was not observed whether NADH was used as a reducing cosubstrate instead of NADPH and whether either NADPH or HMO was absent.

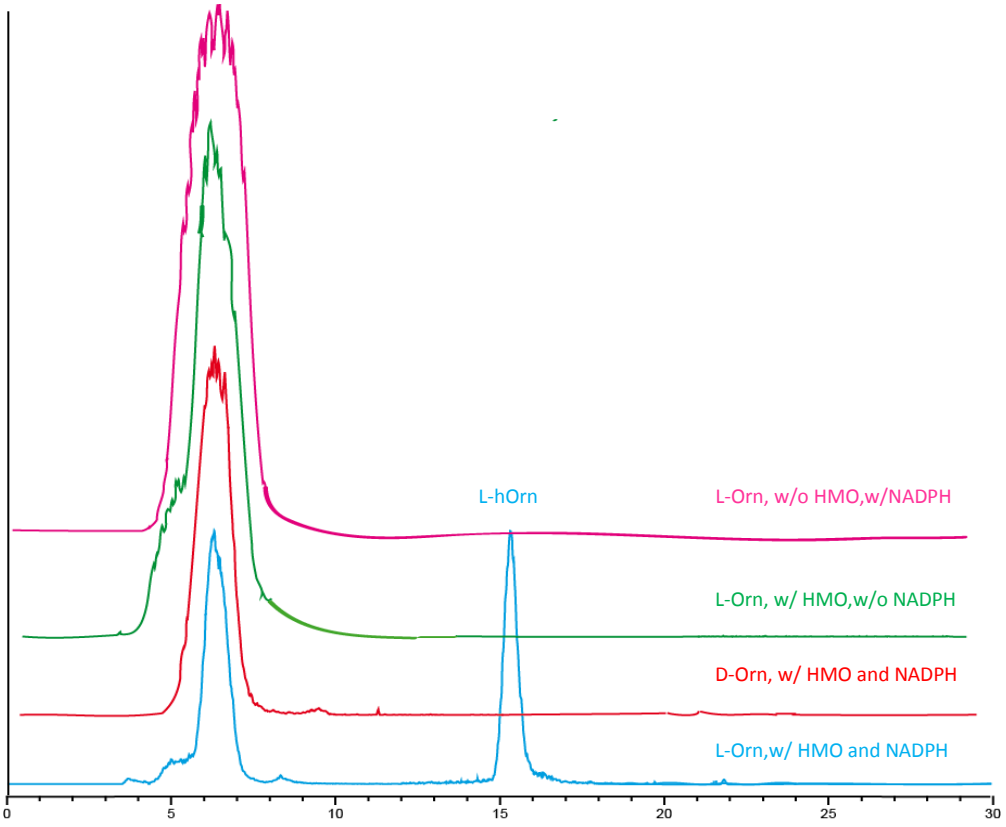

Figure 4.11 HMO-mediated L-Orn hydroxylation. (A) HPLC-MS single-ion chromatogram (SIC) of the hydroxylation assays is shown: in the presence of the L-Orn substrate and the reducing cosubstrate NADPH, HMO catalyzes the conversion of L-Orn to L-hOrn (blue trace). The control reactions evidence that HMO is unable to hydroxylate D-Orn (red trace) and that the reaction does not proceed if either NADPH or the enzyme is missing (green and purple traces, respectively).

4.4.4 Substrate specificity assay of HMO

In order to investigate the substrate specificity of HMO, the recombinant protein was incubated with a variety of amino acids: L-Orn, D-Orn, L-Val, L-Gln, L-Glu, L-Lys and L-Arg. Interestingly, the enzyme displays limited substrate specificity toward L-Orn over a variety of amino acids, Table 4.2.

Table 4.2 Overview of the substrate specificities evaluated for the HMO-mediated hydroxylation.

Substrate	*m/z* $[M+H]^+$ substrate	*m/z* $[M+H]^+$ expected hydroxylation	*m/z* $[M+H]^+$ observed	Hydoxylation
L-Orn	133.1	149.1	149.1	√
D-Orn	133.1	149.1	133.1	×
L-Val	118.1	134.1	118.1	×
L-Gln	147.1	163.1	147.1	×
L-Glu	148.1	164.1	148.1	×
L-Lys	147.1	163.1	147.1	×
L-Arg	175.1	191.1	175.1	×
L-Orn wo/ NADPH	133.1	149.1	133.1	×

4.4.5 Determination of the kinetic parameters of HMO

Catalyzed L-Orn *δ-N*-hydroxylation was determined spectrophotometrically by measuring the initial rates of the assay with different concentrations of L-Orn. The calculation of kinetic parameters was carried out using a Michaelis-Menten equation plot and was calculated to an apparent K_M = 1.8 ± 0.5 mM and k_{cat} = 0.32 ± 0.01 s^{-1}, with a catalytic efficiency of $k_{cat}/k_M = 0.17\ ^{s-1}mM\ ^{-1}$.

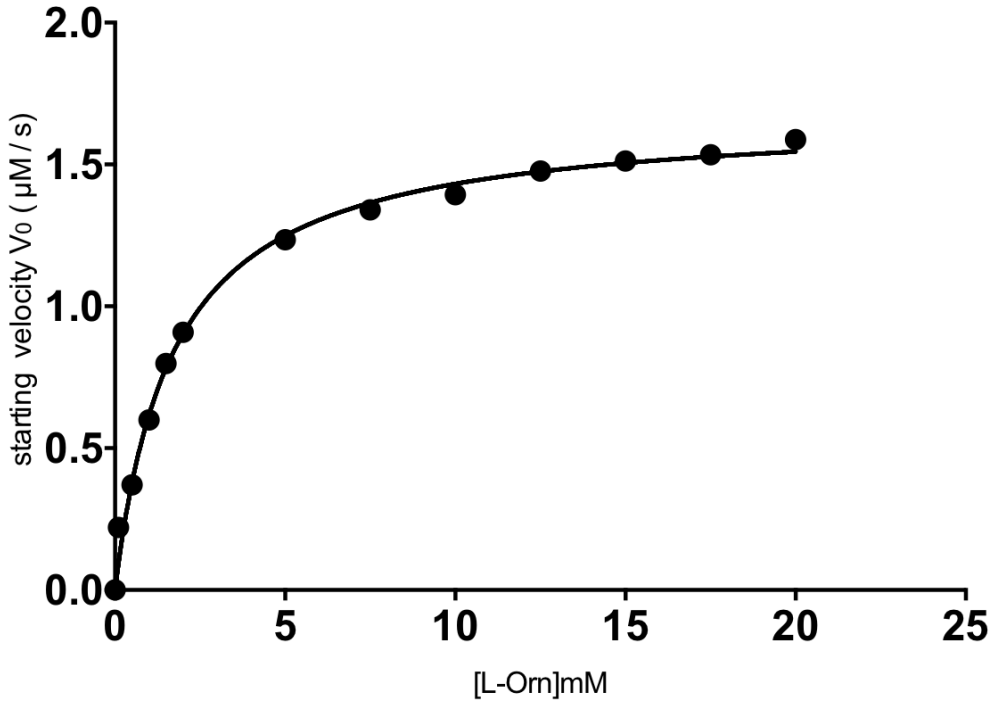

Figure 4.12 Michaelis-Menten kinetics for HMO. NADPH concentration was fixed at 500 µM, FAD at 20 µM and HMO at 10 µM. L-Orn substrate concentration was varied between 0.10 and 20 mm.

4.5 Iron-siderophore Binding Protein

4.5.1 Bioinformatic analysis of HtbH (iron-siderophore binding protein)

A bioinformatic analysis of the biosynthetic gene cluster of heterobactin A demonstrated that the *htbH* gene encodes for a putative iron-siderophore binding protein which is involved in the iron-siderophore uptake system. The multiple sequence alignment of the different siderophore binding proteins, FhuD, FepB from *E.coli,* FeuA, YicQ from *B. subtilus*, CeuA from *Mannheimia haemolytica,* CeuE from *Campylobacter jejuni* to HtbH from *R. erythropolis* PR4 was carried out by using the Clustal Omega algorithm.

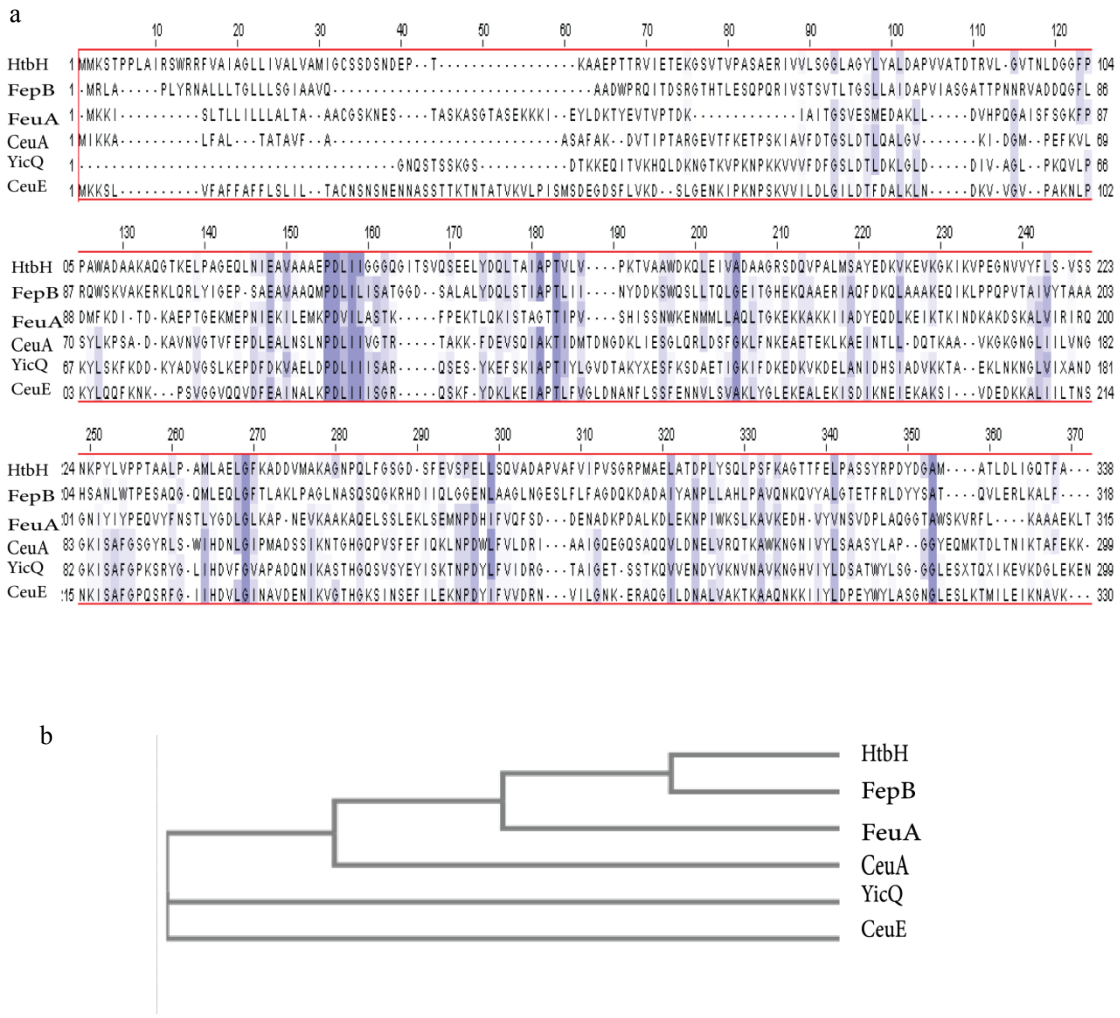

Figure 4.13 (a)The multiple sequence alignment of the different Catecholates siderophore binding proteins, FepB, FeuA, CeuA, YicQ, and CeuE to HtbH from *R. erythropolis* PR4, carried out by using the clustal omega algorithm. (b) Phylogenetic tree of the different Catecholates binding proteins with HtbH.

a

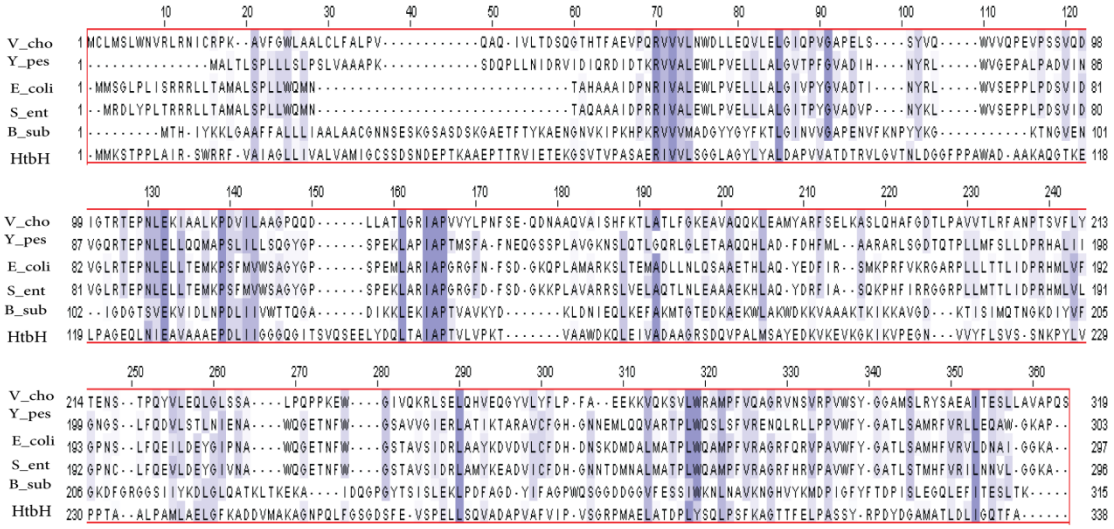

b

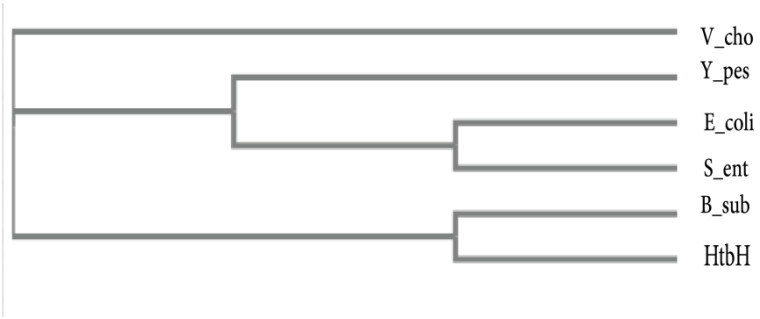

Figure 4.14 (a)The multiple sequence alignment of the different FhuD hydroxamates siderophore binding proteins to HtbH from *R. erythropolis* PR4, carried out by using the clustal omega algorithm. (b) Phylogenetic tree of the different FhuD hydroxamates binding proteins and HtbH.

The results exhibit 27.4 % identity and 44.6 % similarity with FepB, 18.9 % identity and 36.7 % similarity with FeuA, finally 22.2 % identity and 37.9 % similarity with FhuD (*B_sub*) as shown in (Figure 4.13) and (Figure 4.14). The open reading frame encodes a protein with 338 amino acids. The first 32 amino acids are characterized as a lipoprotein signal peptide, which contains the lipoamino acid *N*-acyl glyceride cysteine at the N-terminal. The glyceryl-cysteine serves as a attachment site for two ester-linked fatty acids and one amid-linked fatty acid. The mature protein contained 306 amino acids.

4.5.2 Biochemical characterization of iron-siderophore binding protein (HtbH)

In order to verify the binding function of HtbH, the corresponding gene was cloned as a N-terminal His-tag fusion in pET28a(+). The correct sequences of the plasmid inserts was confirmed by DNA sequencing (GATC Biotech), heterologously produced in *E. coli* BL21(DE3) for protein overproduction and purified via affinity chromatography and size exclusion chromatography, respectively, with yields of 10 mg/L of bacteria culture, (Figure 4.15).

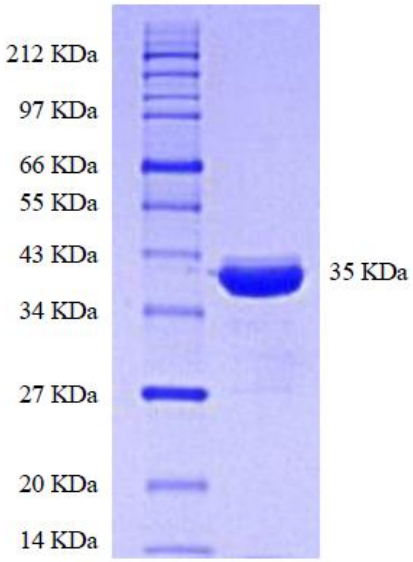

Figure 4.15 Coomassie blue staining of the SDS-PAGE of purified recombinant HtbH.

4.5.3 Secondary structure analysis of iron-siderophore binding protein (HtbH)

The protein was analyzed by circular dichroism (CD) spectroscopy in the far UV region (Fig. 4.16) to estimate the folding efficiency as well as the secondary structure.

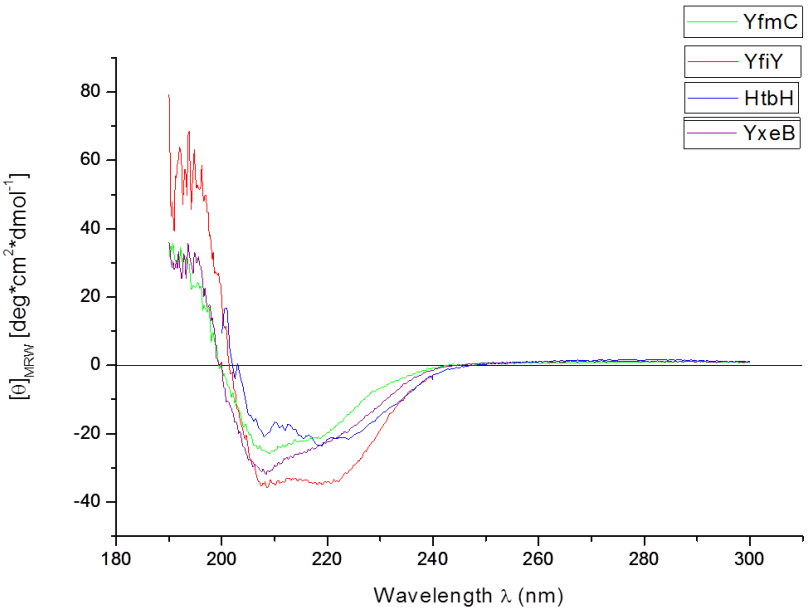

Figure 4.16 CD spectroscopy of siderophore-binding proteins YfmC, YxeB, YfiY[171] and HtbH in the far UV region. The control curve was monitored in 5 mM K_2HPO_4/KH_2PO_4, pH 7.0. [Θ]MRW is the mean residue ellipticity.

Table 4.3 Percentages of secondary structure elements in different SBPs determined by CD spectroscopy in the far UV region. Data extraction from spectral information was carried out by using a data deconvolution tool.

Secondary structure	Proportion (%) HtbH	Proportion (%) YfiY	Proportion (%) YxeB	Proportion (%) YfmC
α-helix	34.0	36.4	27.1	29.2
β-sheet	14.5	11.7	18.1	18.7
Coil	12.5	12.5	12.5	12.5
Random	33.4	32.0	35.0	34.0
Sum	94.4	92.7	92.8	94.4

4.5.4 Characterization of binding affinity by fluorescence titration spectroscopy

The purified iron-siderophore binding protein HtbH was used in a binding affinity assay by fluorescence titration spectroscopy (FP-6500 spectrofluorometer JASCO). The loss of the binding ability of HtbH towards ferric-siderophores is shown by a dramatic decrease of fluorescence quenching. If fluorescence quenching was observed during titration, data were set to 100 % starting fluorescence intensity and fitted by nonlinear regression analysis (Graphpad prism 6 software) using equation (3), according to the Law of Mass Action in a one-site binding model, where $[P]_t$ and $[L]_t$ are total protein and ligand concentrations, respectively, f_P, f_L and f_{PL} are the relative molar fluorescence coefficients of the free protein, the free ligand and the proteinligand complex, respectively, and K_D is the dissociation constant. K_D and f_{PL} were set as free parameters, and f_P was set to 100 % μM^{-1} according to the starting value. The data obtained from the spectroscopic measurements are shown in (Figure 4.12). The fluorescence intensity is plotted against the concentration of ferric-heterobacti A, ferric-heterobactin S2, ferric-erythrochelin and ferric-mecam. K_D values were calculated using equation (3) and are given in Table 4.4. The estimated binding affinities for all complexes are in the micromolar range.

$$F = ([P]_t - [L]_t - K_D) \times \frac{f_P}{2} + ([L]_t - [P]_t - K_D) \times \frac{f_L}{2} + ([P]_t + [L]_t + K_D) \times \frac{f_{PL}}{2} + (f_P + f_L - f_{PL}) \times \sqrt{\frac{([P]_t + [L]_t + K_D)^2}{4} - [P]_t \times [L]_t} \quad (3)$$

Table 4.4 Binding of different ferric-siderophores by HtbH.

Siderophore	K_D (µM)
Heterobactin A	4.1±1.95
Heterobactin S2	27.0 ±0.4
Mecam	7.24±1.34
Erythrochelin	~ 430

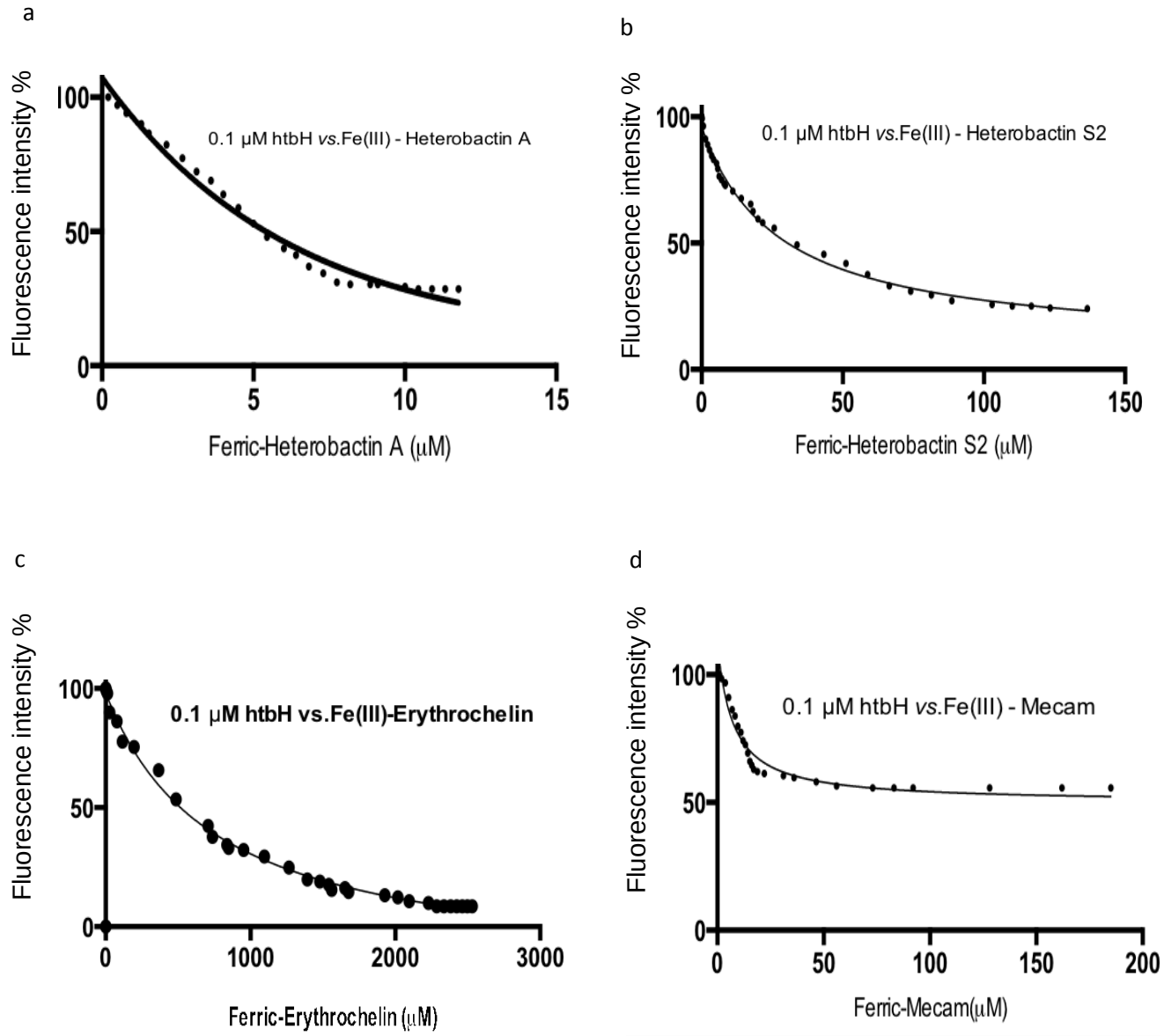

Fig 4.17 Fluorescence titration analysis of iron-siderophore binding protein htbH with (a) ferric-heterobactin A, (b) ferric-heterobactin S2, (c) ferric erythrochelin and (d) ferric-mecam.

Chapter 5

Discussion

5.1 Heterobactin Isolation and Structural Elucidation

5.1.1 Genome analysis of *R. erythropolis* PR4

R. erythropolis PR4 genome contains 17 secondary metabolite gene clusters based on antiSMASH secondary metabolite analysis, six of them encode for NRPS and two of PKS, suggesting the chance of a wide secondary metabolite range. As has been previously suggested, natural product gene clusters are among the most diverse and rapidly evolving genetic elements of a chromosome. This feature reflects the genome plasticity toward the selective pressure that continuously remodels the genetic elements of a species to best fit the environment.[146]

Table 5.1 Secondary metabolite gene cluster in *R. erythropolis* PR4. antiSMASH antibiotics and secondary metabolite analysis shell.[147,151]

No.	Cluster location	Predicted product
1	*R*PR4_ 233553 – 278496	PK I
2	*R*PR4_ 398578 – 444757	PK I
3	*R*PR4_ 591684 - 635601	Other
4	*R*PR4_1055114 – 1111808	NRPS
5	*R* PR4_1957706 – 2052893	NRPS
6	*R*PR4_2501139 – 2543676	Other
7	*R*PR4_2870647 – 2926165	NRPS
8	*R*PR4_3257161 – 3314570	NRPS-Terpene
9	*R*PR4_3342469 – 3409060	NRPS
10	*R*PR4_3641373 – 3724431	NRPS
11	*R*PR4_3772211 – 3828404	NRPS
12	*R*PR4_3907729 – 3928673	Terpene
13	*R*PR4_4128539 – 4138937	Ectoine
14	*R*PR4_5848307 – 5859194	Butyrolactone
15	*R*PR4_5875372 – 5896607	Amglyccycl
16	*R*PR4_6068957 – 6093890	Lantipeptide
17	*R*PR4_6463713 – 6475643	Bacteriocin

In this context, the chemical diversity among the siderophores isolated from several closely related *Rhodococcus* spp. is the most prominent sign of molecule evolution to best fit the environment under the constant force of selective pressure. In addition, the evidence of complex cross-talk mechanisms between distant gene clusters for the biosynthesis of a single natural product has been proposed.[121,152] As more complex regulatory mechanisms can control the biosynthesis of a single natural product, the rational discovery of new natural products using genome-mining strategies has become more challenging. In this context, the isolation and structural characterization of new siderophore molecules can provide both new information about the chemical diversity and NRPS-catalyzed biosynthesis of new natural products.

5.1.2 Heterobactin isolation and structural elucidation

The present work revises the structure of the siderophore heterobactin A,[123] the major compound secreted from *R. erythropolis* PR4 under iron-limiting conditions, and newly introduces the structures of its two sulfonated variants. In addition, the genetic and biochemical characterization of the biosynthetic elements allow the connection of the natural product with its gene cluster. In analogy to rhodochelin and rhodobactin (the other *Rhodococcus* siderophores characterized so far), heterobactins belong to the hydroxamate−catecholate mixed type family, with the common presence of 2,3-DHB and differently modified ornithine residues (Figure 5.1), truly suggesting these common features to be a shared motif among the *Rhodoccus* genus.[121,122]

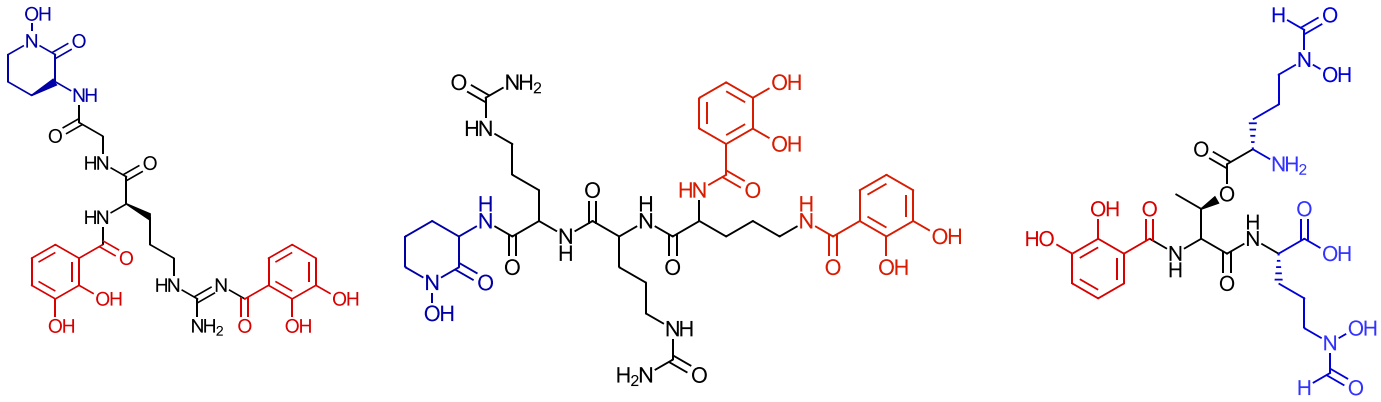

Heterobactin A Rhodobactin Rhodochelin

Figure 5.1 Chemical structures of heterobactin A, rhodobactin and rhodochelin with iron-coordinating functionalities: 2,3-DHB and ornithines.

5.1.3 Revise the chemical structure of heterobactin A (by Carrano et al. in 2001)

The present study revises the structure of heterobactin A that was described by Carrano et al. in 2001,[123] in which siderophore heterobactin A was characterized from *R. erythropolis* IGTS8. In this study, HR-MS measurements of the heterobactn A compound revealed this compound to have an *m/z* of 616.2357 and not 599.20959 $(M+H]^+$) as previously reported. This result suggests that the loss of an ammonia molecule occurred by spontaneous degradation during the isolation of the sample, as it has sometimes been observed during the purification of the sample when more than 30 °C was used to evaporate the MeOH in rotary evaporation.

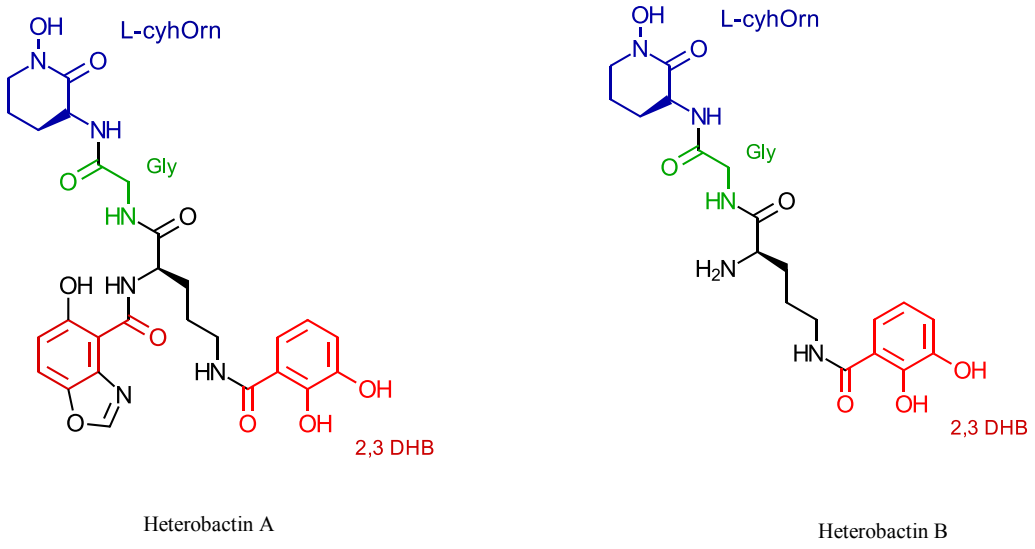

Figure 5.2 Chemical structures of heterobactin A and heterobactin B that were described by Carrano et al. in 2001.[123]

Additionally, the proposed structure of the original heterobactin A (containing a 1-carboxy-2 hydroxybenzoxazole (DHB) moiety) was recently synthesized by Bergeron *et al.*[153] A close inspection of the NMR data revealed a discrepancy with respect to those described by Carrano *et al.* The singlet signal at 8.35 ppm (s, ^{1}H) observed for the synthetic heterobactin A (characteristic of the 1-carboxy-2-hydroxybenzoxazole) was not observed by Carrano *et al*. In its place, three one-proton signals in multiplets have been assigned to 1-carboxy-2-hydroxybenzoxazole, which is obviously not correct. Therefore, the successful synthesis of the heterobactin A proposed originally provides the possibility of a direct comparison of the respective NMR results and allows the revision of the homonymous structure proposed by Carrano et al.[123]

5.2 Heterobactin Siderophores Sulfonation

5.2.1 Microbial natural products sulfonation

In this study, new sulfonated siderophores are reported; in the presence of inorganic sulfate in the medium, heterobactin A is partly modified *in vivo*, leading to heterobactins S1 and S2. The sulfonation occurs on the aromatic ring of one of the 2,3-DHB rings, probably without affecting octahedral iron coordination, as was observed for other sulfonated siderophores, such as petrobactin (Figure 5.3) and the pyoverdins.[154–156] The biological reason for the sulfonation is, as yet, unknown. It is believed that the modification increases the hydrophilicity of the compounds or could be necessary to prevent other strains in the same ecological niche from stealing the iron-siderophore complex. The sulfonation modification is probably an enzyme-catalyzed reaction, as sulfonation could not be observed spontaneously over time after incubation of purified heterobactin A in M9 minimal medium (data not shown). A BLAST search using the characterized arylsulfatase RHA1_ro259525 revealed the presence of five different enzyme homologues in *R. erythropolis* PR4 (Table 5.2). They are located outside the NRPS cluster, and, at the current point of knowledge, it is not possible to identify which one could be involved in the tailoring of heterobactin A.

Table 5.2 Bioinformatic identification of the homologues of the arylsulfatase RHA1_ro02595 in *R. erythropolis* PR4 that could be responsible for the sulfonation tailoring modification of heterobactin S1 and S2.[84]

locus name	refseq accession	protein size (aa)	% identity / similarity	
RER_11900	YP_002764637	786	69	83
RER_53450	YP_002768792	788	39	55
RER_45150	YP_002767961	778	38	54
RER_16070	YP_002765054	773	35	51
RER_19580	YP_002765405	545	26	38

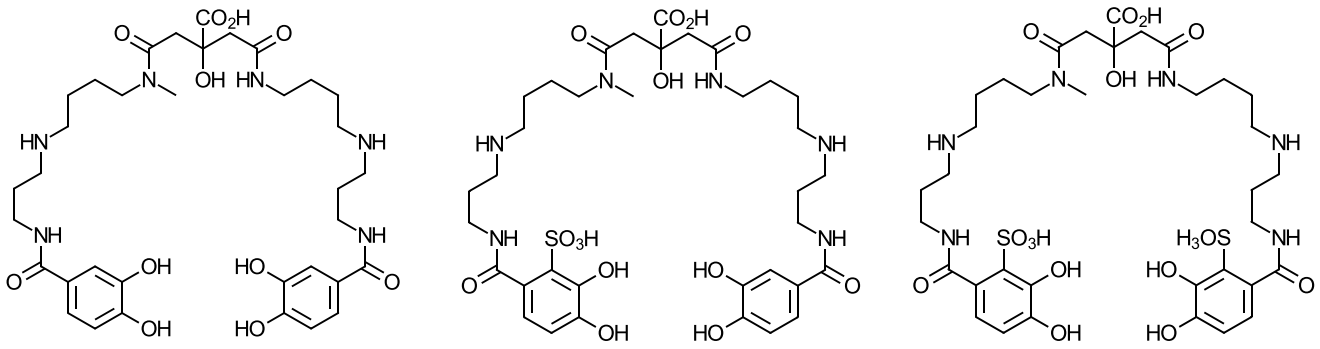

Petrobactin | Petrobactin sulfonate | Petrobactin disulfonate

Figure 5.3 Petrobactins and their sulfonated derivatives structures.

In addition, no information about the timing of the sulfonation reaction is known: it could occur either before the incorporation of 2,3-DHB into the peptide scaffold or, more likely, as a postassembly tailoring event. The purification of heterobactin S1 led to the recovery of an amount of material insufficient for NMR-based structure elucidation. Therefore, the structure of heterobactin S1 presented is solely based on the hypothesis that the sulfonation modification occurs on the alternate 2,3-DHB moiety (resulting in a different chromatographic retention), and is pictured in Figure 4.6C. Sulfonation of the aromatic ring would increase the water solubility of aromatic compounds[157] and might also lead to stabilization of the catechol ring against oxidation, and affect the Fe^{III} stability constant.

5.3 The Biosynthesis of Heterobactin A Requires NRPS Cross-talk

5.3.1 Identification of the gene set associated with heterobactin A biosynthesis

The whole set of gene cluster for biosynthesis of heterobactin A was identified by bioinformatic tools. The HtbG cluster comprises the complete trimodular NRPS synthetase. The presence of 2,3-DHB within the heterobactin A structure led to the investigation of the *R. erythropolis* PR4 genome to identify all the genes involved in biosynthesis of the aryl moiety. The isochorismatase enzyme has already been found to be encoded in the Htb cluster (HtbA) . Since the biosynthesis of aryl-capped

siderophore bacilibactin requires the activation of 2,3-DHB by the stand-alone A-domain HtbE prior to NRPS-catalyzed assembly, a gene homologous to htbE was identified in a different genomic region, along with two others genes involved in 2,3-DHB biosynthesis, namely htbB and htbC. These three genes are arranged in an operon-like way and, together with htbA, cover the entire 2,3-DHB pathway from the chorismate precursor to its activation as adenylate. The activated 2,3-DHB is then, subsequently, transferred to the *htbD* gene, which is described as an aryl carrier protein. The *htbH* gene is the putative iron-siderophore binding protein which was investigated later as a member belonging to the mixed-type catecholate–hydoxamate siderophore binding protein in this work. There are other siderophore export and iron-release genes, such as *htb*I putative siderophore exporter and *htb*J putative siderophore interactive protein. The latter, which is found in *E.coli* (*YqjH*), is able to catalyze the release of iron from a variety of iron chelators, including ferric triscatecholates and ferric dicitrate, displaying the highest efficiency for the hydrolyzed ferric enterobactin complex ferric (2,3-dihydroxybenzoylserine). The *htbF* was found in the gene cluster as a NADPH-dependent flavin mononucleotide (FMN) reductase. Finally, there is the putative MFS transporter (*htbK*) located upstream of the gene cluster.

5.3.2 Genome comparison between sequenced *Rhodococcus* strains

Genome comparison of *R. erythropolis* PR4 with other sequnced *Rhodococcus* strains displays a high degree of similarity with *Rhodococcus qingshengii* (90 %) and shares an identical gene arrangment within all essential genes that are involved in heterobactin biosynthesis. The three mixed-type catecholate–hydroxamate siderophores that were isolated from *Rhodococcus* (Figure 5.1) show that rhodobactin and heterobactin A exhibit chelator groups which are more tightly linked than rhodochelin siderophore: they have two catecholate groups and one hydroxamate group, while the rhodochelin has two hydroxamate groups and one catecholate group. Catecholates are known to bind iron more tightly than hydroxamates. This would lead to a siderophore with increased iron-siderophore complex binding affinity, providing an evolutionary advantage to the organism's capability to achieve under iron-limited conditions.

5.4 Biosynthesis of Canonical Amino Acid L-Orn

The hydroxamate moieties are crucial for iron coordination; biosynthesis of hydoxylated ornithine residue would require monooxygenase mediating of the *δ-N*-hydroxylation of lysine or L-Ornithine. This mechanism is used by NRPS-dependent and NRPS-independent pathways for siderophore biosynthesis, followed by the additional transfer of an acetyl or formyl group to the secondary amine intermediate to generate the functional hydroxamate moiety. This moiety subsequently incorporates enzymes into the siderophore scaffold by the NRPS-dependent or NRPS-independent assembly.[36,68]

5.4.1 Biochemical characterization of the L-Orn monooxygenase HMO

According to a bioinformatic analysis, HMO was predicted to belong to the *N*-hydroxylating flavoprotein monooxygenase, and it shares significant sequence identity and similarity with different homologues which have previously been characterized through inclusive biochemical and strucural studies.[121,71,158–164]

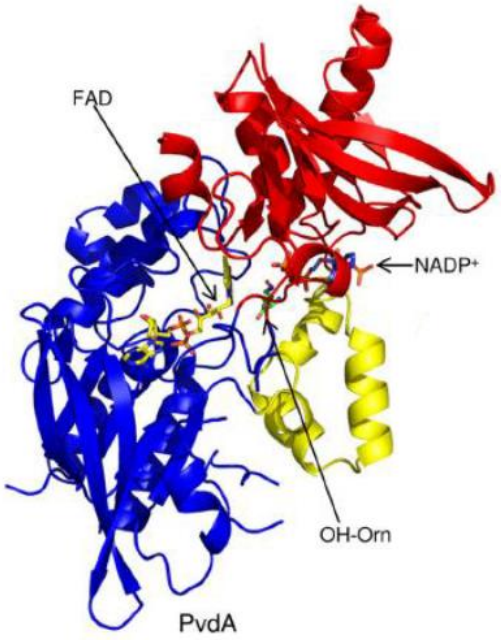

Figure 5.4 The crystal structure of the *P. aeruginosa* L-Orn monooxygenase PvdA. The FAD-binding domain is colored in blue, the NADPH-binding domain in red and the L-Orn binding domain in yellow. The catalytic pocket is located at the interface of the three domains. FAD, NADPH and L-Orn are shown in the PvdA structure as CPK-colored sticks.[165]

The bioinformatic analysis revealed the gene HMO exhibits 77.5 % sequential identity with Rmo from (*R. jostii* RHA1), 86.6 % similarity to the characterized FAD-dependent monooxygenase and PvdA (*Pseudomonas aeruginosa*, 30.6 % sequence identity, 42.9 % sequence homology), AmcK (Amycolatopsis sp.MJM2582 47.9%, 60.5%), CchB (*S.coelicolor*, 47.8 %, 61.68 %) and EtcB (*S.erythraea* 50%, 63.6%). Those flavoprotein monooxygenases share many characteristics, such as being encoded by a single gene, containing a tightly bound FAD cofactor, depending on NADPH as a coenzyme and electron donor and keeping the coenzyme bound during catalysis, and, finally, are composed of two dinucleotide binding domains (Rossmann fold) binding FAD and NADPH, respectively,[69] (Figure 5.4) and (Figure 5.5).

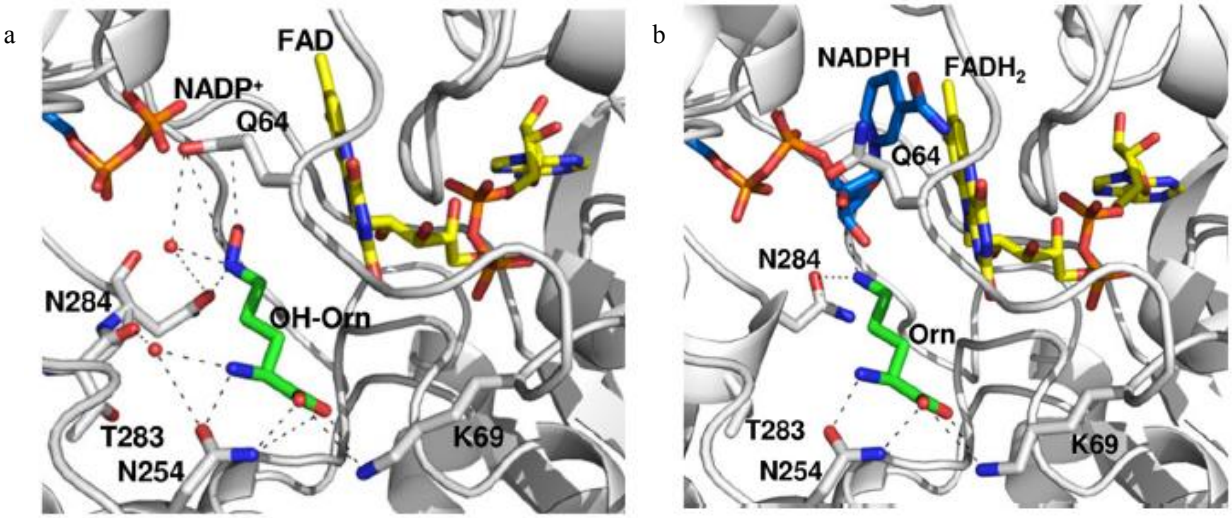

Figure 5.5 (a,b) Comparison of the oxidized and reduced active sites of PvdA, stereo views of the active site of the oxidized and reduced structures, respectively, oxygen atoms are *red*, nitrogen atoms are *dark blue* and phosphorus atoms are *orange*. Carbons are colored as per the molecule: PvdA, *slate blue* or *gray*; FAD(H2), *yellow*; ornithine, *green*; and NADP(H), *bright blue*. Hydrogen bonds are shown as *dashed lines*.[165]

An HMO catalyzed the first step in the formation of hydroxamates by oxidizing the terminal amino group of the (L-Orn) to produce the corresponding hydoxylamines (L-hOrn) in the presence of molecular oxygen, NADPH and FAD. HMO displays preference activity toward its cognate amino acid substrate and reducing the electron

donor NADPH. In addition, HMO shows classical Michaelis-Menten behavior compared with other L-Orn monooxygenase homologues; the kinetic parameters determination shows that HMO possesses similar catalytic efficiency to Rmo, while this catalytic activity is less than the high catalytic efficiency in EtcB or VbsO (Table 5.3).[72,164]

Table 5.3 Kinetic parameters for HMO-mediated L-Orn hydroxylation and comparison with others homologue L-Orn monooxygenases involved in siderophore biosynthesis.

Enzyme	Siderophore	K_M (mM)	k_{cat} (S^{-1})	k_{cat}/k_M ($^{s-1}$ mM^{-1})
HMO	Heterobactin A	1.8 ± 0.5	1.6 ± 0.01	0.35
Rmo[75]	Rhodochelin	1.6 ± 0.2	0.2331 ± 0.008	0.15
CchB[158]	Coelichelin	3.6 ± 0.58	0.290 ± 0.01	0.081
PvdA[159]	Pyoverdin	0.60 ± 0.07	0.4000± 0.05	0.67
EtcB[72]	Erythrochelin	0.286 ± 0.035	0.3267 ± 0.0005	1.14
VbsO[164]	Vicibactin	0.305 ± 0.024	1.80 ± 0.03	5.90

5.5 Biochemical and genetic model for heterobactin biosynthesis

5.5.1 Biosynthetic model for the assembly of heterobactins

The results obtained in this study allow the postulation of a model for heterobactin biosynthesis (Figure 5.6). The assembly of heterobactin A is initiated by HtbE, which activates 2,3-DHB, which is, subsequently, transferred to its cognate stand-alone aryl carrier protein HtbD. The first module of the NRPS HtbG assembles the tripeptide (DHB)2-Arg via an iterative mechanism, condensing two 2,3-DHB molecules with one PCP-bound arginine residue. Before the elongation of the peptide chain, the Arg side chain is epimerized by the E-domain.[54] The tripeptide is, subsequently, elongated by the incorporation of the fourth building block (Gly) in the following module, according to the classic linear logic of NRPS assembly lines. Interestingly, this second HtbG NRPS module features a highly unusual domain organization consisting of C-PCP-A; no other known NRPS features a similar modular domain organization. This peculiar organization may help to orient the Gly-S-PCP intermediate and the branched tripeptide (DHB)2-Arg in closer proximity on the acceptor and donor sites of the C-domain, respectively.

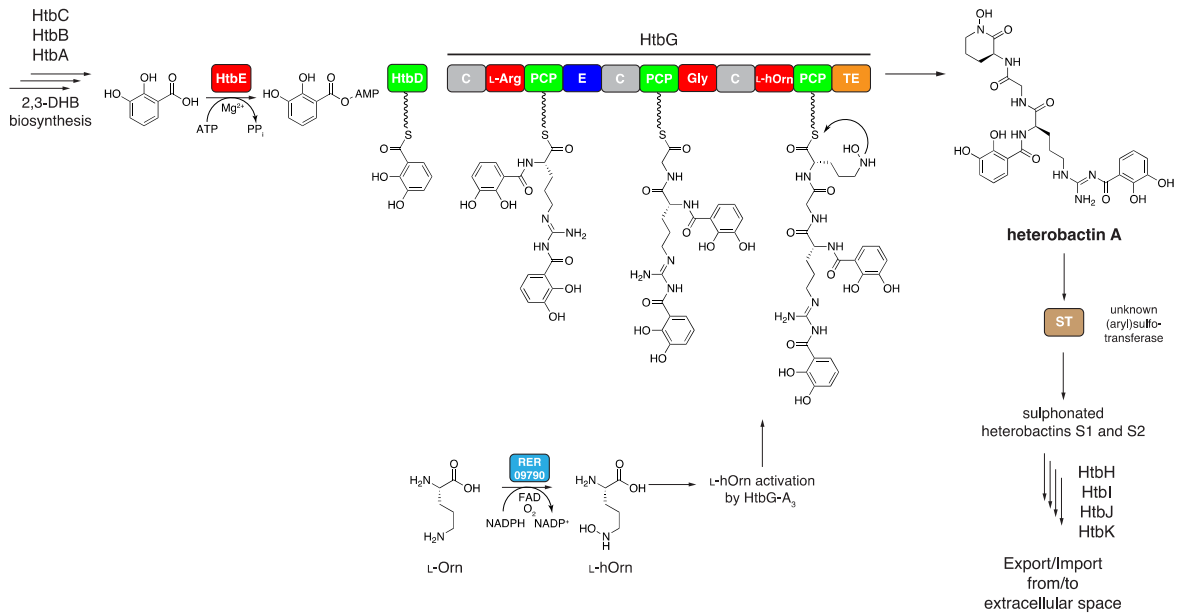

Figure 5.6 Proposed biosynthetic pathway for heterobactin assembly. The two nonproteinogenic building blocks 2,3-DHB and L-hOrn are synthesized by the corresponding pathways. The NRPS HtbG assembles the pentapeptide via an iterative mechanism on its initiation module and releases it through the L-hOrn side chain cyclization.

Next, the HtbG C-terminal module attaches the fifth and last L-hOrn building block (which is synthesized by the L-Orn monoxygenase RER_09790)[75,68] to the main peptide scaffold. Finally, the terminal TE-domain catalyzes the assembly of heterobactin A through cyclization of the L-hOrn side chain. Before the export to the extracellular space to carry out its biological function, one of the two catecholate moieties could be further tailored by an unknown (aryl)sulfotransferase (Table 5.2), giving rise to the sulfonated heterobactin variants S1 and S2.

5.6 Iron-siderophore Binding Protein

5.6.1 Bioinformatic analysis of HtbH (iron-siderophore binding protein)

The sequence of HtbH indicates that it encodes a hydrophilic protein with a signal sequence and a consensus sequence for a signal peptide, which indicate an N-terminal glycryl-cisteine-lipid anchor for the mature protein; this structure is found in FhuD from *B.subtilis*.[166] The lipid anchor may keep the hydrophilic protein associated with the outside of the cytoplasmic membrane of *R.erythropolis* PR4 and prevent its escape into the surrounding medium, and may be a special adaptation to the lack of an outer membrane in Gram-positive bacteria.[112] HtbH displays low but significant homologues to the catecholate-binding proteins FepB, CeuA, YicQ and FeuA, and hydroxamate-binding protein FhuD; the high homology is found in FepB (27.4 % identity, 44.6 % similarity) and in FhuD (*B_sub*) (22.2 % identity, 37.9 % similarity), that indicate the unique mixed-type binding protein sequence in HtbH.

5.6.2 Structure analysis of iron-siderophore binding protein (HtbH)

HtbH iron-siderophore binding protein was recombinanty produced and purified in the mature form with yelds of 10 mg/mL of bacteria culture. The circular dichroism (CD) spectroscopy analysis displays the deconvolution of the spectra revealing that HtbH was efficienty folded with dominating proportions of α-helical elements at a 1.5- to 3.0-fold higher abundance compared with the estimated percentage of β-sheet elements. This character shows that HtbH belong the type III periplasmic-binding proteins, that adopt structure containing two globular domains connected by short stretches of β-strand allowing interdomain movement via a “Venus flytrap” like Packman. The electrostatic environments of the siderophore-binding pocket reflect the chemical nature of their potential ligands very well. Recent structural studies on type III periplasmic-binding protein display a better understanding of how ferric-siderophore complexes are bound in the active site. The hydroxamate siderophore generally prefers the hydrophobic-binding pocket, whereas for catecholate and α-hydroxycaroxylate siderophores, basic Arg or Lys residues are required to reduce the net negative charge of the ferric-siderophore complex.[106,107] According to the chemical nature of the HtbH mixed-type (catecholate–hydroxamate) iron-siderophore binding protein, its binding pocket could be comprised of both hydrophobic and basic residues and, hence, reflects the chemical

nature of the mixed-type siderophores; interestingly, this is a unique iron-siderophore binding protein structure. HtbH, similar to an FhuD ferric-hydroxamate binding protein, exhibits that binding occurs in a hydrophobic-binding pocket when bound with hydroxamate moieties (Figure 5.7).[106]

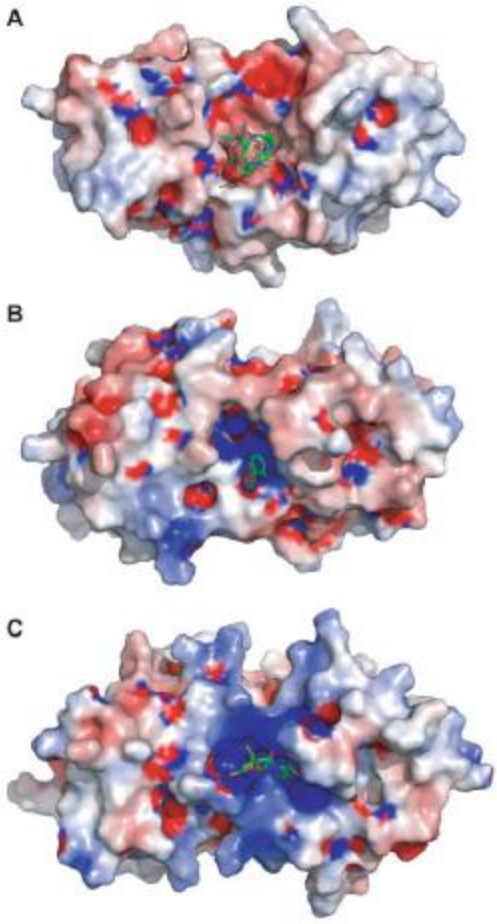

Figure 5.7 Electrostatic surface potential plots of (A) FhuD bound with ferrichrome, (B) FeuA bound with ferric-bacillibactin and (C) HtsA bound with ferric-staphyloferrin A. The basic binding pockets of FeuA and HtsA are clearly seen here, and the more hydrophobic-binding pockets of FhuD are apparent. Electrostatic potentials are plotted, where blue and red represent positive and negative electrostatic potentials, respectively.[167]

The side chain of Arg 84 appears to be an essential recognition-binding factor, forming hydrogen bonds with two of three carbonyl oxygen atoms of the hydroxamate acid moieties. In CeuE, a catecholate-siderophore binding protein (such as FeuA, Figure (5.8), and FepB), which shows homologues with HtbH, the binding of a ferric-

catecholate by a single CeuE molecule is mediated by three Arg residues which neutralize the net negative charge of each ferric-catecholate molecule along with coordinating ligands from Gln 98, Lys 121 and Tyr 288.[113]

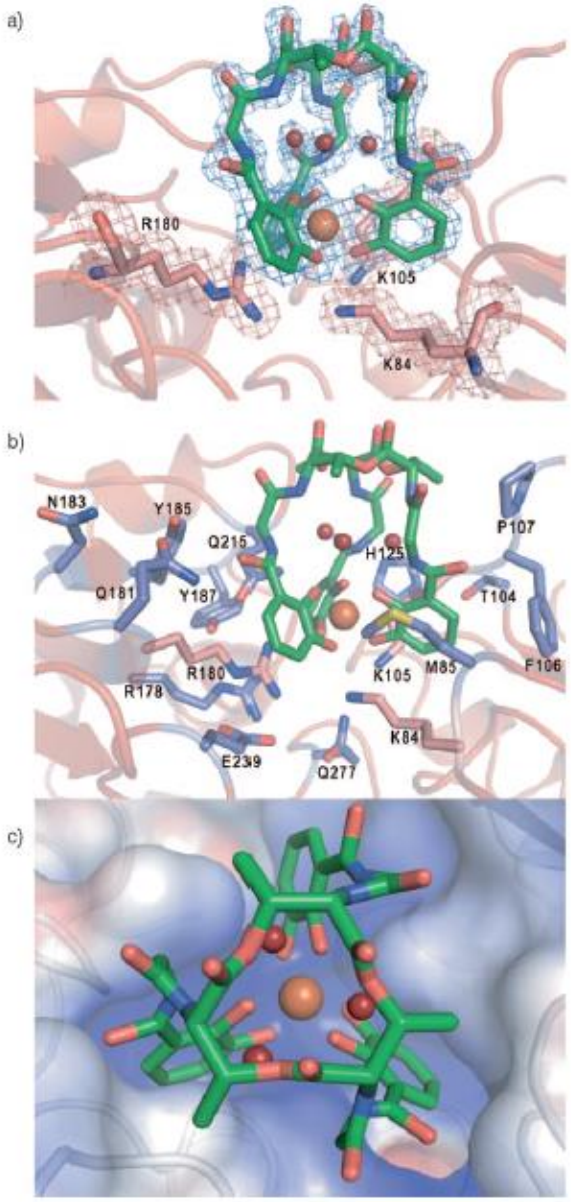

Figure 5.8 Detailed view of the siderophore-binding pocket of FeuA; ligand atoms: green C, red O, blue N, orange sphere Fe. a) SIGMAA weighted ($F_{obs} - F_{calc}$) electron-density difference (blue) calculated at 1.7 Å resolution (contour level 2.7σ) for $[FeIII(BB)]^{3-}$ and the three water molecules (dark red spheres); b) The side chains of other residues which make up the binding site are also illustrated (C light blue). c) Electrostatic surface representation of the binding pocket (from -5 (red) to +5 (blue)k_BT/e_c.[13]

The crystal structure of YciQ mixed-type (catecholate/α-hydroxycarboxylate) iron-siderophore binding protein from *B.subtilis* is a close structural homologue of CeuE (41 % sequence idintity). The structure of YciQ displays a positively charged pocket similar to that of CeuE and should accommodate a negatively charged ferric-petrobactin molecule.[168] The carboxyl in the citrate moiety may be stabilized by a hydrogen bond with His-214, Lys-84 and Arg-236 are in carbonyl group to make direct contact with ferric-petrobactin. YfiY is predicted to bind ferric citrate-hydroxamate, such as a ferric arthrobactin or schizokinen, then their binding pocket consists of hydrophobic and basic residues.[169] According to the previous, HtbH iron-siderophore binding protein mixed-type (catecholate–hydroxamate) siderophore binds with both the catecholate and hydroxamate siderophore. Finally, the crystal structure for α-hydroxycarboxylate HtsA-binding protein isolated from *Staphyloococcus aureus* was solved and shows a positively (basicity) charged binding pocket.[170]

5.6.3 Characterization of Siderophore Specificities and Binding Affinities by Fluorescence Titration Spectroscopy

5.6.3.1 HtbH is an SBP specific for heterobactin A

Ligand specificity of the recombinant HtbH was determined by fluorescence spectroscopy. Quenching of intrinsic protein fluorescence during titration with different siderophore solutions indicates specific binding of a ligand. Fluorescence data were analyzed by nonlinear regression analysis using a one-site binding model (Graphpad prism6 software) that allowed for the determination of dissociation constants (K_D). HtbH was found to bind mixed-type siderophore ferric-heterobactin A with higher (K_D ~ 4 μM), such as all endogenous siderophores which have been studied previously.[114,171] On the other hand, the ferric-heterobactin S2 displays lower binding affinity toward HtbH (K_D ~ 27 μM), which indicates the sulfonation effects on the binding affinity toward HtbH. The K_D values defining the binding of HtbH to heterobactin A, a mixed catecholate–hydroxamate siderophore, is, therefore, in the range of the affinity displays by other ferric mixed-type siderophores, such as ferric-aerobactin (carboxylate–hydroxamate) toward YfiY (K_D ~ 6 μM), ferric-arthrobactin (carboxylate–hydroxamate) toward YxeB (K_D ~ 1 μM), and ferric-arthrobactin toward

FhuD (K_D ~ 5 μM).[171] The binding affinity of HtbH for ferric-mecam (K_D ~ 7 μM) is only slightly lower than for the ferric-heterobactin A ligand, indicating that the catecholate siderophore has less binding affinity toward HtbH than the mixed-type (catecholate–hydroxamate) siderophore. Compared with other catecholate siderophores, such as ferric-bacilibactin towards the FeuA-binding protein from *B.subtilis* where the binding affinity was (K_D ~ 15 nM)[172] or ferric-enterobactin towards the FepB-binding protein from *E.coli* where the binding affinity was (K_D ~ 30 nM),[118] the binding affinity of HtbH for ferric-mecam is weaker than other catecholate siderophores toward their binding proteins. Surprisingly, the binding affinity of HtbH for ferric-erythrochelin (hydroxamate siderophore) shows very low affinity compared with other types of siderophore (K_D ~ 430 μM); this indicates that HtbH has a very low binding affinity toward hydroxamate siderophores. The ferric-ferrichrom (hydroxamate siderophore) displays binding affinity (K_D ~ 7 μM) toward YfiY- and YxeB-binding proteins,[171] and these are higher than the binding affinity of HtbH for ferric-erythrochelin.

5.7 Outlook

5.7.1 Heterobactins sulfonation (sulfation)

There are five enzymes belonging to the arylsulfatase (ARS) superfamily (in the chromosomal DNA of *R. erythropolis* PR4) which could be the reason for the posttranslation modification that catalyzed Heterobactin A to its sulfonation derivatives S1 and S2. There are other classes of enzymes that may be responsible for sulfonation: so-called sulfotransferase enzymes.

5.7.2 Biochemical and genetic analyses of NADPH-dependent FMN reductase and the siderophore interacting protein

There are two known general mechanisms that lead to iron release from siderophores. The first is used TE-domain and the second is the reduction of siderophore-bound Fe^{III} to Fe^{II}. The soluble flavin reductases that catalyze reduction of several flavin-based substrates such as FMN, FAD and riboflavin by using NAD(P)H or NADH as an electron donor. The siderophore interacting protein is able to catalyze the release of iron from a variety of iron chelators.

5.7.3 Crystallization and structural studies of the *N*-htdroxylating flavoprotein monooxygenase

Crystallization-studies of HMO, with and without the substrate L-Orn or, the coenzymes-FAD and NADPH, were initiated, Crystals were obtained (only in the absence of substrate and coenzymes) by combining 0.5-2.0 µL of 15.8 mg/mL enzyme (in 150 mM NaCl, 10 mM HEPES pH 7.5) with 0.5 µL of 1.6 M ammonium sulfate, 0.1 M sodium chloride, 0.1 M HEPES pH 7.5. Through whole-crystal seeding experiments, crystal size was increased and diffraction quality was improved (from ~8 Å to ~3.8 Å); however, the resolution was not adequate for phasing by molecular replacement. Further crystal optimization will be necessary to achieve higher resolution for structure elucidation. (Figure 5.9) shows the crystals for HMO monooxygenase.

Figure 5.9 The crystals of HMO monooxygenase.

5.7.4 X-ray crystallography structure of the *R. erythropolis* PR4 iron-siderophore binding protein (HtbH) bound to a mixed-type (catecholate-hydroxamate) Heterobactin A siderophore

HtbH was initially screened for crystals in sparse-matrix conditions at 10 mg/mL protein (in 150 mM NaCl, 10 mM HEPES pH 7.5), but very little precipitation was observed. The concentration was therefore increased to 75 mg/mL, which yielded a suitable amount of precipitation, but no crystals could be obtained. The study was carried out with and without the ferric-siderophore complex.

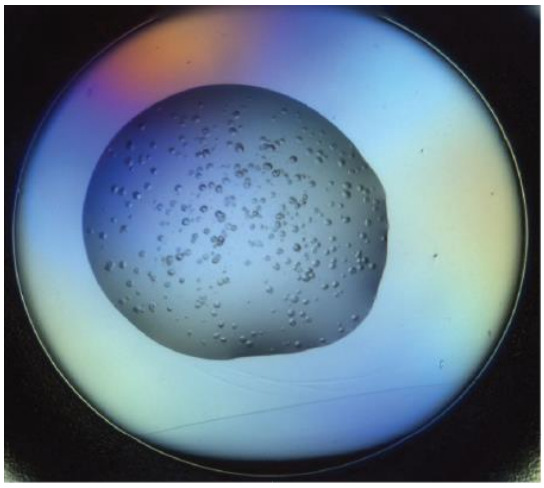

Figure 5.10 The crystals of HtbH iron-siderophore binding protein.

References

References

1. Kagawa Y, Mitani Y, Yun H-Y, Nakashima N, Tamura N, Tamura T. Identification of a methanol-inducible promoter from *Rhodococcus erythropolis* PR4 and its use as an expression vector. *J Biosci Bioeng*. 2012;113(5):596-603.

2. Mitani Y, Watanabe T, Kondo K, Tamura T. Identification of Strain-specific genes in *Rhodococcus erythropolis* using a modified HiCEP method. *Open Biotechnol J*. 2007;1:66-71.

3. Sekine M, Tanikawa S, Omata S, et al. Sequence analysis of three plasmids harboured in *Rhodococcus erythropolis* strain PR4. *Environ Microbiol*. 2006;8(2):334-346.

4. Zerikly M, Challis GL. Strategies for the discovery of new natural products by genome mining. *Chembiochem*. 2009;10(4):625-633.

5. Wandersman C, Delepelaire P. Bacterial iron sources: from siderophores to hemophores. *Annu Rev Microbiol*. 2004;58:611-647.

6. Touati D. Iron and oxidative stress in bacteria. *Arch Biochem Biophys*. 2000;373(1):1-6. doi:10.1006/abbi.1999.1518.

7. Halliwell B, Gutteridge JM. Oxygen toxicity, oxygen radicals, transition metals and disease. *Biochem J*. 1984;219(1):1-14. doi:10.1016/j.siny.2010.04.003.

8. Neilands JB. Siderophores: structure and function of microbial iron transport compounds. *J Biol Chem*. 1995;270(45):26723-26726.

9. Schaible UE, Kaufmann SHE. A nutritive view on the host–pathogen interplay. *TRENDS Microbiol*. 2005;13(8):373-380.

10. Miethke M, Marahiel M. A. Siderophore-based iron acquisition and pathogen control. *Microbiol Mol Biol Rev*. 2007;71(3):413-451.

11. Miethke M, Klotz O, Linne U, May JJ, Beckering CL, Marahiel M. A. Ferri-bacillibactin uptake and hydrolysis in *Bacillus subtilis*. *Mol Microbiol*. 2006;61(6):1413-1427.

12. Andrews SC, Robinson AK, Rodríguez-Quiñones F. Bacterial iron homeostasis. *FEMS Microbiol Rev*. 2003;27(2-3):215-237.

13. Peuckert F, Miethke M, Albrecht AG, Essen LO, Marahiel M. A. Structural basis and stereochemistry of triscatecholate siderophore binding by FeuA. *Angew Chemie - Int Ed*. 2009;48(42):7924-7927. doi:10.1002/anie.200902495.

14. Takase H, Nitanai H, Hoshino K, Otani T. Impact of Siderophore Production on *Pseudomonas aeruginosa* Infections in Immunosuppressed Mice. *Infect Immun*. 2000;68(4):1834-1839.

15. Pandey A, Bringel F, Meyer J-M. Iron requirement and search for siderophores in lactic acid bacteria. *Appl Microbiol Biotechnol*. 1994;40(5):735-739.

16. Weinberg ED. The Lactobacillus anomaly: total iron abstinence. *Perspect Biol Med*. 1997;40(4):578-583. doi:10.1353/pbm.1997.0072.

17. Neilands JB, Winkelmann G, Van der Helm D. *Iron Transport in Microbes, Plants, and Animals*. VCH; 1987.

18. Voßen W, Fuchs R, Taraz K, Budzikiewicz H. Can the peptide chain of a pyoverdin be bound by an ester bond to the chromophore? - The old problem of pseudobactin 7SR1. *Zeitschrift fur Naturforsch - Sect C J Biosci*. 2000;55(3-4):153-164.

19. Twort FW, Ingram GLY. A Method for Isolating and Cultivating the Mycobacterium enteritidis chronicae pseudotuberculosae bovis, Johne, and some Experiments on the Preparation of a Diagnostic Vaccine for Pseudo-tuberculous Enteritis of Bovines. *Proc R Soc London Ser B, Contain Pap a Biol Character*. 1912:517-542.

20. Francis J, Madinaveitia J, Macturk HM, Snow GA. Isolation from acid-fast bacteria of a growth-factor for *Mycobacterium johnei* and of a precursor of phthiocol. *Nature*. 1949;163(4140):365.

21. Neilands JB. A crystalline organo-iron pigment from a rust fungus (*ustilago sphaerogena*) 1. *J Am Chem Soc*. 1952;74(19):4846-4847.

22. Hesseltine CW, Pidacks C, Whitehill AR, Bohonos N, Hutchings BL, Williams JH. Coprogen, a new growth factor for coprophilic fungi. *J Am Chem Soc*. 1952;74(5):1362.

23. Snow GA. Mycobactin. A growth factor for *Mycobacterium johnei*. Part II. Degradation, and identification of fragments. *J Chem Soc*. 1954:2588-2596.

24. Burton MO, Sowden FJ, Lochhead AG. Studies on the isolation and nature of the'terregens factor'. *Can J Biochem Physiol*. 1954;32(4):400-406.

25. Garibaldi JA, Neilands JB. Formation of iron-binding compounds by micro-organisms. 1956.

26. Ito T, Neilands JB. Products of "Low-iron Fermentation" with *Bacillus subilis*: Isolation, Characterization and Synthesis of 2, 3-Dihydroxybenzoylglycine1, 2. *J Am Chem Soc*. 1958;80(17):4645-4647.

27. Emery T, Neilands JB. The Iron-Binding Centre of Ferrichrome Compounds. 1959.

28. Bickel H, Gäumann E, Nussberger G, et al. Stoffwechselprodukte von Actinomyceten. 25. Mitteilung. Über die Isolierung und Charakterisierung der Ferrimycine A1 und A2, neuer Antibiotika der Sideromycin-Gruppe. *Helv Chim Acta*. 1960;43(7):2105-2118.

29. Bickel H, Bosshardt R, Gäumann E, et al. Stoffwechselprodukte von Actinomyceten. 26. Mitteilung. Über die Isolierung und Charakterisierung der Ferrioxamine A—F, neuer Wuchsstoffe der Sideramin- Gruppe. *Helv Chim Acta*. 1960;43(7):2118-2128.

30. Bickel H, Hall GE, Keller-Schierlein W, Prelog V, Vischer E, Wettstein A. Stoffwechselprodukte von Actinomyceten. 27. Mitteilung. Über die Konstitution von Ferrioxamin B. *Helv Chim Acta*. 1960;43(7):2129-2138.

31. Anderegg G, l'Eplattenier F, Schwarzenbach G. Hydroxamate complexes. III. Iron (III) exchange between sideramines and complexones. A discussion of the formation constants of the hydroxamate complexes. *Helv Chim Acta*. 1963;46:1409-1422.

32. O'Brien IG, Gibson F. The structure of enterochelin and related 2,3-dihydroxy-N-benzoyne conjugates from *Eschericha Coli*. *Biochim Biophys Acta - Gen Subj*. 1970;215(2):393-402. doi:10.1016/0304-4165(70)90038-3.

33. Pollack JR, Neilands JB. Enterobactin, an iron transport compound from *Salmonella typhimurium*. *Biochem Biophys Res Commun*. 1970;38(5):989-992.

34. Barry SM, Challis GL. Recent advances in siderophore biosynthesis. *Curr Opin Chem Biol*. 2009;13(2):205-215.

35. Pattus F, Abdallah MA. Siderophores and Iron-Transport in Microorganisms. *J Chinese Chem Soc*. 2000;47(1):1-20.

36. Challis GL. A widely distributed bacterial pathway for siderophore biosynthesis independent of nonribosomal peptide synthetases. *Chembiochem*. 2005;6(4):601-611.

37. Buyer JS, De Lorenzo V, Neilands JB. Production of the siderophore aerobactin by a *halophilic pseudomonad*. *Appl Environ Microbiol*. 1991;57(8):2246-2250.

38. Finking R, Marahiel M. A. Biosynthesis of nonribosomal peptides 1. *Annu Rev Microbiol*. 2004;58:453-488.

39. De Lorenzo V, Bindereif A, Paw BH, Neilands JB. Aerobactin biosynthesis and transport genes of plasmid ColV-K30 in *Escherichia coli* K-12. *J Bacteriol*. 1986;165(2):570-578.

40. Thariath A, Socha D, Valvano MA, Viswanatha T. Construction and biochemical characterization of recombinant cytoplasmic forms of the IucD protein (lysine: N6-hydroxylase) encoded by the pColV-K30 aerobactin gene cluster. *J Bacteriol*. 1993;175(3):589-596.

41. Coy M, Paw BH, Bindereif A, Neilands JB. Isolation and properties of N. epsilon.-hydroxylysine: acetyl coenzyme A N. epsilon.-transacetylase from *Escherichia coli* pABN11. *Biochemistry*. 1986;25(9):2485-2489.

42. Kadi N, Oves-Costales D, Barona-Gomez F, Challis GL. A new family of ATP-dependent oligomerization-macrocyclization biocatalysts. *Nat Chem Biol*. 2007;3(10):652-656.

43. Kadi N, Arbache S, Song L, Oves-Costales D, Challis GL. Identification of a gene cluster that directs putrebactin biosynthesis in Shewanella species: PubC catalyzes cyclodimerization of N-hydroxy-N-succinylputrescine. *J Am Chem Soc*. 2008;130(32):10458-10459.

44. Schwarzer D, Marahiel M. A. Multimodular biocatalysts for natural product assembly. *Naturwissenschaften*. 2001;88(3):93-101.

45. Walsh CT, Fischbach MA. Natural products version 2.0: connecting genes to molecules. *J Am Chem Soc*. 2010;132(8):2469-2493.

46. Marahiel M. A. Working outside the protein-synthesis rules: Insights into non-ribosomal peptide synthesis. *J Pept Sci*. 2009;15(12):799-807. doi:10.1002/psc.1183.

47. Condurso HL, Bruner SD. Structure and noncanonical chemistry of nonribosomal peptide biosynthetic machinery. *Nat Prod Rep*. 2012;29(10):1099. doi:10.1039/c2np20023f.

48. Sieber S a, Marahiel M. A. Molecular Mechanisms Underlying Nonribosomal Peptide Synthesis: Approaches to New Antibiotics. *Chem Rev*. 2005;105(2):715-738. doi:10.1021/cr0301191.

49. Conti E, Stachelhaus T, Marahiel M. A, Brick P. Structural basis for the activation of phenylalanine in the non-ribosomal biosynthesis of gramicidin S. *EMBO J*. 1997;16(14):4174-4183.

50. Reuter K, Mofid MR, Marahiel M, A. Ficner R. Crystal structure of the surfactin synthetase-activating enzyme sfp: a prototype of the 4'-phosphopantetheinyl transferase superfamily. *EMBO J*. 1999;18(23):6823-6831. doi:10.1093/emboj/18.23.6823.

51. Lambalot RH, Gehring AM, Flugel RS, et al. A new enzyme superfamily-the phosphopantetheinyl transferases. *Chem Biol*. 1996;3(11):923-936.

52. Weber T, Baumgartner R, Renner C, Marahiel M. A, Holak T a. Solution structure of PCP, a prototype for the peptidyl carrier domains of modular peptide synthetases. *Structure*. 2000;8(4):407-418. doi:10.1016/S0969-2126(00)00120-9.

53. Parris KD, Lin L, Tam A, et al. Crystal structures of substrate binding to *Bacillus subtilis* holo-(acyl carrier protein) synthase reveal a novel trimeric arrangement of molecules resulting in three active sites. *Structure*. 2000;8(8):883-895. doi:10.1016/S0969-2126(00)00178-7.

54. Linne U, Marahiel M. A. Control of directionality in nonribosomal peptide synthesis: role of the condensation domain in preventing misinitiation and timing of epimerization. *Biochemistry*. 2000;39(34):10439-10447.

55. Belshaw PJ, Walsh CT, Stachelhaus T. Aminoacyl-CoAs as probes of condensation domain selectivity in nonribosomal peptide synthesis. *Science (80-)*. 1999;284(5413):486-489.

56. Keating TA, Marshall CG, Walsh CT, Keating AE. The structure of VibH represents nonribosomal peptide synthetase condensation, cyclization and epimerization domains. *Nat Struct Mol Biol*. 2002;9(7):522-526.

57. Samel SA, Schoenafinger G, Knappe TA, Marahiel MA, Essen L-O. Structural and functional insights into a peptide bond-forming bidomain from a nonribosomal peptide synthetase. *Structure*. 2007;15(7):781-792.

58. Leslie AGW. Refined crystal structure of type III chloramphenicol acetyltransferase at 1· 75 Å resolution. *J Mol Biol*. 1990;213(1):167-186.

59. Marahiel M. A, Stachelhaus T, Mootz HD. Modular Peptide Synthetases Involved in Nonribosomal Peptide Synthesis. *Chem Rev*. 1997;97(7):2651-2674. doi:10.1016/S0006-3495(02)75175-8.

60. Linne U, Marahiel M. A. Reactions catalyzed by mature and recombinant nonribosomal peptide synthetases. *Methods Enzymol*. 2004;388(2001):293-315. doi:10.1016/S0076-6879(04)88024-8.

61. Walsh CT. The chemical versatility of natural-product assembly lines. *Acc Chem Res*. 2008;41(1):4-10. doi:10.1021/ar7000414.

62. Pfeifer E, Pavela-Vrancic M, Von Dohren H, Kleinkauf H. Characterization of tyrocidine synthetase 1 (TY1): Requirement of posttranslational modification for peptide biosynthesis. *Biochemistry*. 1995;34(22):7450-7459. doi:10.1021/bi00022a019.

63. Weber G, Schorgendorfer K, Schneider-Scherzer E, Leitner E. The peptide synthetase catalyzing cyclosporine production in *Tolypocladium niveum* is encoded by a giant 45.8-kilobase open reading frame. *Curr Genet*. 1994;26(2):120-125. doi:10.1007/BF00313798.

64. Stachelhaus T, Walsh CT. Mutational analysis of the epimerization domain in the initiation module PheATE of gramicidin S synthetase. *Biochemistry*. 2000;39(19):5775-5787. doi:10.1021/bi9929002.

65. Luo L, Kohli RM, Onishi M, Linne U, Marahiel M. A, Walsh CT. Timing of epimerization and condensation reactions in nonribosomal peptide assembly lines: kinetic analysis of phenylalanine activating elongation modules of tyrocidine synthetase B. *Biochemistry*. 2002;41(29):9184-9196.

66. Schwarzer D, Finking R, Marahiel M. A. Nonribosomal peptides: from genes to products. *Nat Prod Rep*. 2003;20(3):275-287. doi:10.1039/b111145k.

67. Schoenafinger G, Schracke N, Linne U, Marahiel M. A. Formylation domain: an essential modifying enzyme for the nonribosomal biosynthesis of linear gramicidin. *J Am Chem Soc*. 2006;128(23):7406-7407.

68. Olucha J, Lamb AL. Mechanistic and structural studies of the *N*-hydroxylating flavoprotein monooxygenases. *Bioorg Chem*. 2011;39(5):171-177.

69. Van Berkel WJH, Kamerbeek NM, Fraaije MW. Flavoprotein monooxygenases, a diverse class of oxidative biocatalysts. *J Biotechnol*. 2006;124(4):670-689.

70. Kopp F, Linne U, Oberthür M, Marahiel M. A. Harnessing the chemical activation inherent to carrier protein-bound thioesters for the characterization of lipopeptide fatty acid tailoring enzymes. *J Am Chem Soc*. 2008;130(8):2656-2666.

71. Robbel L, Knappe TA, Linne U, Xie X, Marahiel M. A. Erythrochelin–a hydroxamate-type siderophore predicted from the genome of *Saccharopolyspora erythraea*. *FEBS J*. 2010;277(3):663-676.

72. Robbel L, Helmetag V, Knappe TA, Marahiel M. A. Consecutive enzymatic modification of ornithine generates the hydroxamate moieties of the siderophore erythrochelin. *Biochemistry*. 2011;50(27):6073-6080.

73. McMorran BJ, Shantha Kumara HMC, Sullivan K, Lamont IL. Involvement of a transformylase enzyme in siderophore synthesis in *Pseudomonas aeruginosa*. *Microbiology*. 2001;147(6):1517-1524.

74. Lamont IL, Martin LW, Sims T, Scott A, Wallace M. Characterization of a Gene Encoding an Acetylase Required for Pyoverdine Synthesis in *Pseudomonas aeruginosa* Characterization of a Gene Encoding an Acetylase Required for Pyoverdine Synthesis in Pseudomonas aeruginosa. *Society*. 2006;188(8):3149-3152. doi:10.1128/JB.188.8.3149.

75. Bosello M, Mielcarek A, Giessen TW, Marahiel M. A An enzymatic pathway for the biosynthesis of the formylhydroxyornithine required for rhodochelin iron coordination. *Biochemistry*. 2012;51(14):3059-3066. doi:10.1021/bi201837f.

76. Linne U, Schwarzer D, Schroeder GN, Marahiel M. A. Mutational analysis of a type II thioesterase associated with nonribosomal peptide synthesis. *Eur J Biochem*. 2004;271(8):1536-1545.

77. Schwarzer D, Mootz HD, Linne U, Marahiel M. A. Regeneration of misprimed nonribosomal peptide synthetases by type II thioesterases. *Proc Natl Acad Sci*. 2002;99(22):14083-14088.

78. Yeh E, Kohli RM, Bruner SD, Walsh CT. Type II thioesterase restores activity of a NRPS module stalled with an aminoacyl-S-enzyme that cannot be elongated. *ChemBioChem*. 2004;5(9):1290-1293. doi:10.1002/cbic.200400077.

79. Schneider A, Marahiel M. A. Genetic evidence for a role of thioesterase domains, integrated in or associated with peptide synthetases, in non-ribosomal peptide biosynthesis in *Bacillus subtilis*. *Arch Microbiol*. 1998;169(5):404-410.

80. Mougous JD, Green RE, Williams SJ, Brenner SE, Bertozzi CR. Sulfotransferases and Sulfatases in *Mycobacteria*. *Chem Biol*. 2002;9(7):767-776. doi:10.1016/S1074-5521(02)00175-8.

81. Bojarová P, Williams SJ. Sulfotransferases, sulfatases and formylglycine-generating enzymes: a sulfation fascination. *Curr Opin Chem Biol*. 2008;12(5):573-581. doi:10.1016/j.cbpa.2008.06.018.

82. Malojcić G, Glockshuber R. The PAPS-independent aryl sulfotransferase and the alternative disulfide bond formation system in pathogenic bacteria. *Antioxid Redox Signal*. 2010;13(8):1247-1259. doi:10.1089/ars.2010.3119.

83. Negishi M, Pedersen LG, Petrotchenko E, et al. Structure and function of sulfotransferases. *Arch Biochem Biophys*. 2001;390(2):149-157. doi:10.1006/abbi.2001.2368.

84. Cregut M, Piutti S, Slezack-Deschaumes S, Benizri E. Compartmentalization and regulation of arylsulfatase activities in Streptomyces sp., Microbacterium sp. and *Rhodococcus sp*. soil isolates in response to inorganic sulfate limitation. *Microbiol Res*. 2013;168(1):12-21. doi:10.1016/j.micres.2012.08.001.

85. Kertesz M a, Leisinger T, Cook AM. Proteins Induced by Sulfate Limitation. *Notes*. 1993;175(4):1187-1190.

86. Konz D, Klens A, Schörgendorfer K, Marahiel MA. The bacitracin biosynthesis operon of *Bacillus licheniformis* ATCC 10716: molecular characterization of three multi-modular peptide synthetases. *Chem Biol*. 1997;4(12):927-937.

87. Cosmina P, Rodriguez F, Ferra F, et al. Sequence and analysis of the genetic locus responsible for surfactin synthesis in *Bacillus subtilis*. *Mol Microbiol*. 1993;8(5):821-831.

88. Mootz HD, Marahiel M. A. The tyrocidine biosynthesis operon of *Bacillus brevis*: complete nucleotide sequence and biochemical characterization of functional internal adenylation domains. *J Bacteriol*. 1997;179(21):6843-6850.

89. De Crécy-Lagard V, Saurin W, Thibaut D, et al. Streptogramin B biosynthesis in *Streptomyces pristinaespiralis* and *Streptomyces virginiae*: molecular characterization of the last structural peptide synthetase gene. *Antimicrob Agents Chemother*. 1997;41(9):1904-1909.

90. Blanc V, Gil P, Naudin L, et al. Pristinamycin I biosynthesis in *Streptomyces pristinaespiralis* : molecular characterization of the first two structural peptide synthetase genes . Pristinamycin I Biosynthesis in Streptomyces pristinaespiralis : Molecular Characterization of the First Two. 1997;179(3):705-713.

91. Lin TP, Chen CL, Chang LK, Tschen JSM, Liu ST. Functional and transcriptional analyses of a fengycin synthetase gene, fenC, from *Bacillus subtilis*. *J Bacteriol*. 1999;181(16):5060-5067.

92. Tosato V, Albertini AM, Zotti M, Sonda S, Bruschi C V. Sequence completion, identification and definition of the fengycin operon in *Bacillus subtilis* 168. *Microbiology*. 1997;143(11):3443-3450. doi:10.1099/00221287-143-11-3443.

93. Tudzynski P, Hölter K, Correia T, Arntz C, Grammel N, Keller U. Evidence for an ergot alkaloid gene cluster in *Claviceps purpurea*. *Mol Gen Genet*. 1999;261(1):133-141. doi:10.1007/s004380050950.

94. Walsh CT, Chen H, Keating T a., et al. Tailoring enzymes that modify nonribosomal peptides during and after chain elongation on NRPS assembly lines. *Curr Opin Chem Biol*. 2001;5(5):525-534. doi:10.1016/S1367-5931(00)00235-0.

95. Smith DJ, Burnham MKR, Bull JH, et al. Conserved in Clusters in Prokaryotes and Eukaryotes. *EMBO J*. 1982;9(3):741-747.

96. Sawada Y, Baldwin JE, Singh PD, Solomon NA, Demain AL. Valine to Isopenicillin N. 1980;18(3):465-470.

97. Kohsaka M, Demain AL. Conversion of penicillin N to cephalosporin(s) by cell-free extracts of *Cephalosporium acremonium*. *Biochem Biophys Res Commun*. 1976;70(2):465-473. doi:10.1016/0006-291X(76)91069-X.

98. Felnagle E a, Jackson EE, Chan Y a, et al. NIH Public Access. 2011;5(2):191-211. doi:10.1021/mp700137g.Nonribosomal.

99. Mootz HD, Schwarzer D, Marahiel M. A. Ways of assembling complex natural products on modular nonribosomal peptide synthetases. *ChemBioChem*. 2002;3(6):490-504. doi:10.1002/1439-7633(20020603)3:6<490::AID-CBIC490>3.0.CO;2-N.

100. Krewulak KD, Vogel HJ. Structural biology of bacterial iron uptake. *Biochim Biophys Acta*. 2008;1778(9):1781-1804. doi:10.1016/j.bbamem.2007.07.026.

101. Chu BC, Garcia-Herrero A, Johanson TH, et al. Siderophore uptake in bacteria and the battle for iron with the host; a bird's eye view. *BioMetals*. 2010;23(4):601-611. doi:10.1007/s10534-010-9361-x.

102. Chu BCH, Peacock RS, Vogel HJ. Bioinformatic analysis of the TonB protein family. *BioMetals*. 2007;20(3-4):467-483. doi:10.1007/s10534-006-9049-4.

103. Hutchings MI, Palmer T, Harrington DJ, Sutcliffe IC. Lipoprotein biogenesis in Gram-positive bacteria: knowing when to hold 'em, knowing when to fold 'em. *Trends Microbiol*. 2009;17(1):13-21. doi:10.1016/j.tim.2008.10.001.

104. Guerinot ML. Microbial iron transport. *Annu Rev Microbiol*. 1994;48:743-772. doi:10.1146/annurev.micro.48.1.743.

105. Clarke TE, Rohrbach MR, Tari LW, Vogel HJ, Köster W. Ferric hydroxamate binding protein FhuD from *Escherichia coli*: Mutants in conserved and non-conserved regions. *BioMetals*. 2002;15(2):121-131. doi:10.1023/A:1015249530156.

106. Clarke TE, Ku SY, Dougan DR, Vogel HJ, Tari LW. The structure of the ferric siderophore binding protein FhuD complexed with gallichrome. *Nat Struct Biol*. 2000;7(4):287-291. doi:10.1038/74048.

107. Clarke TE, Braun V, Winkelmann G, Tari LW, Vogel HJ. X-ray crystallographic structures of the *Escherichia coli* periplasmic protein FhuD bound to hydroxamate-type siderophores and the antibiotic albomycin. *J Biol Chem*. 2002;277(16):13966-13972. doi:10.1074/jbc.M109385200.

108. Sebulsky MT, Shilton BH, Speziali CD, Heinrichs DE. The role of FhuD2 in iron(III)-hydroxamate transport in *Staphylococcus aureus*: Demonstration that FhuD2 binds iron(III)-hydroxamates but with minimal conformational change and implication of mutations on transport. *J Biol Chem*. 2003;278(50):49890-49900. doi:10.1074/jbc.M305073200.

109. Sebulsky MT, Heinrichs DE. Identification and Characterization of fhuD1 and fhuD2, Two Genes Involved in Iron-Hydroxamate Uptake in *Staphylococcus aureus*. *J Bacteriol*. 2001;183(17):4994-5000. doi:10.1128/JB.183.17.4994.

110. Sitthisak S, Knutsson L, Webb JW, Jayaswal RK. Molecular characterization of the copper transport system in *Staphylococcus aureus*. *Microbiology*. 2007;153(Pt 12):4274-4283. doi:10.1099/mic.0.2007/009860-0.

111. Jin B, Newton SMC, Shao Y, Jiang X, Charbit A, Klebba PE. Iron acquisition systems for ferric hydroxamates , haemin and haemoglobin in *Listeria monocytogenes*. 2006;59(December 2005):1185-1198. doi:10.1111/j.1365-2958.2005.05015.x.

112. Schneider R, Hantke K. Iron-hydroxamate uptake systems in *Bacillus subtilis*: identification of a lipoprotein as part of a binding protein-dependent transport system. *Mol Microbiol*. 1993;8(1):111-121.

113. Müller A, Wilkinson AJ, Wilson KS, Duhme-Klair AK. An [{Fe(mecam)}2]6- bridge in the crystal structure of a ferric enterobactin binding protein. *Angew Chemie - Int Ed*. 2006;45(31):5132-5136. doi:10.1002/anie.200601198.

114. Peuckert F, Ramos-Vega AL, Miethke M, et al. The siderophore binding protein FeuA shows limited promiscuity toward exogenous triscatecholates. *Chem Biol*. 2011;18(7):907-919. doi:10.1016/j.chembiol.2011.05.006.

115. Chu BCH, Otten R, Krewulak KD, Mulder F a. a., Vogel HJ. The Solution Structure, Binding Properties, and Dynamics of the Bacterial Siderophore-binding Protein FepB. *J Biol Chem*. 2014;289(42):29219-29234. doi:10.1074/jbc.M114.564021.

116. Loomis LD, Raymond KN. Solution Equilibria of Enterobactin and Metal-Enterobactin Complexes. *Inorg Chem*. 1991;30(1):906-911. doi:10.1021/ic00005a008.

117. Elkinst MF, Earhart CF. Nucleotide sequence and regulation of the transport protein FepB . Nucleotide Sequence and Regulation of the *Escherichia coli* Gene for Ferrienterobactin Transport Protein FepB. 1989;171(10).

118. Sprencel C, Cao Z, Qi Z, et al. Binding of Ferric Enterobactin by the. 2000;182(19):5359-5364.

119. Banerjee a., Sharma R, Banerjee UC. The nitrile-degrading enzymes: Current status and future prospects. *Appl Microbiol Biotechnol*. 2003;60(1-2):33-44. doi:10.1007/s00253-002-1062-0.

120. Van der Geize R, Dijkhuizen L. Harnessing the catabolic diversity of rhodococci for environmental and biotechnological applications. *Curr Opin Microbiol*. 2004;7(3):255-261. doi:10.1016/j.mib.2004.04.001.

121. Bosello M, Robbel L, Linne U, Xie X, Marahiel M. A. Biosynthesis of the siderophore rhodochelin requires the coordinated expression of three independent gene clusters in *Rhodococcus jostii* RHA1. *J Am Chem Soc*. 2011;133(12):4587-4595. doi:10.1021/ja1109453.

122. Dhungana S, Michalczyk R, Boukhalfa H, et al. Purification and characterization of rhodobactin: A mixed ligand siderophore from *Rhodococcus rhodochrous* strain OFS. *BioMetals*. 2007;20(6):853-867. doi:10.1007/s10534-006-9079-y.

123. Carrano CJ, Jordan M, Drechsel H, Schmid DG, Winkelmann G. Heterobactins: A new class of siderophores from *Rhodococcus erythropolis* IGTS8 containing both hydroxamate and catecholate donor groups. *BioMetals*. 2001;14(2):119-125. doi:10.1023/A:1016633529461.

124. Miranda-CasoLuengo R, Coulson GB, Miranda-CasoLuengo A, Vázquez-Boland J a., Hondalus MK, Meijer WG. The hydroxamate siderophore rhequichelin is required for virulence of the pathogenic actinomycete *Rhodococcus equi*. *Infect Immun*. 2012;80(12):4106-4114. doi:10.1128/IAI.00678-12.

125. Miranda-CasoLuengo R, Prescott JF, Vázquez-Boland J a., Meijer WG. The intracellular pathogen *Rhodococcus equi* produces a catecholate siderophore required for saprophytic growth. *J Bacteriol*. 2008;190(5):1631-1637. doi:10.1128/JB.01570-07.

126. Schäfer A, Tauch A, Jäger W, Kalinowski J, Thierbach G, Pühler A. Small mobilizable multi-purpose cloning vectors derived from the *Escherichia coli* plasmids pK18 and pK19: selection of defined deletions in the chromosome of Corynebacterium glutamicum. *Gene*. 1994;145(1):69-73. doi:10.1016/0378-1119(94)90324-7.

127. Pridmore RD. New and versatile cloning vectors with kanamycin-resistance marker. *Gene*. 1987;56(2-3):309-312. doi:10.1016/0378-1119(87)90149-1.

128. Section M. Properties of an R Factor from. 1974;108(3):199-204.

129. Mazodier P, Petter R a M, Thompson C. Intergeneric conjugation between *Escherichia coli* and Streptomyces species . Intergeneric Conjugation between Escherichia coli and Streptomyces Species. 1989;171(6):3583-3585.

130. Socicly A, Schafer A, Kalinowski RN, Simon R. ·High-Frequency Conjugal Plasmid Transfer froIn Dram-Negative *Escherichia coli* to Various Gram-Positive CoryneforIn Bacteria. 1990:1663-1666.

131. Gay P, Le Coq D, Steinmetz M, Berkelman T, Kado CI. Positive selection procedure for entrapment of insertion sequence elements in gram-negative bacteria. *J Bacteriol*. 1985;164(2):918-921.

132. Jager W, Schafer A, Puhler A, Labes G, Spring S. ~ E. 1992;174(16):5462-5465.

133. Olmo CH del, Santos VE, Alcon A, Garcia-Ochoa F. Production of a *Rhodococcus erythropolis* IGTS8 biocatalyst for DBT biodesulfurization: influence of operational conditions. *Biochem Eng J*. 2005;22(3):229-237. doi:10.1016/j.bej.2004.09.015.

134. Studier FW, Moffatt BA. Use of bacteriophage T7 RNA polymerase to direct selective high-level expression of cloned genes. *J Mol Biol*. 1986;189(1):113-130. doi:10.1016/0022-2836(86)90385-2.

135. Simon R, Priefer U, Pühler a. A Broad Host Range Mobilization System for *In Vivo* Genetic Engineering: Transposon Mutagenesis in Gram Negative Bacteria. *Bio/Technology*. 1983;1(9):784-791. doi:10.1038/nbt1183-784.

136. Van Der Geize R, Hessels GI, Van Gerwen R, Van Der Meijden P, Dijkhuizen L. Unmarked gene deletion mutagenesis of kstD, encoding 3-ketosteroid Δ1-dehydrogenase, in *Rhodococcus erythropolis* SQ1 using sacB as counter-selectable marker. *FEMS Microbiol Lett*. 2001;205(2):197-202. doi:10.1016/S0378-1097(01)00464-5.

137. Bradford MM. A rapid and sensitive method for the quantitation of microgram quantities of protein utilizing the principle of protein-dye binding. *Anal Biochem*. 1976;72(1-2):248-254. doi:10.1016/0003-2697(76)90527-3.

138. Koenig T, Menze BH, Kirchner M, et al. Robust prediction of the MASCOT score for an improved quality assessment in mass spectrometric proteomics. *J Proteome Res*. 2008;7(9):3708-3717. doi:10.1021/pr700859x.

139. Perkins DN, Pappin DJC, Creasy DM, Cottrell JS. Probability-based protein identification by searching sequence databases using mass spectrometry data. *Electrophoresis*. 1999;20(18):3551-3567.doi:10.1002/(sici)1522-2683(19991201)20:18<3551::aid-elps3551>3.0.co;2-2.

140. Schwyn B, Neilands JB. Universal chemical assay for the detection and determination of siderophores. *Anal Biochem*. 1987;160(1):47-56. doi:10.1016/0003-2697(87)90612-9.

141. Bhushan R, Brückner H. Marfey's reagent for chiral amino acid analysis: A review. *Amino Acids*. 2004;27(3-4):231-247. doi:10.1007/s00726-004-0118-0.

142. Miethke M, Skerra A. Neutrophil gelatinase-associated lipocalin expresses antimicrobial activity by interfering with L-norepinephrine-mediated bacterial iron acquisition. *Antimicrob Agents Chemother*. 2010;54(4):1580-1589. doi:10.1128/AAC.01158-09.

143. Santi D V., Webster RW, Cleland WW. [49] Kinetics of aminoacyl-tRNA synthetases catalyzed ATP-PPi exchange. *Methods Enzymol*. 1974;29(C):620-627.

144. Linne U, Marahiel M. A. Reactions catalyzed by mature and recombinant nonribosomal peptide synthetases. *Methods Enzymol*. 2004;388:293-315. doi:10.1016/S0076-6879(04)88024-8.

145. Medema MH, Blin K, Cimermancic P, et al. AntiSMASH: Rapid identification, annotation and analysis of secondary metabolite biosynthesis gene clusters in bacterial and fungal genome sequences. *Nucleic Acids Res*. 2011;39(SUPPL. 2):339-346. doi:10.1093/nar/gkr466.

146. Rausch C, Weber T, Kohlbacher O, Wohlleben W, Huson DH. Specificity prediction of adenylation domains in nonribosomal peptide synthetases (NRPS) using transductive support vector machines (TSVMs). *Nucleic Acids Res*. 2005;33(18):5799-5808.

147. Röttig M, Medema MH, Blin K, Weber T, Rausch C, Kohlbacher O. NRPSpredictor2 - A web server for predicting NRPS adenylation domain specificity. *Nucleic Acids Res*. 2011;39(SUPPL. 2):1-6. doi:10.1093/nar/gkr323.

148. Caboche S. Bioinformatics bolster a renaissance. *Nat Publ Gr*. 2014;10(10):798-800. doi:10.1038/nchembio.1634.

149. Gehring AM, Mori I, Perry RD, Walsh CT. The Nonribosomal Peptide Synthetase HMWP2 Forms a Thiazoline Ring during Biogenesis of Yersiniabactin, an Iron-Chelating Virulence Factor of *Yersinia pestis*. *Biochemistry*. 1998;37(33):11637-11650.

150. Sievers F, Wilm A, Dineen D, et al. Fast, scalable generation of high-quality protein multiple sequence alignments using Clustal Omega. *Mol Syst Biol*. 2011;7(539). doi:10.1038/msb.2011.75.

151. Nett M, Ikeda H, Moore BS. Genomic basis for natural product biosynthetic diversity in the actinomycetes. *Nat Prod Rep*. 2009;26(11):1362-1384. doi:10.1039/b817069j.

152. Lazos O, Tosin M, Slusarczyk AL, et al. Biosynthesis of the putative siderophore erythrochelin requires unprecedented crosstalk between separate nonribosomal peptide gene clusters. *Chem Biol*. 2010;17(2):160-173. doi:10.1016/j.chembiol.2010.01.011.

153. Bergeron RJ, Singh S, Bharti N. Synthesis of heterobactins A and B and Nocardia heterobactin. *Tetrahedron*. 2011;67(18):3163-3169. doi:10.1016/j.tet.2011.03.003.

154. Hickford SJH, Küpper FC, Zhang G, Carrano CJ, Blunt JW, Butler A. Petrobactin sulfonate, a new siderophore produced by the marine bacterium *Marinobacter hydrocarbonoclasticus*. *J Nat Prod*. 2004;67(11):1897-1899. doi:10.1021/np049823i.

155. Budzikiewicz H, Fuchs R, Taraz K, Marek-kozaczuk M, Skorupska a. Dihydropyoverdin- 7-Sulfonic Acids - Unusual Bacterial Metabolites. *Nat Prod Lett*. 1998;12(2):125-130. doi:10.1080/10575639808048280.

156. Homann V V., Edwards KJ, Webb E a., Butler A. Siderophores of *Marinobacter aquaeolei*: Petrobactin and its sulfonated derivatives. *BioMetals*. 2009;22(4):565-571. doi:10.1007/s10534-009-9237-0.

157. Thomas F, Beguin C, Pierre J-L, Serratrice G. Thermodynamic and kinetic studies of the sulfonated derivative of the iron chelator TRENCAM, an analog of enterobactin. *Inorganica Chim Acta*. 1999;291(1-2):148-157. doi:10.1016/S0020-1693(99)00130-9.

158. Pohlmann V, Marahiel M. A. δ-amino group hydroxylation of L-ornithine during coelichelin biosynthesis. *Org Biomol Chem*. 2008;6(10):1843-1848.

159. Meneely KM, Lamb AL. Biochemical characterization of a flavin adenine dinculeotide-dependent monooxygenase, ornithine hydroxylase from *Pseudomonas aeruginosa*, suggests a novel reaction mechanism. *Biochemistry*. 2007;46(42):11930-11937. doi:10.1021/bi700932q.

160. Chocklett SW, Sobrado P. Aspergillus fumigatus SidA Is a highly specific ornithine hydroxylase with bound flavin cofactor. *Biochemistry*. 2010;49(31):6777-6783. doi:10.1021/bi100291n.

161. Franceschini S, Fedkenheuer M, Vogelaar NJ, Robinson HH, Sobrado P, Mattevi A. Structural Insight into the Mechanism of Oxygen Activation and Substrate Selectivity of Flavin-Dependent N - Hydroxylating Monooxygenases. 2012:7043-7045.

162. Mayfield J a., Frederick RE, Streit BR, Wencewicz T a., Ballou DP, DuBois JL. Comprehensive spectroscopic, steady state, and transient kinetic studies of a representative siderophore-associated flavin monooxygenase. *J Biol Chem*. 2010;285(40):30375-30388. doi:10.1074/jbc.M110.157578.

163. Macheroux P, Plattner HJ, Romaguera A, Diekmannz H. FAD and substrate analogs as probes for lysine *N*-6-hydroxylase from *E.coli* EN22. 2004;1002:1-9.

164. Heemstra JR, Walsh CT, Sattely ES. Enzymatic tailoring of ornithine in the biosynthesis of the rhizobium cyclic trihydroxamate siderophore vicibactin. *J Am Chem Soc*. 2009;131(42):15317-15329. doi:10.1021/ja9056008.

165. Olucha J, Meneely KM, Chilton AS, Lamb AL. Two structures of an N-hydroxylating flavoprotein monooxygenase: Ornithine hydroxylase from *Pseudomonas aeruginosa*. *J Biol Chem*. 2011;286(36):31789-31798. doi:10.1074/jbc.M111.265876.

166. Von Heijne G. Membrane protein structure prediction. *J Mol Biol*. 1992;225(2):487-494. doi:10.1016/0022-2836(92)90934-C.

167. Chu BCH, Vogel HJ. A structural and functional analysis of type III periplasmic and substrate binding proteins: their role in bacterial siderophore and heme transport. *Biol Chem*. 2011;392(1-2):39-52. doi:10.1515/BC.2011.012.

168. Zawadzka AM, Kim Y, Maltseva N, et al. Characterization of a *Bacillus subtilis* transporter for petrobactin, an anthrax stealth siderophore. *Proc Natl Acad Sci U S A*. 2009;106(51):21854-21859. doi:10.1073/pnas.0904793106.

169. Winkelmann G, Drechsel H. Microbial siderophores. *Biotechnol Set, Second Ed*. 2008:199-246.

170. Grigg JC, Cooper JD, Cheung J, Heinrichs DE, Murphy MEP. The *Staphylococcus aureus* siderophore receptor HtsA undergoes localized conformational changes to enclose staphyloferrin a in an arginine-rich binding pocket. *J Biol Chem*. 2010;285(15):11162-11171. doi:10.1074/jbc.M109.097865.

171. Miethke M, Kraushaar T, Marahiel M. A. Uptake of xenosiderophores in *Bacillus subtilis* occurs with high affinity and enhances the folding stabilities of substrate binding proteins. *FEBS Lett*. 2013;587(2):206-213. doi:10.1016/j.febslet.2012.11.027.

172. Abergel RJ, Zawadzka AM, Hoette TM, Raymond KN. Enzymatic hydrolysis of trilactone siderophores: Where chiral recognition occurs in enterobactin and bacillibactin iron transport. *J Am Chem Soc*. 2009;131(35):12682-12692. doi:10.1021/ja903051q.

173. Herbst D a., Boll B, Zocher G, Stehle T, Heide L. Structural Basis of the Interaction of MbtH-like Proteins, Putative Regulators of Nonribosomal Peptide Biosynthesis, with Adenylating Enzymes. *J Biol Chem*. 2013;288(3):1991-2003. doi:10.1074/jbc.M112.420182.

Supplementary section

Supplementary section

Supporting tables

Table S1. Table of NMR Spectroscopic Data (500 MHz, DMSO-d_6 296 K) for Heterobactin A.

	Position	$\delta^{13}C$ type	$\delta^{1}H$	$\delta^{15}N$	HMBC[a]
DHB-1	1	116.0, C			
	2	148.5, C	11.86, s (brd)		1, 2, 3
	3	146.1, C			
	4	118.9, CH	6.94, d (7.2)		2, 6
	5	118.2, CH	6.71, t (7.8)		1, 3
	6	118.6, CH	7.42, d (7.8)		2, 4, 1´
D-Arg[1]	1´	168.7, C			
	1	171.4, C			
	2	52.6, CH	4.59, m		3, 4, 1, 1´(DHB-1)
	3	29.0, CH_2	1.91, 1.78, m		2, 4, 5, 1
	4	24.5, CH_2	1.64, m		2, 3, 5
	5	40.7, CH_2	3.31, m		3, 4, 7
	6		9.42, t (5.5)	98.8	
	7	154.3, C			
	NH		8.86, d (7.5)	118.3	2, 1´ (DHB-1)
Gly[2]	1	168.4, C			
	2	41.9, CH_2	3.77, d (5.7)		1, 1 (D-Arg[1])
	NH		8.36, t (5.5)	106.1	2, 1 (D-Arg[1])
L-cyhOrn[3]	1	164.7, C			
	2	49.6, CH	4.33, m		3, 4, 1, 1 (Gly[2])
	3	27.8, CH_2	1.90, 1.62, m		
	4	20.3, CH_2	1.90, 1.86, m		2, 3, 5
	5	51.3, CH_2	3.45, m		3, 5, 1
	NH		8.16, d (8.3)	117.7	2, 1, 1 (Gly[2])
DHB-2	1	118.3, C			
	2	146.9, C			
	3	146.3, C			
	4	119.6, CH	7.03, d (7.2)		2, 6
	5	119.0, CH	6.76, t (7.8)		1, 3
	6	120.0, CH	7.25, d (7.5)		2, 4, 1´
	1´	169.0, C			

[a]HMBC correlation, optimized for 8Hz, are from proton(s) stated to indicated carbon.

Table S2. Bioinformatic overview of the gene clusters involved in heterobactin biosynthesis.

locus name	refseq accession	Gene name	Protein size (a.a)	Proposed function	Sequence similarity organism	Identity/ similarity %	
RER_26950	BAH33403	*htb*C	387	Isochorismate synthase	DhbC *B. subtilis* 168	43	58
RER_26960	BAH33404	*htb*D	76	Aryl carrier protein	DhbB *B. subtilis* 168	49	72
RER_26970	BAH33405	*htb*A	263	2,3-dihydroxybenzoate-2,3-dehydrogenase	DhbA *B. subtilis* 168	49	63
RER_26980	BAH33406	*htb*E	554	2,3dihydroxybenzoate-AMP ligase	DhbE *B. subtilis* 168	58	73
RER_26990	BAH33407	*htb*B	215	Isochorismatase	DhbB *B. subtilis* 168	58	73
RER_27000	BAH33408	*htb*F	150	Multimeric flavodoxin / FMNdependent NAD(P)H:quinone oxidoreductase	WrbA *E. coli*	30	41
RER_27010	BAH33409	*htb*G	4161	Putative NRPS	WP_007735126 *R. qingshengii*	97	98
RER_27020	BAH33410	*htb*H	338	Putative iron-siderophore binding protein	YP_006811531 *N. brasiliensis* ATCC 700358	67	80
RER_27030	BAH33411	*htb*I	443	Putative siderophore exporter	YP_006811530 *N. brasiliensis* ATCC 700358	66	79
RER_27040	BAH33412	*htb*J	281	Putative siderophore interactive protein	YqjH *E. coli*	34	48
RER_27050	BAH33413	*htb*K	482	Putative MFS transporter	WP_010693593 *S. spinosa*	36	57

locus name	refseq accession	Gene name	Protein size (a.a)	Proposed function	Sequence similarity organism	Identity/ similarity
RER_09700	BAH1678		584	ABC transporter permease / ATP binding protein	RHA1_ro04710 *R. jostii* RHA1	71 84
RER_09710	BAH1679		600	ABC transporter ATP-binding protein / permease	RHA1_ro04711 *R. jostii* RHA1	75 86
RER_09720	BAH1680		311	Formyltransferase	RHA1_ro04712 *R. jostii* RHA1	84 92
RER_09730	BAH1681		267	Putative hydrolase	WP_019044796 *N. asteroides*	70 81
RER_09740	BAH1682		89	Hypothetical protein / CsoRlike_ DUF156	MSMEG_5388 *M. smegmatis*	87 96
RER_09750	BAH1683		161	Hypothetical protein	WP_019050331 *N. asteroides*	72 83
RER_09760	BAH1684		715	Conserved hypothetical membrane protein	WP_020108132 *Nocardia* sp. 348MFTsub5.1	77 87
RER_09770	BAH1685		196	Hypothetical protein	WP_009156445 *S. marina* XMU15	58 71
RER_09780	BAH1686		5564	Putative NRPS	RHA1_ro04715 *R. jostii* RHA1	65 78
RER_27040	BAH1687		448	Putative L-ornithine-N5-oxygenase	RHA1_ro04716 / Rmo *R. jostii* RHA1	77 86
RER_27050	BAH1688		82	MbtH-like protein	Rv2377c *M. tubercolosis*	76 88

Supprting figures

Table of Contents

Supporting Information

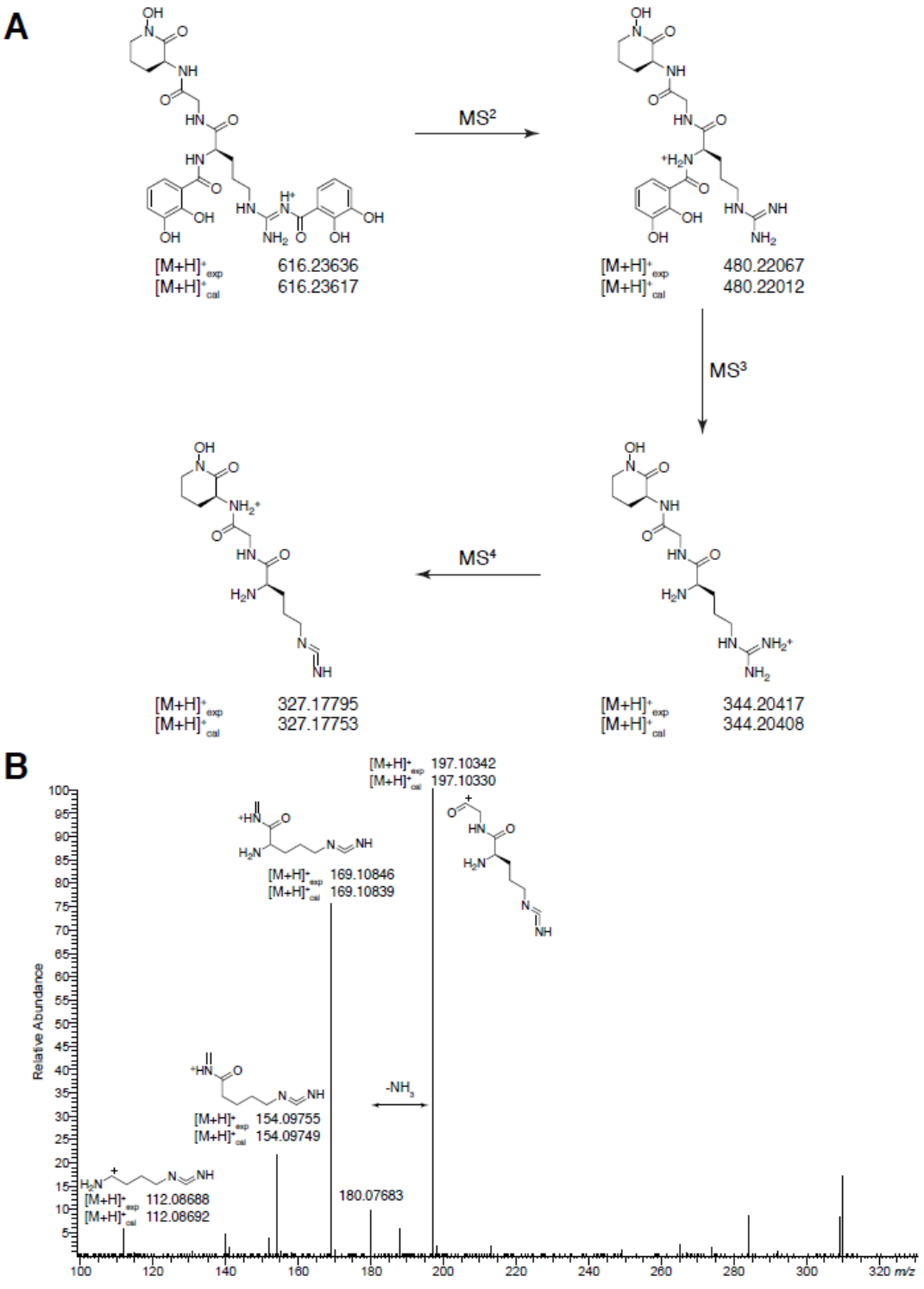

Figure S1. (A) Heterobactin A MS$^{1-4}$-fragmentation. (B) MS^{5}- fragmentation.

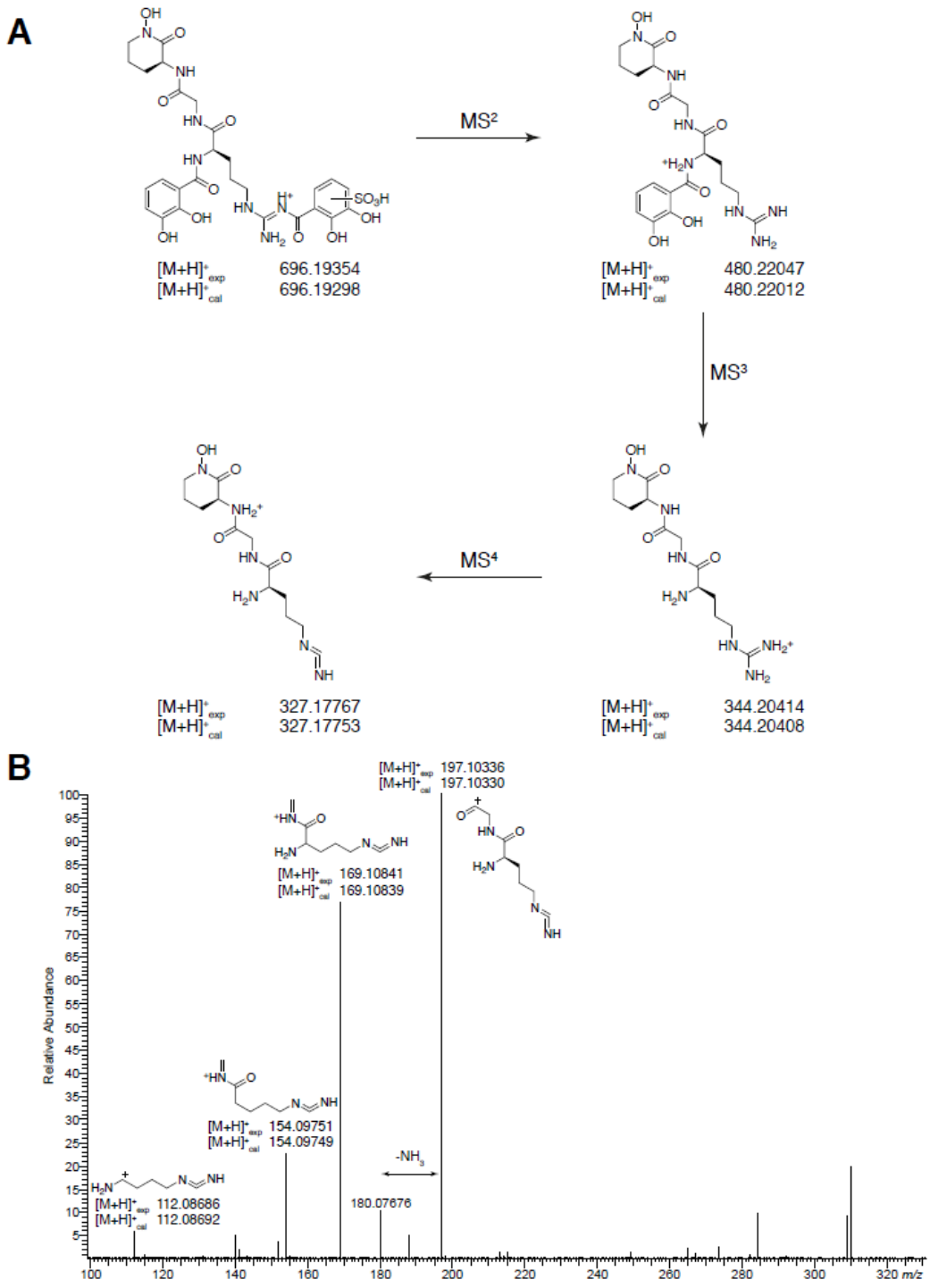

Figure S2. (A) Heterobactin S1 MS$^{1-4}$-fragmentation. (B) MS^{5}-fragmentation.

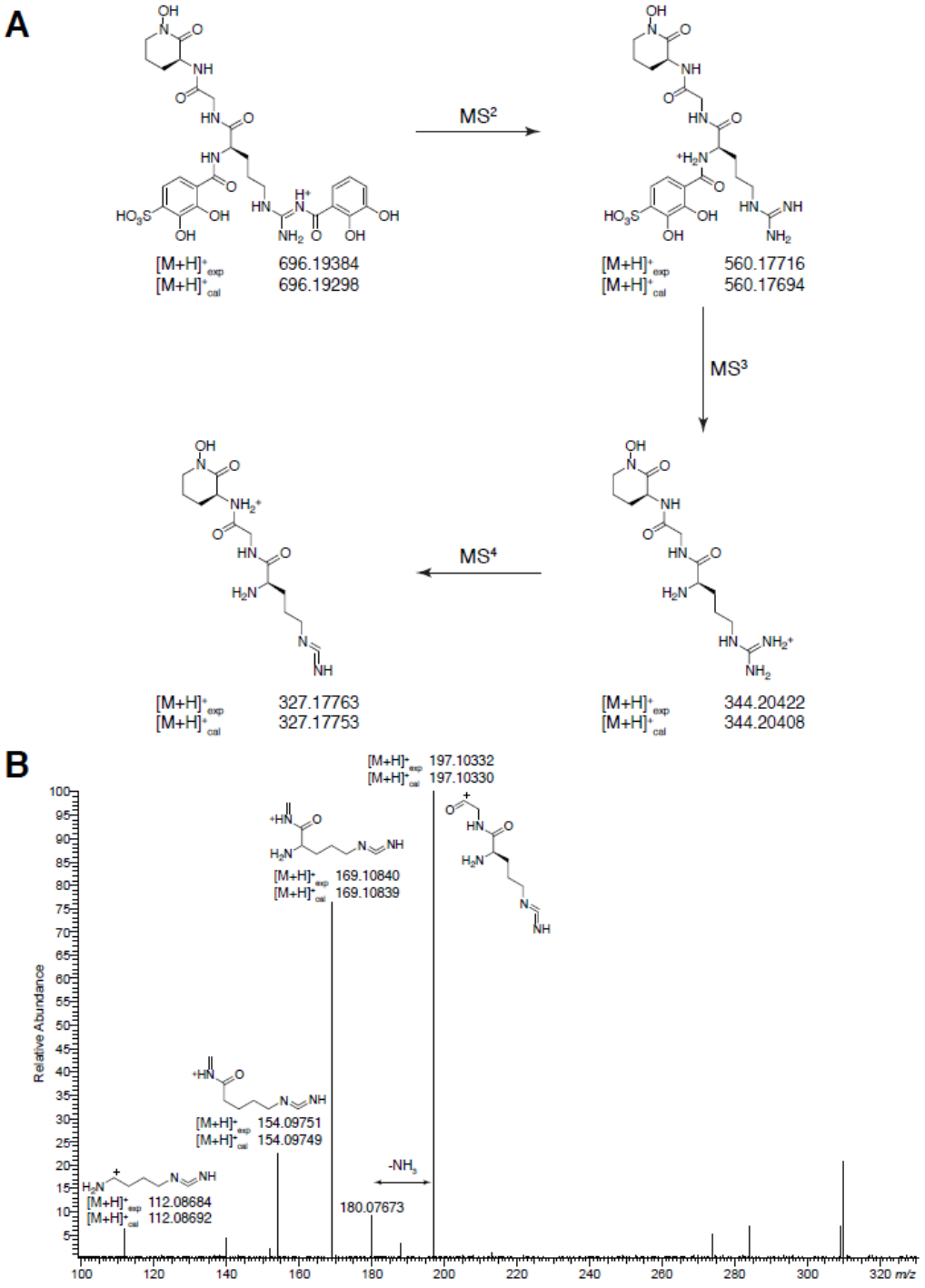

Figure S3. (A) Heterobactin S2 MS$^{1-4}$-fragmentation. (B) MS^{5}-fragmentation.

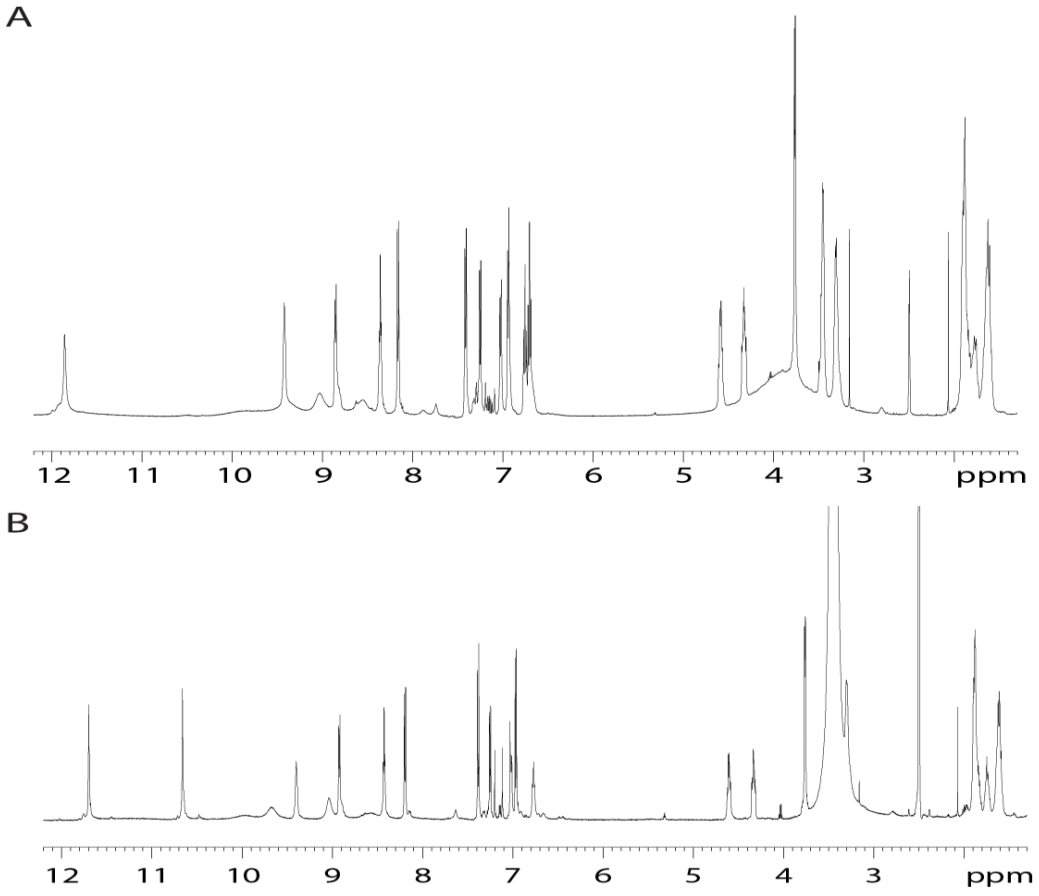

Figure S4. ^{1}H spectra of heterobactin A (A) and S2 (B) in DMSO-*d*6 at 296 K.

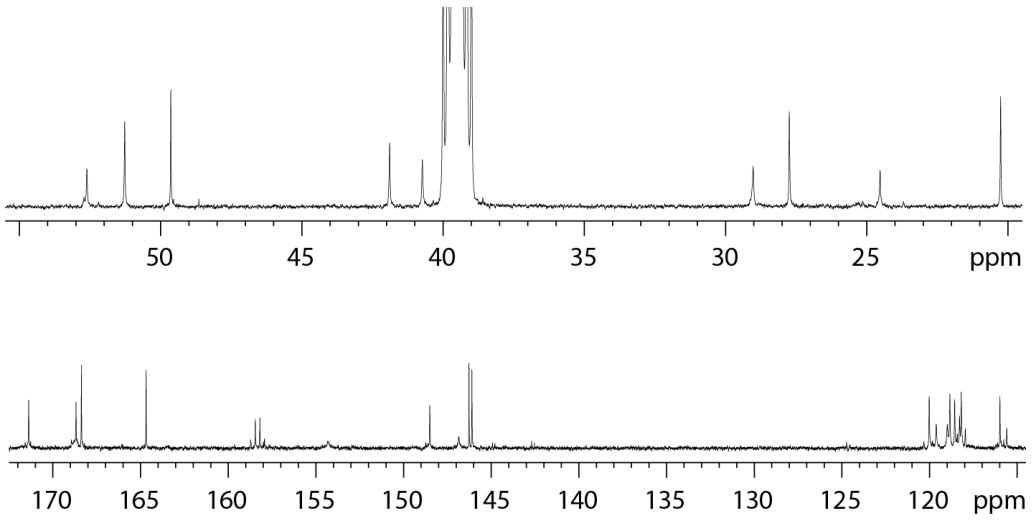

Figure S5. ^{13}C spectrum of heterobactin A in DMSO-*d*6 at 296 K.

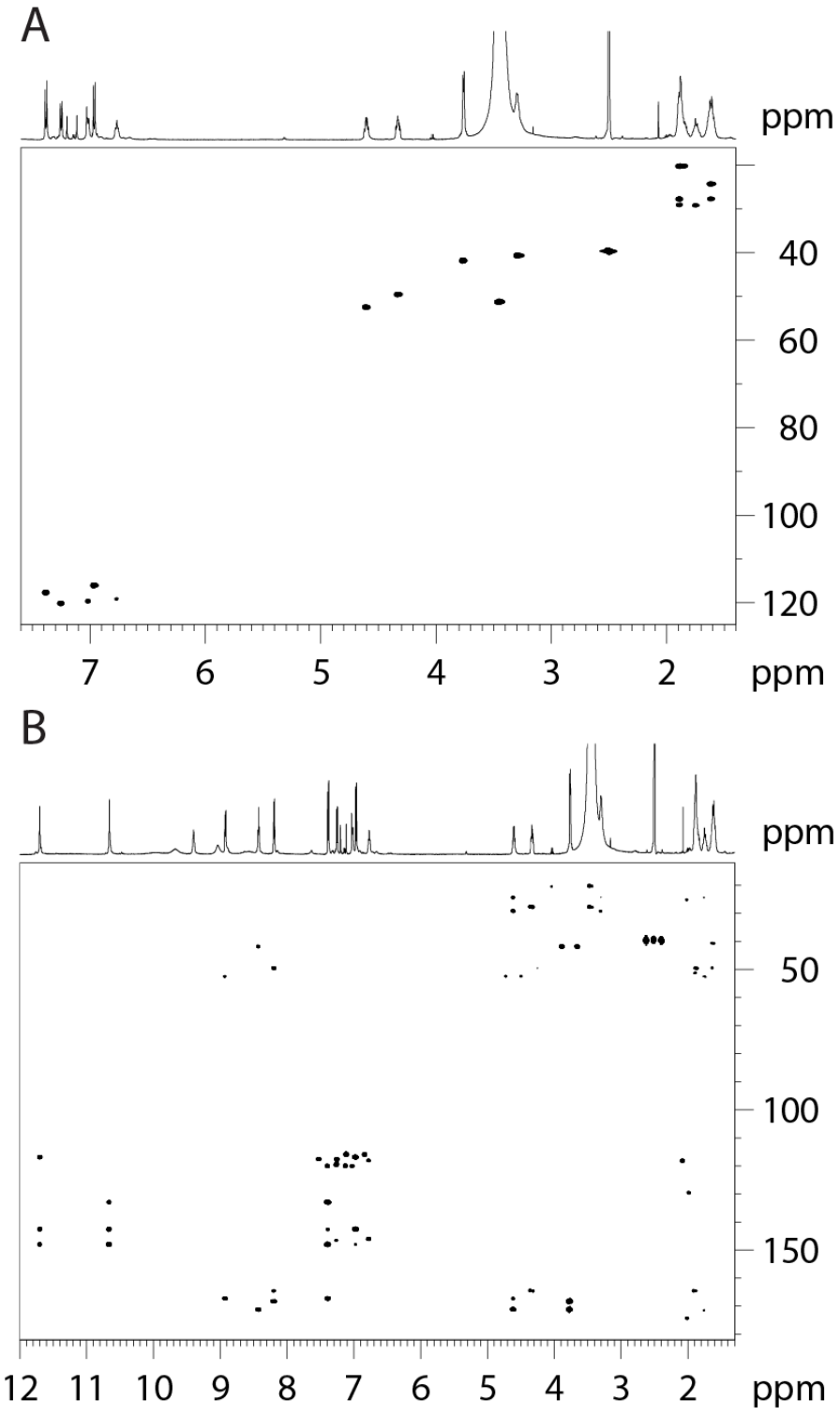

Figure S6. ^{1}H-^{13}C HSQC (A) and HMBC (B) spectra of heterobactin S2 in DMSO-*d*6 at 290 K.

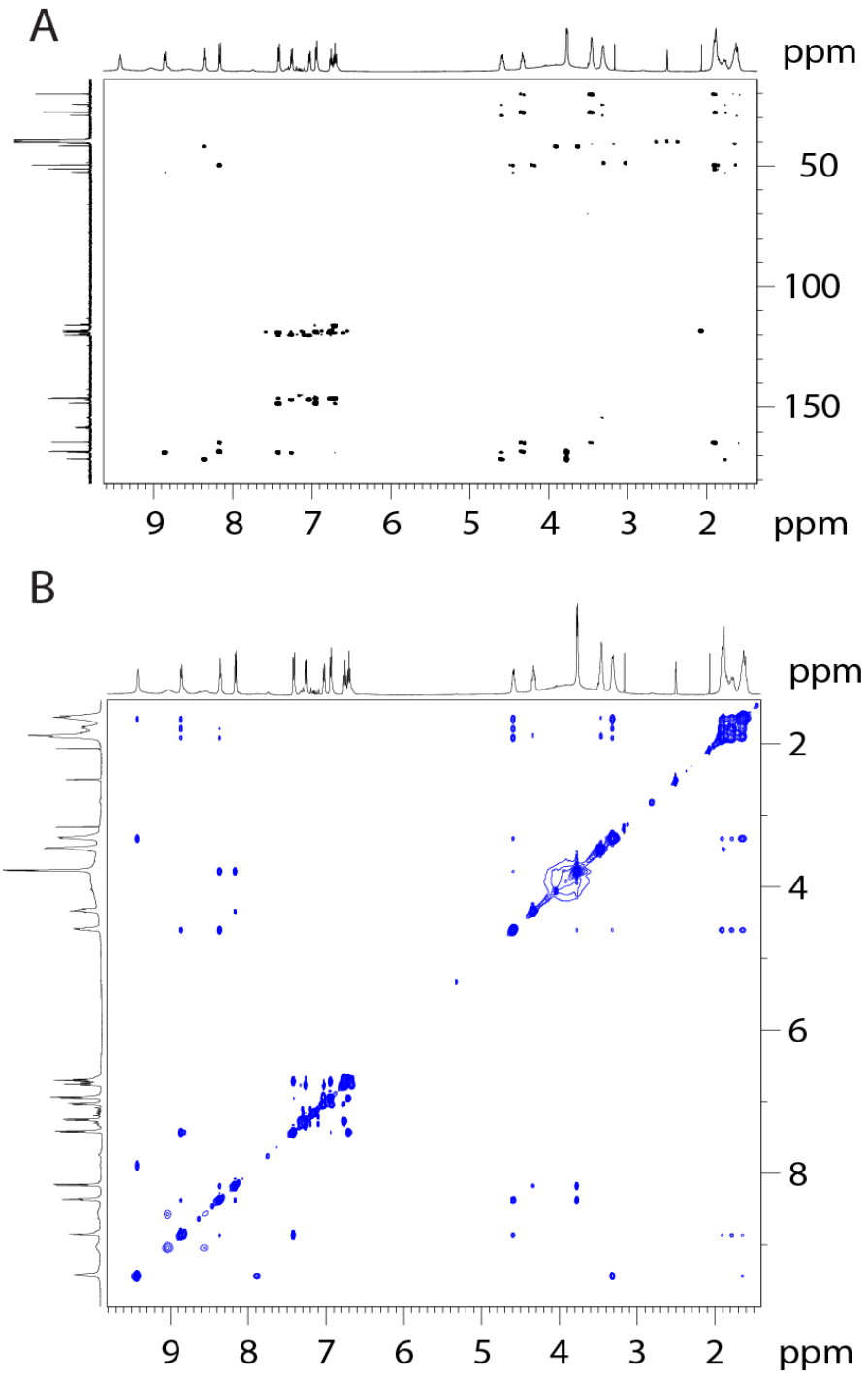

Figure S7. ^{1}H, ^{13}C-HMBC (A) and NOESY (B) spectra of heterobactin A in DMSO-*d*6 at 296 K.

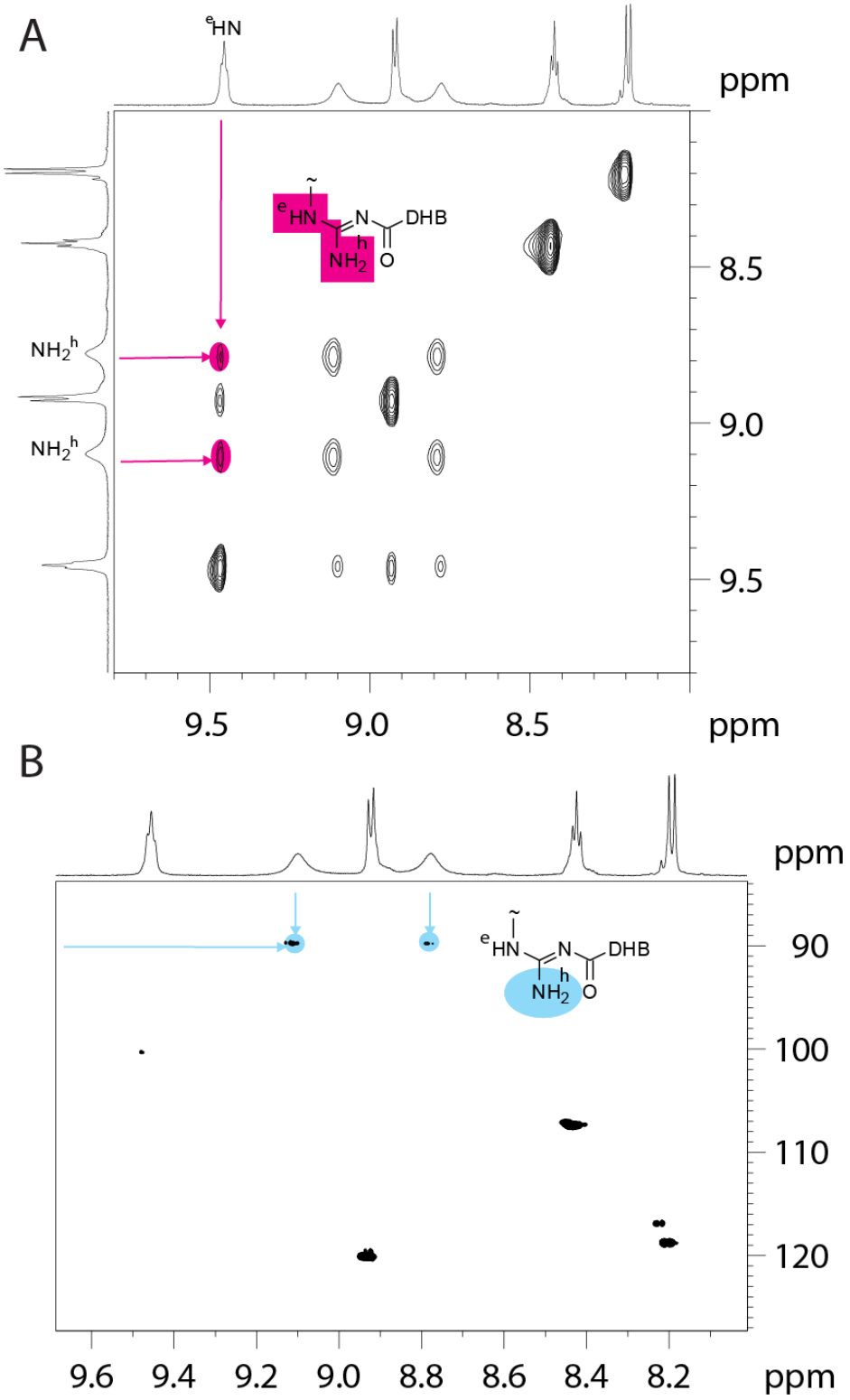

Figure S8. TOCSY (A) and ^{1}H-^{15}N HSQC (B) spectra of heterobactin S2 in DBSO-*d*6 with 1:1 molar ratio TFA at 290 K.

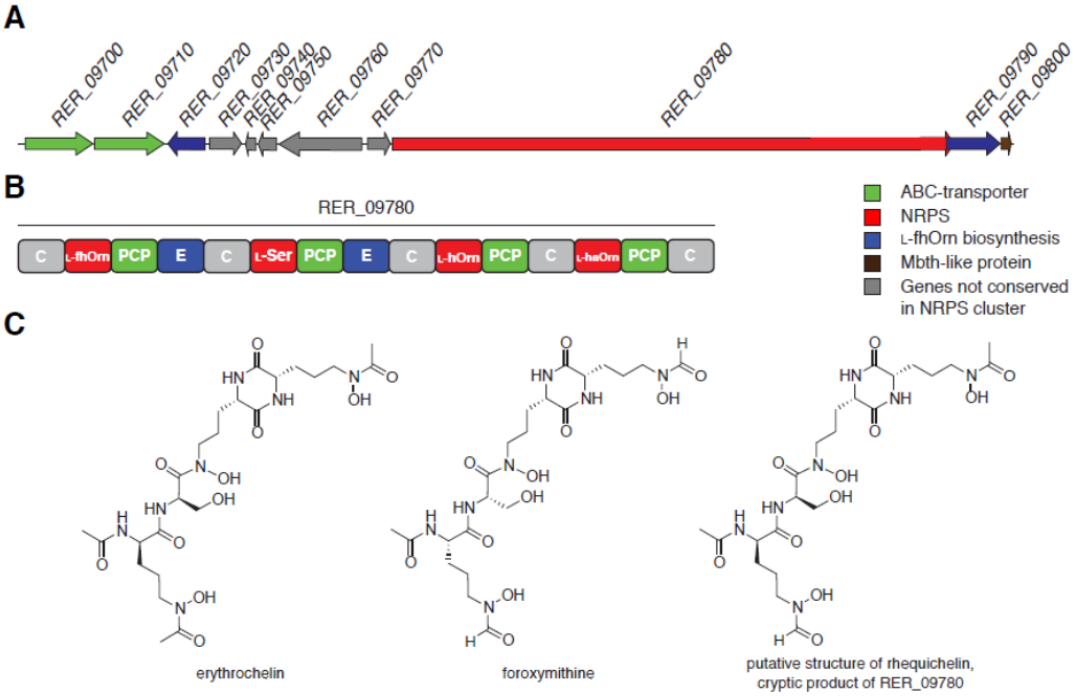

Figure S9. (A) Schematic overview of the cryptic siderophore gene cluster in *R. erythropolis* PR4. As previously reported, in some extent this genic arrangement is conserved among other *Rhodococcus* spp., despite the insertion of a variable number of additional genes within the different *Rhodococcus* isolates. (B) Modular arrangement and adenylation domains substrate specificity prediction of the NRPS RER_09780. (C) Structures comparison of the sideorophores erythrochelin[4] and foroxymithine and the proposed one of rhequichelin, isolated from *R. equii*.

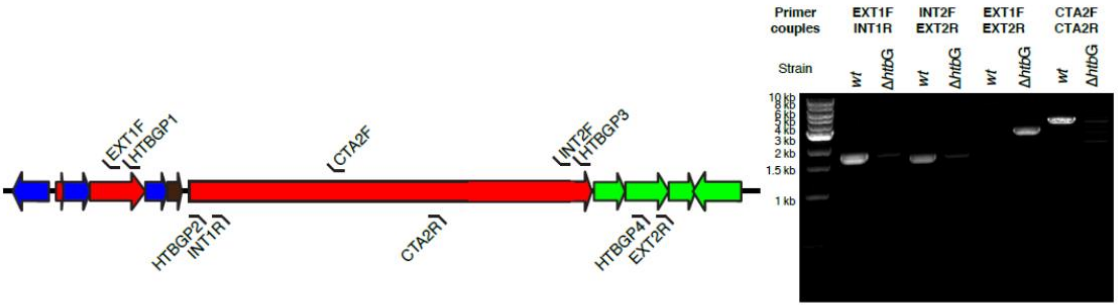

Figure S10. Agarose gel electrophoresis of the PCR reactions amplified with primer pairs spanning the *htb*G gene deletion. On the left, a schematic overview of the primers' annealing within the genome.

```
                                                  *
SgIn1  DDLKPAANGA LGELYVAGAG LAHGYVSRPA LTAERFVADP FAGPGGERMY RTGDLARRRA DGVLEYVGRA 465
MbtF   SWLRPVPDGV AGELYLAGAQ LTRGYLGRPA ETAARFVAEP NG-R-GSRMY RTGDVVRRLP DGGLEFLGRS 855
GlbF   AALRPVPVGA TGELYVAGAG LARGYLGRPA LTAQRFVADP FGAS-GSRMY RTGDLARWRA DGGLDFLGRA 875
CloH   NALRPAAVGE IGELYISGAG LARGYLNRPD LTAQLFVANP FAAD-GERMY RTGDLASMRA DGDILFHGRI 417
SimH   EALRPVPAGV PGELYLGGAG LARGYLGRPG MTAERFVANP FAGD-GSRMY RTGDLVSWRS DGGLDFLGRS 801
PczA361.18 DRLHPVPDGD VGELYMTGPG LARGYLRRPA ATAERFLPNP FGGP-GERMY RTGDRVWAGS DGQLVFVGRV 397
MbtE   DSLQPVPTGV IGEIYIGGTH VAYGYHRRAG LTAERFVADP FN-P-GSRMY RSGDLARRNA DGDIEFVGRA 821
CmnO   --LEPVGDG- LFELHVGGPT LAWGYRDRPA ATAERFPPDE R-----GRRF RTGDLVRVAD DGALVFVGRA 404
VioO   --LVPSDDG- PDELWTGGPG LAWGYADRPA LTAAAFGPAP G--A-GGRFY RTGDLVRTLP DGSLVHAGRA 414
HtbG-A1 SALEPVADGE RGELYLAGPQ LARGYLGRAG ATSERFVADP FGAP-GDLMY RAGDVARWVP GRGYDFIGRS 884
HtbG-A2 DDLREVPEGV AGELYLGGAQ VVRGYLNRPD LTVARFVADP SL-P-GARLY RTGDLVRRR- RGVLQFLRRA 2732
HtbG-A3 SGLREVPIGA AGELYMSGDG TAMGYLHRTA LTSAVFVADP YS-V-GKRMY RTGDVVLRRR DGELEYLGRA 3738
```

Figure S11. Multiple sequence alignment of the dissected HtbG A-domains with know MbtHdependent adenylation domains. The asterisk marks the conserved alanine residue involved in the interaction with two conserved tryptophan residues on the corresponding MbtH-like proteins. Residues are colored according to Herbst *et al*., 2013.[173]

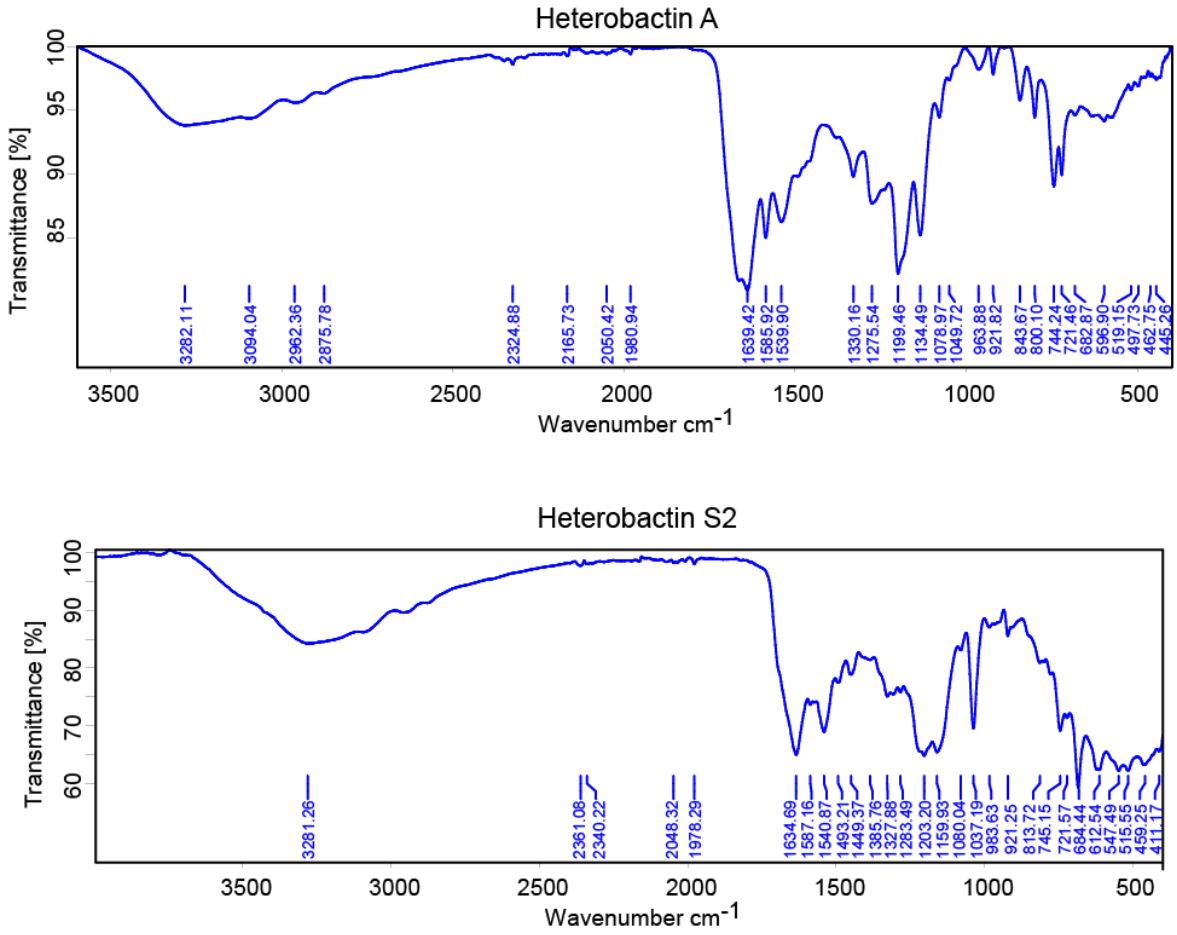

Figure S12. ATR-IR spectra of dried purified heterobactin A and heterobactin S2.

$$FeDye^{3-\gamma} + L^{x-} \longrightarrow FeL^{3-x} + Dye^{\gamma-}$$

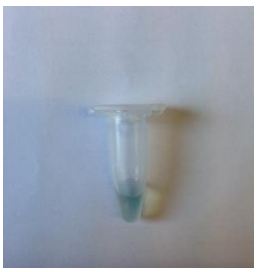

CAS (-) **CAS (+)**

Figures S13.The change in color of the blue dye-(CAS) chrome azurol sulfhonate- assay solution to red indicating the presence of siderophore.

Acknowledgements

First and foremost, I would like to thank my supervisor **Prof. Dr. Mohamed. A. Marahiel** for letting me join his research group and for providing scientific guidance and broad support during my PhD study time. I gratefully acknowledge his open-mindedness towards new ideas and enthusiasm about science, which was a constant source of motivation and resulted in great benefit for my work. I am also grateful for the opportunity he gave me to attend the "Marburg Meeting on Microbiology," 9–11 March 2014, the "2nd Transnational Workshop on Genomics and Transcriptomics in Geobiotechnology and White Biotechnology," 26–29 October 2014 in Freiberg, at which I received the poster prize, and, finally, the "Annual Conference 2015 of the Association for General and Applied Microbiology VAAM," 1–4 March 2015 in Marburg. I gratefully thank **Dr. Gert Bange** for reviewing this thesis and, together with **Prof. Dr. Wolfgang Buckel** and **Prof. Dr. Norbert Hampp**, for being part of the thesis committee. I would also like to thank my university, the **King Abdulaziz University,** for giving me the scholarship and the **Saudia Arabian Cultural Bureau** for all its support. I am also grateful to **Dr. Mattia Bosello** for his support and advice. I am thankful to **Roswitha Roller-Müller** for her administrative help. I would like to thank **Dr. Uwe Linne** for his excellent support with HPLC and MS and for his expert advice. I am deeply in debt to **Dr. Xiulan Xie** for conducting extensive and challenging NMR analyses for heterobactin structure elucidation. A special "thank you" goes to everyone in the Marahiel group for their support, the fruitful discussions and the great time in the lab. I would like to thank current and former colleagues of lab 4710 (L5) for the nice working atmosphere: **Dr. Andreas Mielcarek** and **Bastian Blaunberg**. In addition, **, Dr. Marcel Zimmermann, Dr. Julian Heagmann, and Zhu Shaozhou** from the lasso peptide group and **Dr. Tobias Gießen, Dr. Femke Krass and Dr.Chris Fage** for their support during my PhD study time. **Antje Schäfer, Christiane Bomm** and **Gabriele Schimpff Weiland** are gratefully acknowledged for the technical assistance through the years. Special thanks go to my friends **Alaa Hussein Jalil**, **Mohamed Abdulmajeed** and **Mohamed El-Awady** as well as to anyone from Saudi Arabia who supported me. Finally, I am completely grateful to my parents (**Adnan Zeyadi** and **Fatema Alshareef**), my wife (**Emtinan Alshareef**) and my Children (**Joud, Jumanah** and **Adnan**), who have been a continuous support throughout my whole life. Their constant encouragement has made all of this possible. For this, I dedicate this thesis to them.

Erklärung

Ich versichere, dass ich meine Dissertation „ **Strukturelle Charakterisierung des Heterobactin Siderophors aus *Rhodococcus erythropolis* PR4 und Untersuchung seiner biosynthetischen Maschinerie**" selbständig, ohne erlaubte Hilfe angefertigt und michdabei keiner als der von mir ausdrücklich bezeichneten Quellen und Hilfen bedient habe.

Die Dissertation wurde in der jetzigen oder einer ähnlichen Form noch bei keineranderen Hochschule eingereicht und hat noch keinen sonstigen Prüfungszwecken gedient.

Marburg, 27 October 2015 _____

Mustafa Adnan Zeyadi